ARMY RESEARCH LABORATORY

Embedded Fiber Optic Sensors for Integral Armor

by Bruce K. Fink
and Kelli Corona-Bittick

ARL-TR-2267 September 2000

The findings in this report are not to be construed as an official Department of the Army position unless so designated by other authorized documents.

Citation of manufacturer's or trade names does not constitute an official endorsement or approval of the use thereof.

Destroy this report when it is no longer needed. Do not return it to the originator.

Army Research Laboratory
Aberdeen Proving Ground, MD 21005-5069

ARL-TR-2267 **September 2000**

Embedded Fiber Optic Sensors for Integral Armor

Bruce K. Fink
Weapons and Materials Research Directorate, ARL

Kelli Corona-Bittick
Production Products Manufacturing & Sales, Inc.

Abstract

This report describes the work performed with Production Products Manufacturing & Sales (PPMS), Inc., under the "Liquid Molded Composite Armor Smart Structures Using Embedded Sensors" Small Business Innovative Research (SBIR) Program sponsored by the U.S. Army Research Laboratory (ARL). In the Phase I effort, fiber optic sensor systems were investigated for in-process cure monitoring and in-service health and dynamic response monitoring of monocoque and hybrid liquid molded composite armor structural parts. Sensor embedding techniques during resin infusion molding were developed, thick panels with varying residual stress characteristics were fabricated, two fiber optic sensor types were utilized and compared, several demodulation techniques were studied, and information processing programs were written for converting the sensor signal to engineering data. Bragg grating and fluorescence optrode fiber optic sensors were selected and embedded in armor panels to monitor the cure of the systems and health of the panels during impact and four-point bend tests. During panel curing, the Bragg gratings detected the change in strain in the material at the onset of cross-linking as well as the strain changes (residual stress) resulting from panel processing. The Bragg gratings, serving a dual purpose, measured the resulting strain from the external loads applied due to impact and bending. The fluorescence optrode was used during the cure process only to measure the changes in the material as it cured (degree of cure). Stitching of thick-section fiberglass preforms was also investigated.

Acknowledgments

This research was supported in part through the Small Business Innovative Research (SBIR) Program in a project sponsored by the U.S. Army Research Laboratory (ARL) under Contract No. DAAL01-97-C-0034. The authors gratefully acknowledge the research efforts of Eric Udd (Blue Road Research, Inc.) and Dr. Don Ames (Fluotech, Inc.).

INTENTIONALLY LEFT BLANK.

Table of Contents

List of Figures

INTENTIONALLY LEFT BLANK.

List of Tables

INTENTIONALLY LEFT BLANK.

1. Introduction

This report describes the work performed with Production Products Manufacturing & Sales (PPMS), Inc., St. Louis, MO, under the "Liquid Molded Composite Armor Smart Structures Using Embedded Sensors" Small Business Innovative Research (SBIR) Program sponsored by the U.S. Army Research Laboratory (ARL). In the Phase I effort, fiber optic sensor systems were investigated for in-process cure monitoring and in-service health and dynamic response monitoring of monocoque and hybrid liquid molded composite armor structural parts. In this program, sensor embedding techniques during resin infusion molding (RIM) were developed, thick panels with varying residual stress characteristics were fabricated, two fiber optic sensor types were utilized and compared, several demodulation techniques were studied, and information processing programs were written for converting the sensor signal to engineering data. PPMS was assisted in the area of fiber optic sensor development and demodulation by Mr. Eric Udd of Blue Road Research (BRR) and Dr. Don Ames of Fluotech. Eric Udd has developed the Bragg grating sensor technology and demodulation techniques for strain measurement (in-process and in-service), and Dr. Don Ames is the inventor of fluorescence optrode technology for cure monitoring.

During Phase I, the team selected the composite armored vehicle (CAV) as the platform to demonstrate the sensor system's capabilities for cure and health monitoring. Several 12- × 24- × 1-in-thick flat panels (E-glass/epoxy and E-glass/vinylester) were designed and fabricated to simulate the CAV's armor architecture composite backing plate. Bragg grating and fluorescence optrode fiber optic sensors were selected and embedded in the panels to monitor the cure of the systems as well as the health of the panels during impact and four-point bend tests. During the cure of the panels, the Bragg gratings were able to detect the change in strain in the material at the onset of cross-linking as well as the strain changes (residual stress) resulting from processing the panels. The Bragg gratings, serving a dual purpose, were then capable of measuring the resulting strain from the external loads applied due to impact and bending. The fluorescence optrode was used during the cure process only to measure the changes in the

material as it cured (degree of cure). Along with the sensor studies, stitching of thick-section fiberglass preforms was also investigated.

Composites offer lightweight alternatives for armor. One effective means of manufacturing composite armor is by using liquid molding processes, such as resin transfer molding (RTM) and RIM. Fiber optic sensors embedded in the RTM and RIM composite part can be used for cure monitoring to determine residual stress and degree of cure. The SMARTweave sensor system developed by ARL has the capability of monitoring cure at a number of points in a structure using a wire grid (Fink et al. 1995; England et al. 1996). These residual stress data points can be used to verify analytical models being developed at ARL and the University of Delaware (UD) for residual stress effects on RIM or RTM parts (Bogetti and Gillespie 1991, 1992a, 1992b; Haung et al. 1996; Fuhs et al. 1996). This capability will allow optimization of tools for RIM and RTM structures. These same or other sensors could be used throughout the service of the manufactured part as smart structure material sensors in a static or dynamic mode for in-service damage detection or for active control of, for example, vibration responses.

There are many Army composite structures in use that require service inspection and real-time structural health monitoring. Currently, the cost of this inspection is great and sometimes a complete failure occurs before we know that a problem exists. Future armored vehicles and lines-of-communication (LOC) bridging assets will require lifetime health monitoring and damage assessment. Conventional strain gauges are limited in their use for health monitoring since they are easily damaged, difficult to bond onto the structure, affected by electromagnetic fields, and difficult to ingress/egress. Fiber optic sensors can also be used to monitor the state of cure of composites to improve part quality. A sensor system is needed, which will allow cure monitoring and real-time structural health monitoring of composite structures at low cost. Fiber optic sensor embedment technology, however, is currently also costly. This program deals directly with the cost issue with directed research to commercialize a low-cost liquid molding manufacturing and sensor installation technique while at the same time implementing it into a high-volume Army composite armor application, which will ultimately

lower the cost of the sensors for implementation into many military and commercial product lines.

There are several benefits for having a liquid molded composite structure with fiber optic sensors. These sensors, for instance, can perform internal strain, static, vibration, shock loading, and thermal measurements. The technology allows for monitoring of multiple Bragg grating sensors along a single optical fiber. The systems could be used to accurately define loading and fatigue spectrums. These systems could reduce the maintenance cost by reducing inspections for routine maintenance and by providing detailed information of the status of the structure. Liquid molding is currently being studied for a large number of Army and commercial structures, and development of low-cost techniques to incorporate fiber optic sensors will have a large potential market. The RTM process is typically used for highly loaded structures (high fiber volumes) that have complex geometries, require positive pressure for fabrication, and are produced in large quantities to amortize tooling costs. We also use resin infusion molding (RIM) processing techniques on low-volume/prototype applications that are less critically loaded parts that have simpler geometries, can accommodate lower fiber volumes, and vacuum bag pressure.

2. Requirements Definition

Key requirements for the sensor system include the ability to be embedded and survive the manufacturing process without performance degradation or perturbing the structural integrity of the part. Internal parameters that are of interest include degree of cure, residual strain, strain and temperature during the manufacturing process, and measurement of strains and strain gradients to support health and damage assessment of the parts. Since impact sensing would be performed, it was also necessary that the system have high bandwidth and dynamic response.

The selected demonstration articles for the program are 24- × 12- × 1-in-thick flat composite panels that are resin infusion molded. Four panels were fabricated using E-glass woven fabric: two of the panels are epoxy and two are vinylester. The panels were selected to simulate the integral armor-thick composite sections as an article that could benefit from sensor technology.

The interest for sensing in the CAV articles covers both in-process sensing and structural health sensing. The following describes the sensing desires for vehicles incorporating composite armor:

(1) A low-cost manufacturing technique, vacuum-assisted resin transfer molding (VARTM), is being developed and was used on the CAV program. Since the CAV is such a large structure, it is advantageous to know where the resin is throughout the infusion process and the state of the resin throughout the cure process. Furthermore, in-process inspection is desired to enable measurement of residual stresses throughout the part and degree of cure due to the cure cycle. Knowing this information will enable optimization of the VARTM and cure process for ongoing production articles.

(2) Health monitoring of the structure in service is also desired: detecting damage after impact, using a critical delamination size of 4 in circular; detecting delamination between the various layers of the structure; and detecting excessive strains and ballistic impact damage.

3. Background

The sensor systems used in the demonstration articles were selected, sensor locations identified, and several demodulation techniques for retrieving sensor information were evaluated.

3.1 Sensor Systems. Bragg grating fiber optic sensors and fluorescence optrode sensors were selected for use in this phase of the program. The Bragg grating sensor was selected as a dual-use sensor capable of measuring process-induced strain/residual stress during the manufacturing process and capable of health monitoring in-service. The fluorescence optrode sensor was selected to monitor the cure of the parts (gel time and degree of cure) and to be used as a comparison point for the Bragg gratings.

Fiber Bragg Grating Sensors

There are several methods to manufacture fiber gratings, two of which have been demonstrated to meet high-temperature performance requirements. One method, which was developed by United Technology (Meltz et al. 1989), uses two short wavelength laser beams that are side-imaged to form an interference pattern through the fiber. The resulting bright and dark fringes caused after a long exposure (that can range from minutes to hours) create an index of refraction modulation of the core of the fiber producing a fiber grating. This method is referred to as the "holographic" method of writing fiber gratings. These fiber gratings operate up to about 500 °C before the grating starts to fade. They are characterized by high optical quality and reflectivities that are over 50%. The Naval Research Laboratory has adopted a somewhat different approach by side-imaging very intense short-duration pulses to induce a fiber grating. Unlike the United Technology approach, the index difference in this case appears to be due to optical damage and the temperature at which they operate before fading occurs at about 800 °C. The Naval Research Laboratory has demonstrated that these fiber gratings may be manufactured while the fiber is being drawn, resulting in the potential for very low-cost units. The optical quality of the fiber gratings is comparatively low with a reflectivity of about 2% being achieved.

Ken Hill of the Communications Research Laboratory (CRL) in Canada devised an earlier approach to making fiber gratings based on side imaging of a short wavelength light source using a phase mask (Hill et al. 1978). The light source need not be a laser but could be a highly intense ultraviolet (UV) lamp. These fiber gratings exhibit high optical quality and temperature performance up to about 500 °C. This approach is also being widely used by fiber researchers investigating fiber gratings, as the equipment needed for fabrication is relatively low in cost. CRL has also pioneered an approach where fiber gratings may be written line by line, resulting in high-performance fiber gratings that operate near 800 °C. The high cost of these fiber gratings may be justified for certain applications.

The costs of fiber gratings are beginning to drop dramatically due to considerable efforts by a number of vendors to support requirements of the telecommunication industry. Prices for

single-element devices made via phase mask currently range from $200 to $300 each, as opposed to $500–1,000 each about 2 years ago. Large-volume prices have fallen perhaps even more dramatically. In the 1991 timeframe, prices for hundreds of units were approximately $300 each. Today, BRR has received a quote from a vendor for $50 each for a 1,000-unit buy. Although they are unwilling to commit today, other vendors are promising similar prices in the next year or so. Other techniques being used for writing fiber gratings may have higher prices. Generally, holographically side-written fiber gratings are about double the price of the phase mask fiber gratings. This may be due largely to the high cost of facilitization. The line-by-line approach used by CRL is perhaps the highest cost of all, as it is quite time consuming and difficult to implement. A simple fiber grating being written by this method would cost approximately $1,000 today in small quantities.

More complex fiber grating structures such as the dual overlaid fiber grating have higher costs, mainly because the quantities being sold are low. A few pieces generally range from $400 to $700 each. In quantities of about 20, the price range drops to about $300 for the 21st and subsequent fiber gratings purchased. In very large quantities, 1,000 or more, the price would be less than $100.

The previously mentioned prices reflect the situation for 1997. As vendors move to support the massive number of fiber gratings needed to support telecom and cable TV requirements, the price will drop substantially.

Strain and Temperature Measurement Using Fiber Gratings

One of the issues associated with fiber-grating-based strain sensors and other strain sensors is temperature dependence. This is particularly important when accurate strain measurements are to be made in situations where the temperature varies widely and rapidly. Manufacturing composite materials when parts start to consolidate is an example of this situation. While at McDonnell Douglas, Mr. Eric Udd invented a dual overlaid fiber grating approach (Udd and Clark 1995) that involves writing two fiber gratings directly over each other at well-separated

wavelengths (e.g., 1.3 and 1.5 μ). The spectral outputs of the overlaid fiber gratings result in two equations in two unknowns, strain and temperature, that can be rapidly processed and solved. This approach has been demonstrated, and papers on it have recently begun to appear in the literature (Xu et al. 1994).

Also at McDonnell Douglas, Mr. Eric Udd realized the problem of off-axis strain measurements and devised a method of overlaying four fiber gratings, two of which are angled in the direction of the transverse axes. Although fiber gratings of this type were made, demonstrations of transverse sensitivity were, to the best of our knowledge, never made. The previous approaches, as well as demodulation methods, have McDonnell Douglas patents pending, on which BRR holds the licenses.

An improved multiple-strain sensing approach using fiber gratings was devised at BRR by Mr. Eric Udd (1997) and involves writing two overlaid fiber gratings onto birefringent fiber. In this program, the fiber would be polarization preserving fiber with a beat length of about 2 mm. The wavelengths of the fiber gratings were written at 1.300 and 1.550 μ. By writing onto the highly birefringent fiber, four gratings are established; in the case of a 2-mm beat length, they would be about 1300.0, 1300.5, 1550.0, and 1550.7 nm. Also, because the birefringent axes are well defined, transverse strains can be measured along with longitudinal strain and temperature through four equations in four unknowns. Figure 1 illustrates how overlaid fiber gratings may be used to measure three axes of strain and temperature.

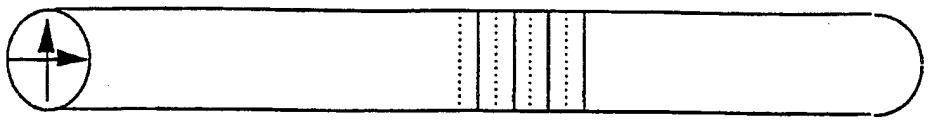

Figure 1. Three-Axis Strain and Temperature Sensor Based on Dual Overwritten Fiber Gratings on Polarization Preserving Fiber.

Selection of Fiber Bragg Grating Sensors

For Phase I of this program, both ordinary single-element fiber Bragg gratings and three-axis fiber gratings consisting of dual overlaid fiber grating on polarization maintaining fiber were selected. Six ordinary fiber gratings and two three-axis fiber gratings were used to support the program. These sensors offered the ability to measure strain, temperature, and strain gradients in the four composite panels that were fabricated. Each panel contained two fiber gratings, one located four plies down from the surface and the other located in the center of the part. Both three-axis fiber grating sensors were located in the center of the part because of their unique ability to measure transverse strain gradients.

Fluorescence Optrode Cure Sensors (FOCSs)

Description of Material Reaction to Measure Degree of Cure

A high-molecular-weight solid thermosetting epoxy polymer is formed through a chemical reaction between a low-molecular-weight hydrocarbon monomer containing glycidyl/epoxy group(s) ($RCHOCH_2$ or $ArCHOCH_2$) and/or hydroxyl group (OH) and a primary (RNH_2) or secondary amine (RNHR', where R and R' represent an alkyl or aryl group). Although the two reactants will react at ambient temperature, the reaction rate is so low that insignificant amounts of the polymer are produced. Thus, to produce a specific polymer form, the reaction rate is enhanced by heating the mixed reactants to a higher temperature. Once this temperature is reached, the heat of reaction increases the temperature, thereby increasing the reaction rate. Unfortunately, the reaction rate is diffusion controlled such that the solid polymer formed prevents reactant diffusion, producing a limited amount of cured polymer. To cure or react a desired amount of the two reactants, they are heated to a sufficiently high temperature where reactant diffusion does not limit the reaction (Eloundou et al. 1996).

As the reaction proceeds, the molecular weight increases, the liquid reactants' viscosity increases, a gel (rubber) involving cross-linked oligomer molecules is formed, and the ratio of

gel to sol increases with reaction time, yielding a dramatic increase in viscosity. Then vitrification (change from rubber to glass) occurs as curing time proceeds. The vitrified polymer contains gel and sol because vitrification retards reactant mobility, thereby quenching the reaction (stopping the cure). Consequently, complete stoichiometric reaction does not occur. Since the time-temperature-transformation behavior of the polymer system used to prepare a composite is required to optimize the composite properties, the extent of the chemical reactions involved in the cure state throughout the composite provides intelligent process control rather than a simple recipe (Gillham and Enns 1994). Furthermore, the composite mechanical properties and the dimensional accuracy are strongly dependent on the chemo-rheological events occurring during the laminate consolidation process (Loos and Springer 1983). Such cure state information is best provided by in-situ on-line monitoring because the last curing reactions occur in the middle of the mold. Since the fibers used in the composite do not change their properties or react during the cure, some polymer physical or chemical property must be measured to determine the percent of the cure reaction(s).

Candidate Systems for Measuring Cure State

There are several systems available for measuring cure state and a sample of those techniques are described in Table 1. For this program, we have selected to investigate the fluorescence technique. Fluorescence is a luminescence stimulated by radiation, not continuing no more than 10 ns after the stimulating radiation is extinguished. It is attributed to atomic or molecular energy level changes. Absorption of radiation of energy, E, produces an atomic or molecular energy level change from the ground electronic energy level, E_G, to an excited electronic energy level, E_F. The electronic energy levels of all molecules have rotational and vibrational energy (vibrotor) levels; each vibrational level is associated with a series of rotational levels. Upon excitation, the first two electronic energy levels with their associated vibrotor levels are populated and the excited vibrotor levels must decay to the lowest vibrotor level before fluorescence can occur because of spectroscopic selection rules. The excess energy, which is

Table 1. In-Situ Cure State Monitoring

Classification	Approach	Details
Fluorescence spectrometry	Fluorescence spectrometer plus optical fiber	Optical fiber embedded in composite; follow fluorescence with time
Frequency dependent dielectric response	Impedance analyzer plus Dekdyne microsensor	Measure dielectric impedance to obtain viscosity
UV reflection spectrometry	UV-Vis spectrometer plus specular reflection attachment plus optical fiber	Measure the absorbance against wavelength; use Kramers-Kronig transformation to obtain absorptivity
Near-infrared Fourier-transform infrared (FTIR) spectrometry	FTIR spectrometer plus optical fiber	Large-core optical fibers axially centered to face each other (2–3 mm apart); follow IR absorption of several vibrotor bands
Phosphorescence spectrometry	Fluorescence spectrometer plus optical fiber	Follow phosphorescence
Raman spectroscopy	Monochromator, laser optical fiber	Follow frequency shift with time

small compared with the fluorescence radiation, is dissipated by radiationless collisions. When the lowest excited energy level is completely populated (i.e., no excited vibrotor level is populated), fluorescence occurs at higher wavelengths than the excitation wavelengths. The vibrotor energy levels of the ground energy level become populated during the fluorescent emission, which extends over several tens of nanometers and is longer than the excitation wavelengths (Winans and Seldin 1967; Lackowicz 1991). A large number of optical sensing techniques based on fluorescence have been proposed (Wolfbeis 1991).

Selection of FOCSs

The selected fluorescence technique has been shown to be effective for the cure characterization of polymers because of its sensitivity and selectivity, its capability for nondestructive in-situ monitoring when combined with optical fibers, its applicability to environmental effects on composites, and the off-the-shelf availability of applicable instrumentation (Levy and Ames 1984; Levy and Schwab 1988; Levy 1986; Wang et al. 1986; Stroeks et al. 1988; Scarlata and Ors 1986; Noel et al. 1986; Dousa et al. 1989; Strehmel et al. 1992; Song and Sung 1993; Sun and Sung 1996).

Since fluorescence is both sensitive, related to the consolidation processes indicating aging and water sorption, and can be miniaturized using optical fibers, it has been selected for monitoring the polymer cure. Fluorescence from polymers is divided into two types: intrinsic, where one or more groups of the polymer fluoresce, and extrinsic, where a fluorophore is added at a low concentration to the reactants prior to polymerization. Both approaches provide viscosity-related information on the cure state. Viscosity-dependent fluorescence occurs in excited molecules that can reach the lowest excited energy level by nonradiative vibrotor transitions. Aromatic moieties present in a polymer will display viscosity-dependent fluorescence when irradiated with electromagnetic energy at low wavelengths (Forster and Hoffmann 1971; Loutfy 1981). In low-viscosity solvents, the fluorescence yield is low because of nonradiative decay caused by group rotation/vibration (torsional motion) (Loutfy 1986). As the reactants gel, the fluorescence intensity will increase because less degrees of freedom exist within the cross-linked network. As the percent of gel increases, the fluorescence intensity increases; thus, as the polymer vitrifies, the fluorescence intensity increases. Hence, fluorescence may be used to monitor the aging of the composite (Schwab and Levy 1990; Royal and Torkelson 1992, 1993). Furthermore, sorbed water or other liquids increase the number of degrees of freedom, thereby decreasing the fluorescence intensity (Levy and Ames 1985; Sun and Sung 1993; Jacobs et al. 1994; Miller et al. 1995). A cure state monitor can then monitor sorbed liquids, the rate of sorption, and the rate of aging, in addition to the extent of polymer reaction (cure). As the polymer cross-linkage increases, the maximum wavelength for the

fluorescent emission shifts toward the red for intrinsic fluorescence, whereas a blue wavelength shift occurs for extrinsic fluorescence (Sun and Sung 1996).

An optical fiber was selected for monitoring the cure because (1) its dimensions are similar to the glass/carbon fibers used in the composite, (2) it can be located anywhere in the composite panel, (3) it causes no reduction in laminate strength, (4) it transmits electromagnetic radiation with little loss, (5) radiation at different wavelengths does not interfere with one another, (6) the fiber can be used to monitor other parameters during the composite life, (7) off-the-shelf instrumentation for its use is readily available, and (8) techniques for fiber egress have been developed and demonstrated by PPMS.

3.2 Demodulation Techniques. A variety of demodulation techniques were investigated during this phase of the program. For the Bragg grating, the methods are selected based on the required response time (ranging from low velocity and ballistic impact events) and the resolution. For the FOCS, techniques were selected based on response time and intensity.

Demodulation Techniques for Fiber Bragg Gratings

One of the key issues in successfully implementing fiber optic grating sensor systems is the method used to extract the spectral content of the signal. Since a 1,000-με input corresponds to approximately 1 nm of spectral change, a demodulator capable of resolving 10 με must be able to resolve 0.01 nm. There are many methods that have been proposed, including fiber gratings, optical spectrometers, overcoupled beamsplitters, Fabry-Perot etalons, acoustooptic modulators, interferometers and CCD/dispersive element approaches.

One approach is a modulated fiber grating demodulation system. A broadband light source, which might be a light-emitting diode, is coupled into an optical fiber and used to illuminate a fiber grating. The returned spectrally modulated signal from the fiber grating is then directed by a coupler through a modulated fiber reference grating. In the case of open-loop operation, with the two spectral profiles of the sensing and reference fiber grating overlapped, the resulting

signal on the detector is predominantly second and other even-order harmonics. When the signal fiber grating is stretched or compressed first, order harmonics appear whose amplitude is proportional to the compression or extension and whose phase determines direction in analogy to demodulation methods used in association with the fiber gyro. For the closed loop, a system would have to be designed to compress and extend the reference fiber grating. Since this is difficult, only open-loop implementations of this approach are likely to be commercially viable.

A second fiber grating approach is to use a broadband chirped fiber grating filter. In this case, a broadband light-emitting diode is used to illuminate a fiber grating and the narrow band reflected signal is directed onto the fiber grating filter element by a set of two beamsplitters. A portion of the resultant light beam is directed through the fiber grating filter onto the first detector, and a second portion of the light beam is reflected off the fiber grating filter, via one of the beamsplitters, onto the second detector. The ratio of the resultant output of the two detectors establishes a unique wavelength and consequently a strain or temperature value. One advantage of this approach is that the bandwidth of this system is limited solely by the detector bandwidth, which could be multiple GHz, and the offset in path length between the transmitted and reflected legs of the light paths off the fiber grating filter (which could easily be adjusted to supported multiple GHz operation). This allows impact and ballistic events to be supported. This approach was devised by Mr. Eric Udd of BRR and is currently being developed into an educational kit (under another Phase II PPMS/BRR Program), which is under beta test at PPMS.

Another approach is to use a broadband filter such as an overcoupled coupler. This approach has been used by BRR to implement a low-cost demodulation system at 1.3 μm and works well for relative strain measurements of a single fiber grating or, using wavelength division multiplexing methods, fiber gratings that are well separated spectrally. The primary issues associated with this approach are sensitivity that is about an order or magnitude less than the fiber grating filter, as well as temperature and polarization stability issues.

A higher cost approach that offers good resolution and moderate speed is a Fabry-Perot etalon-based demodulator. When two semireflective mirrors are placed internal to the fiber

through the process of cleaving, coating, and refusing the fibers, an intrinsic fiber etalon is formed. This method has been used extensively by Texas A&M for strain measurements. An alternative Fabry-Perot etalon for sensing is the extrinsic Fabry-Perot, which consists of cleaved fiber ends that may or may not be coated placed in a capillary tube. This embodiment is called the extrinsic Fabry-Perot etalon and has been used primarily by Virginia Tech and their affiliates. For demodulation purposes, a variable Fabry-Perot etalon, based on two cleaved and end-coated fibers separated by an air gap that is controlled by a piezoelectric element, has been commercialized by a number of companies including Queensgate Instruments. The transmission of these Fabry-Perot etalons depends upon the mirror reflectivity and the spacing between the mirrors. Increasing the mirror reflectivity (higher values of the finesse F) increases the sharpness of the transmission lines, allowing better resolution of the fiber grating spectral envelope (as the half-width spectral transmission curves of the fiber etalon approach that of the fiber grating).

Various approaches can be used to adjust the tuning range (free spectral range) and sharpness of the transmission peaks, including using a length of optical fiber to form part of the cavity as well as the air gap. The main advantage of this approach is that it allows for the possibility of wide tuning ranges capable of supporting multiple-strain sensors by wavelength division multiplexing. When time division multiplexing techniques are also used, larger numbers of sensors can be supported.

A precision optical spectrometer can also be used to support the measurement of many fiber grating sensors and offers the advantage of detailed measurements of the spectral profiles of the fiber gratings. This is a particular advantage when strain gradients induced by the manufacturing process or during compression tests are of high interest. State-of-the-art optical spectrum analyzers, such as those available from Ando, Anritsu, and Hewlett-Packard, offer sufficient resolution to make high-accuracy measurements.

Other methods, such as using acoustooptic, interferometric, and charge-coupled device (CCD)-based demodulators can be used. The interferometric approach has the advantage of

providing extremely high sensitivity, while the CCD method offers the possibility of supporting very large numbers of fiber grating sensors.

The most promising acoustooptic method involves tunable filters implemented in integrated optics form. By controlling the radio frequency (RF) signal input, the spectral transmission profile may be controlled, and demodulation methods analogous to those described in association with the fiber Fabry Perot etalon may be used. Currently, the price of these integrated optic devices is higher than the fiber etalons, and electrical interference problems associated with frequencies on the order of 100 MHz have limited implementation of this demodulation system.

Interferometric approaches involve using a Mach-Zehnder or Michelson interferometer to form an optical spectral filter. If the interferometer has a large offset, it has high sensitivity but very poor thermal stability. Usually this approach has been used to support acoustic sensing rather than slowly varying strain measurements. BRR has licensed the patent on this technology from the Naval Research Laboratory for certain market areas and is cooperating with Corning on the development of a miniature Mach-Zehnder interferometer that offers the prospect of improved thermal stability, allowing strain measurements to be made successfully.

BRR has also devised novel methods of using CCD arrays to demodulate fiber gratings that are in the early stages of development. In this case, the reflected signal is directed to a special beamsplitter with flattened ends arranged to generate an interference pattern on a CCD array. The period of the interference pattern is then analyzed to determine the wavelength of the light source and, in turn, the state of the fiber grating.

Selected Fiber Grating Demodulation Techniques

The demodulation systems selected for the program were (1) a system based on a state-of-the-art optical spectrum analyzer and (2) a high-speed, low-cost demodulation system being developed by BRR that uses a fiber grating filter.

The high-speed, low-cost demodulation system based on the fiber grating spectral filter was selected since it could be used to monitor cure and to support impact and ballistic tests. This system also has the potential to be fielded in rugged environments and at costs that are compatible with widespread field use. The high-performance optical spectrum analyzer approach was selected because it is highly accurate and was used to correlate and verify the results of the other more cost-effective system. It provides a highly accurate absolute calibration source.

Demodulation Technique for the FOCS

The signal obtained from a fluorescent sensor is a product of a multitude of instrumental parameters: the intensity of the light source, the light throughput of the optical system in the excitation part, the light throughput of the optical system in the emission part, the molar absorption coefficient of the fluorophore at the excitation wavelength, the molar absorption coefficient of the indicator/fluorophore at the emission wavelength, the optical path length for the exciting light in the sensor element, the optical path length for the emitted light in the sensor, the fluorescence quantum efficiency, and the detector sensitivity (Draxler and Lippitsch 1993; Park and Song 1997).

The instrumentation selected for the current work includes a lamp housing equipped with a condenser lens and an optical fiber connector (Model No. 60000 lamp, Model No. 77799 fiber bundle focusing assembly, and Model No. 77780 fiber optic input accessory, Oriel Corp., 250 Long Beach Blvd., P.O. Box 872, Stratford, CT 06497); a 75-W xenon fused-silica lamp and DC power supply (Model No. C2576, Hamamatsu Corp., 360 Foothill Road, P.O. Box 6910, Bridgewater, NJ 08807-0910); bare 200-μm-diameter silica optical fibers (CS-90-1812, 3M Specialty Optical Fibers, 420 Frontage Road, West Haven, CT 06516) terminated on one end with a 905 SMA connector; a bifurcated optical fiber with a central 200-μm fiber surrounded by six fibers of the same diameter (General FiberOptics Inc., 1 Washington Avenue, Fairfield, NJ 07004); a miniature spectrometer with a wavelength range of 320–1,080 nm (Model S2000, Ocean Optics, 1104 Pinehurst Road, Dunedin, FL 34698-5427), equipped with a charge coupled

detector and optical fiber input; and software compatible with a personal computer (PC or clone) (see Figure 2). The Windows-based software was capable of displaying the transmission absorption or reflection mode. With a bifurcated optical fiber or two parallel fibers, the excitation radiation is passed through one fiber and the other fiber(s) transmits the fluorescent radiation to the spectrometer. This transmitted radiation was monitored with the spectrometer and was displayed on the personal computer. Figure 3 is the spectrum of the xenon lamp transmitted through a silica optical fiber.

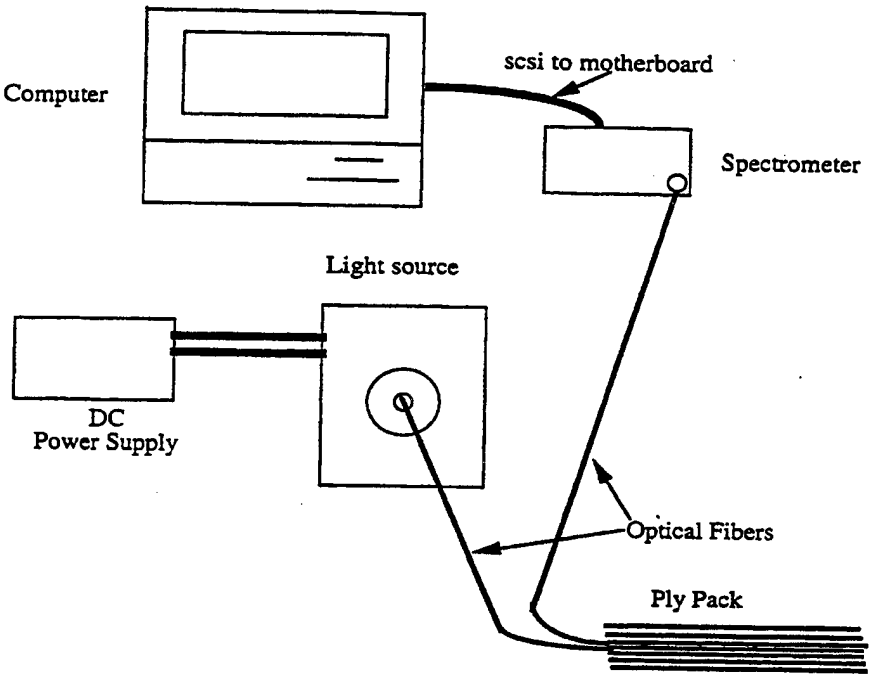

Figure 2. Instrumentation for Monitoring the Cure Using Embedded FOCS.

Data Interpretation Software

Bragg Grating and Fluorescence Optrode Spectra

The wavelength spectra recorded by the Ando spectrum analyzer for the Bragg gratings and the Ocean Optics spectrum analyzer for the fluorescence optrode sensors were stored periodically into computer files. These two-column files contained the wavelength and intensity

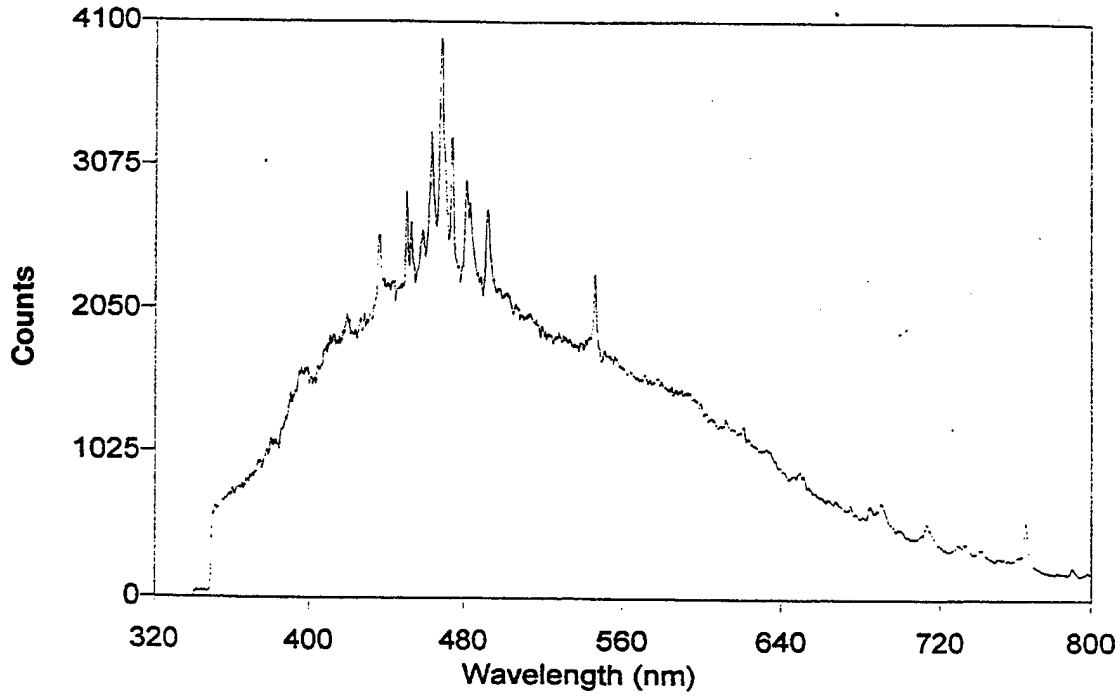

Figure 3. Spectrum of Xenon Lamp Transmitted Through a Silica Optical Fiber.

of the spectrum at 1,001 (Ando) or 2,048 (Ocean Optics) points over the selected wavelength range. A C++ program was developed to read the data from all files recorded at different times during a test, analyze the spectra, and output the results at each time to a text file for plotting in Excel and trend analysis. The characteristics studied were maximum intensity, wavelength at maximum intensity, mean wavelength, and mean-squared wavelength. The program was modified to locate both peaks from the double-peak Bragg grating spectra.

BRR Demodulator

The BRR demodulator outputs two voltage values that are proportional to the intensity of the light reflected back to the OptiPhase detector boxes. The average wavelength of the Bragg grating being read by the demodulator is a function of these intensities. The intensity of the voltage varies as the strain in the grating changes. Voltages were read and recorded with a high-resolution Keithley Metrabyte analog-to-digital (A/D) data acquisition card installed in a

personal computer in all phases of the test program. Data acquisition rates varied from one reading every 6 s during the panel cure to 2,000 readings/s during impact and ballistic tests.

A computer program was developed using Visual C++ to read, record, and interpret the data. All load, deflection, resistive strain, acceleration, and optical fiber strain output was fed to the A/D card. The program converted the voltage readings to engineering values and stored these in a data file as well as outputting them to the screen in low-rate tests. Functions were incorporated in the program to convert the voltages from the BRR demodulator to approximate strain values. The demodulator is in the beta-test stage, so software to accurately interpret the data is still in development.

The greatest challenge in interpreting the results comes from the noise in the signal. Testing was performed in a manufacturing plant with large electrical equipment. This led to significant 60-Hz noise, which can be easily seen in the raw 2-kHz data taken during impact testing. An 8-Hz noise was also detected in some tests, which is probably due to mechanical vibration from a nearby compressor. We are studying methods to further amplify the signal from the source or shield the computer hardware in order to minimize the effect of electrical noise. Voltages are currently in the range of 50–300 mV. These could be boosted to several volts to improve the signal quality. The results from this test program were averaged over a period of time to produce a more steady signal. One hundred data points covering 100–600 s were averaged in the cure tests, and 35 data points covering about 1/60th of a second were averaged in the impact tests performed at 2 kHz. Averaging was discontinued at high-voltage changes since the noise was no longer as significant and to preserve the approximate magnitude of the short-duration strain changes. No averaging was performed in the flexural tests since very few data points are recorded during the load changes. Overall, these methods yielded good results.

The relationship between the voltages and strain is determined by analyzing the spectrum of the output at the detector boxes from a broadband light source. A plot of the spectra for the beta-test demodulator is shown in Figure 4. Since the intensity of the light reaching the Bragg grating will vary due to losses at splices along the line and bending of the optical fiber, which is

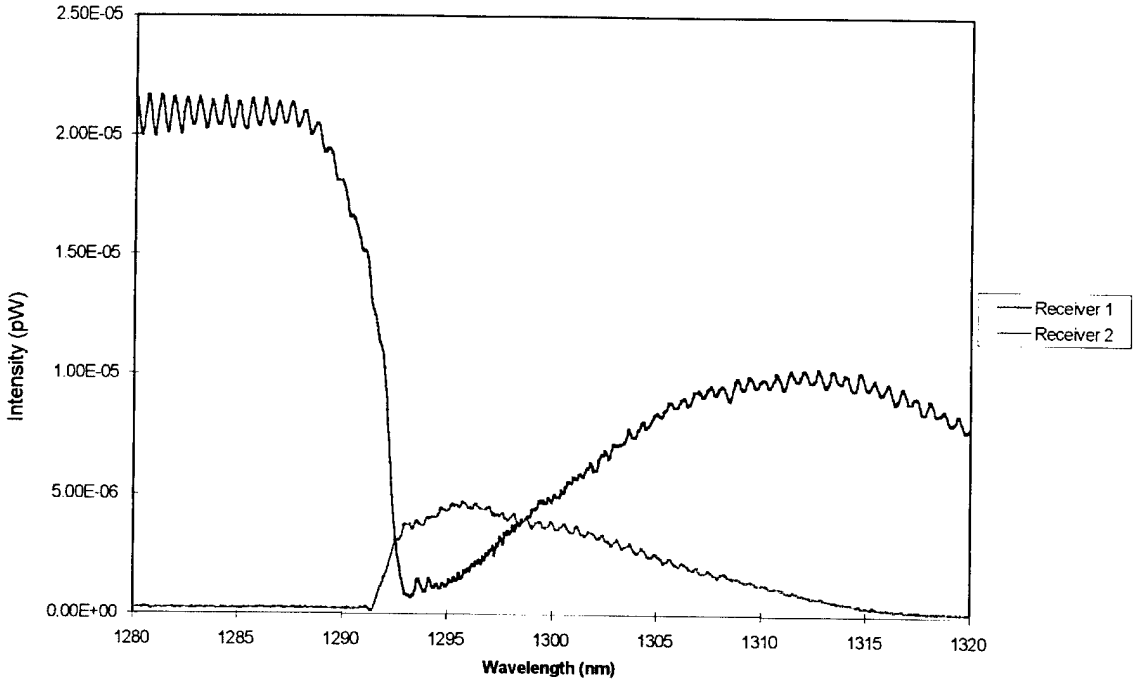

Figure 4. BRR Demodulator Receiver Spectra.

sometimes induced by test loads, a demodulation technique was developed based on the ratio of the two voltages so that the reading would be independent of the input intensity. Figure 5 is a plot of the wavelength vs. two times the Receiver 2 intensity divided by the Receiver 1 intensity for a segment of the spectrum. A smooth curve was fit through the function to quickly estimate the wavelength. The current average wavelength of a Bragg grating can then be determined from Figure 5 using the ratio of the output voltages from the two detector boxes on the BRR demodulator.

This is a simple conversion if a high level of accuracy is not needed and the smooth curve can be used. However, the wavelength is not a *function* of this ratio since, due to waviness in the spectrum, more than one wavelength can be associated with a single ratio. The use of a smoothed spectrum will lead to errors of ± 100 με. The waviness is not noise but a characteristic of the Bragg grating in the demodulator. Prototype software was developed to track the changes in the ratio along the actual curve in order to achieve accuracies on the order of 10 με; however, the noise in the signal from our current test configuration made this difficult to automate since a

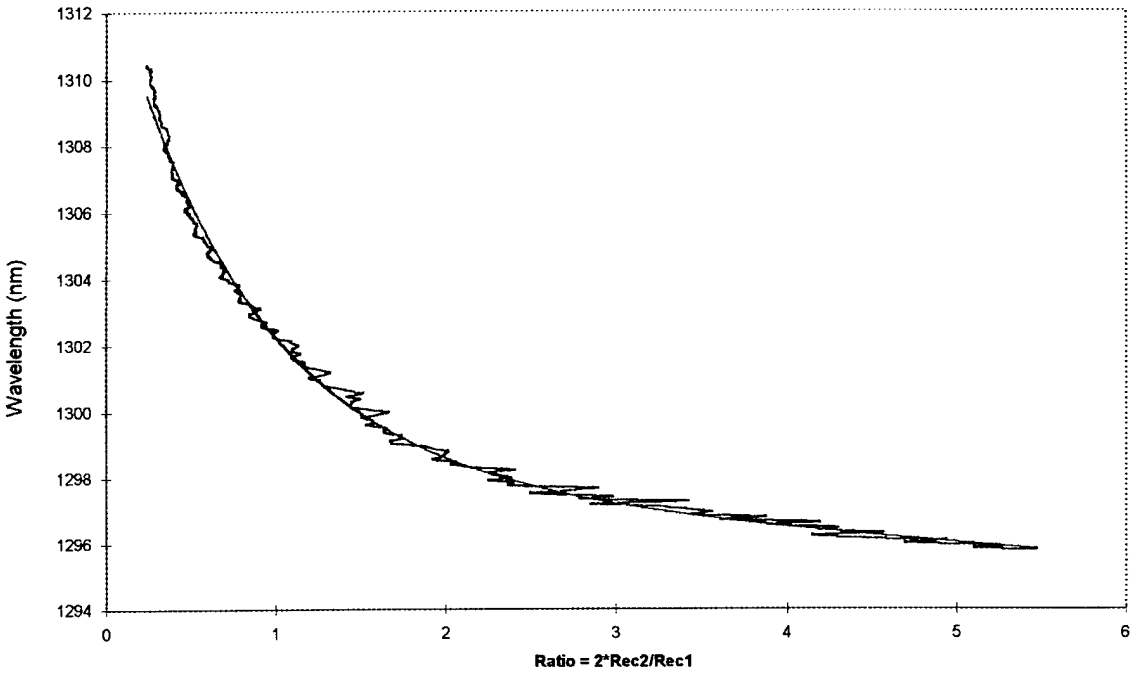

Figure 5. Wavelength vs. Receiver Ratio.

small change in the ratio due to "noise" would cause a jump from one "bump" to the next, leading to a rapid, apparent change in the strain. Attempts to smooth input voltages led to a loss of some important characteristics of the data. This issue will continue to be addressed in the development of the BRR demodulator. In the meantime, all results in this program were interpreted using the smooth curve. Strains are calculated by subtracting the initial "zero" wavelength from the current wavelength and multiplying by 1,000 με/nm. The strain was "rezeroed" for all load tests.

4. Sensor Integration

We developed an RTM composite demonstration panel design with embedded fiber optic systems utilizing ongoing concurrent engineering involving composite structure and sensor design, composite manufacturing methods, sensor embedment methods, sensor demodulation techniques, and structure/sensor performance evaluation.

4.1 Demonstration Article Design With Sensors.

Panel No. 1

Panel no. 1 is a 12- × 24- × 1-in-thick fiberglass/epoxy panel. The fiberglass preform is made up of 108 plies of 0/90 E-glass cloth (plain weave, 7.5 oz, 0.011-in thick, from Fiberglast). The epoxy is an anhydride system made up of the following mix ratio of material:

2,500 g	CIBA 6005 (preheated 8 hr at 110 °F)
2,250 g	MTHPA
25 g	BDMA
25 g	BYK A525

This panel was cured to intentionally induce maximum residual stresses to investigate the detection ability of the sensors. The cure cycle was as follows: After infusion of the panel, ramp to 275 °F, hold for 4 hr; after the hold cycle, cool the part quickly with oven doors open and apply an ice pack.

Panel no. 1 contained two single-element fiber gratings. Each of the fiber gratings had a nominal center wavelength of approximately 1,300 nm and was written into a low-cost Corning SMF-28 standard telecom optical fiber. The full-width half-maximum spectral width of the fiber gratings was 0.2 nm, and the reflectivity was approximately 80%. One of the fiber gratings (BRR-7) was embedded in the center of the panel, and the other (BRR-8) was embedded four plies from the tool surface.

Panel no. 1 was also monitored using a FOCS. A General FiberOptics bifurcated optical fiber was used. The fiber common end was placed perpendicular to the glass fibers and on the outside of the vacuum bag. Figure 6 shows the wooden support fixture for the sensor to enable looking through the bag during cure.

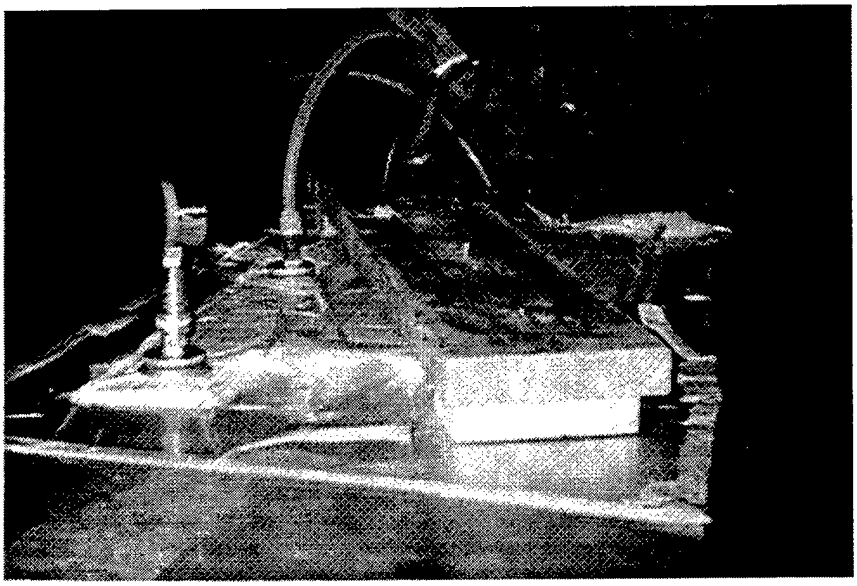

Figure 6. Bifurcated Optical Fiber Setup to Look Through the Vacuum Bag During Cure of Panel No. 1.

Panel No. 2

Panel no. 2 is a 12- × 24- × 1-in-thick fiberglass/epoxy panel with stitching. The fiberglass preform is made up of 108 plies of 0/90 E-glass cloth (plain weave, 7.5 oz, 0.011-in thick, from Fiberglast). Prior to infusion, the fiberglass preform was stitched with size E Kevlar thread using the stitch pattern shown in Figure 7. The stitching technique available to us for the panels did not allow stitching through the 1-in thickness; therefore, smaller ply packs were stitched and stacked for the panels. The ply pack stacking was as follows: 1 pack of 4 plies, 5 packs of 20 plies each, and 1 pack of 4 plies. Section 4.3 describes the stitching process and gives recommendations for the Phase II demonstration.

The epoxy in this panel is an amine system made up of the following mix ratio of material:

3,000 g	DER 383 (preheated 8 hr at 110 °F)
960 g	Jeffamine D230
30 g	BYK A525

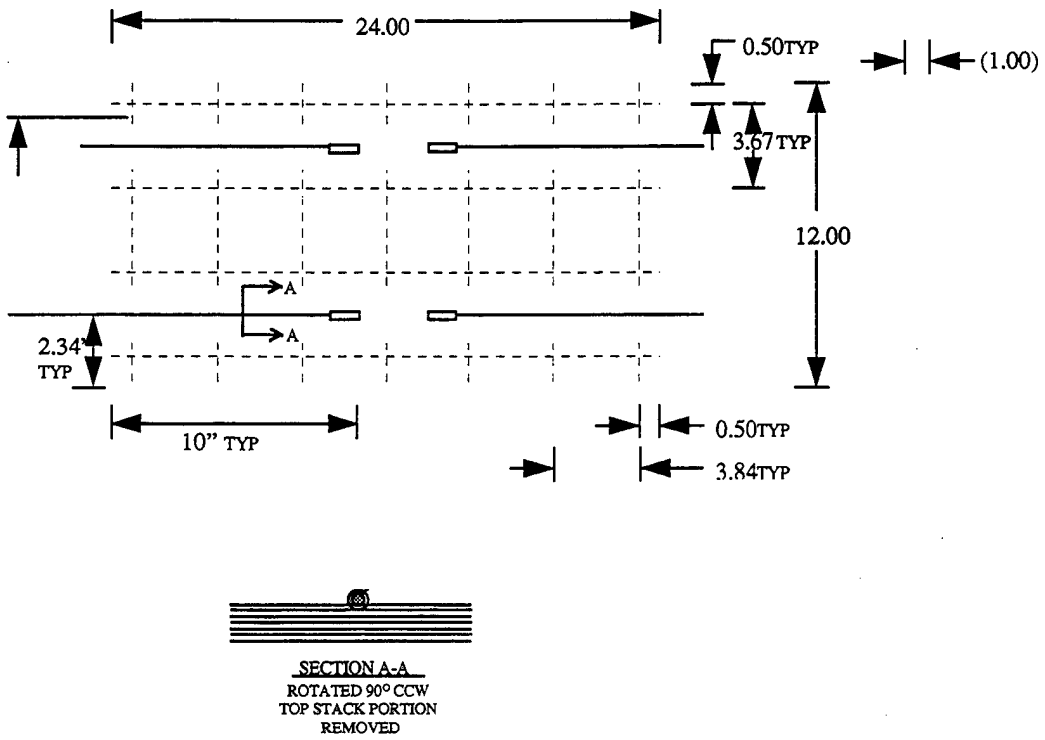

Figure 7. Stitch Pattern for 12- × 24-in Panels.

The cure cycle for this panel was used to minimize residual stresses in order to investigate the detection capability of the sensors. The cure cycle was as follows: After infusion of the panel, ramp to 175 °F, hold for 2 hr, ramp to 250 °F, hold for 2 hr; after the hold cycle, cool at 8°/min.

Panel no. 2 contained one single-element fiber grating (BRR-49-3) with a center wavelength of approximately 1,300 nm, reflectivity of about 80%, and full-width half-maximum spectral width. This sensor was embedded four plies from the tool surface. It also contained one dual overlaid fiber grating (Fibercore 5) at 1,300 and 1,550 nm, respectively, that was written into Fibercore polarization preserving fiber so that transverse strain gradients in this panel could be studied. The full-width half-maximum spectral width of the fiber gratings was approximately 0.2 nm, and the reflectivity was about 50%. This three-axis Bragg grating sensor was embedded at the midplane of the panel.

Panel no. 2 also contained a FOCS embedded at the midplane of the panel. The FOCS was two bare 200-μm silica fibers. The two distil fiber ends were placed as close together as possible during embedding in the preform.

Panel No. 3

Panel no. 3 is a 12- × 24- × 1-in-thick E-glass/vinylester panel with stitching. The fiberglass preform is made up of 108 plies of 0/90 E-glass cloth (plain weave, 7.5 oz, 0.011-in thick, from Fiberglast). Prior to infusion, this fiberglass preform was also stitched with Kevlar thread as described in panel no. 2. The ply pack stacking was as follows: 1 pack of 4 plies, 5 packs of 20 plies each, 1 pack of 4 plies. The objective of this panel was minimum residual stresses, and the vinylester mix ratio used to achieve this goal follows:

3,000 g	DOW 411-C-50
3 g	DMA (0.1%)
60 g	Trigonox (2%)
9 g	CoNap (0.3%)
1.5 g	2,4P

The cure cycle was as follows: After infusion of the panel and exotherm of the material, ramp to 250 °F, hold for 2 hr; after the hold cycle, cool at 8°/min.

Panel no. 3 contained the same type of Bragg grating sensors as panel no. 2. One single element fiber grating (BRR-49-5) embedded four plies from the tool surface, and one dual overlaid fiber grating (Fibercore 4) embedded at the midplane of the panel.

Panel No. 4

Panel no. 4 is a 12- × 24- × 1-in-thick fiberglass/vinylester panel. The fiberglass preform is made up of 108 plies of 0/90 E-glass cloth (plain weave, 7.5 oz, 0.011-in thick, from Fiberglast).

The objective of this panel was maximum residual stresses, and the vinylester mix ratio used to achieve this goal follows:

3,200 g	DOW 411-C-50
40 g	MEKP (1.25%)
9.6 g	CoNap (0.3%)
1.6 g	DMA (0.05%)

The cure cycle was as follows: After infusion of the panel and exotherm of the material, ramp to 175 °F, hold for 1 hr, ramp to 250 °F, hold for 2 hr; after the hold cycle, cool at 8°/min.

Panel no. 4 contained the same type of Bragg grating sensors as panel no. 1, two single-element fiber gratings. One of the fiber gratings (BRR-124-1) was embedded in the center of the panel; and the other was embedded (BRR-94-6) four plies from the tool surface. Panel no. 4 also contained a FOCS embedded at the midplane of the panel. The FOCS was two bare 200-μm silica fibers. The two distil fiber ends were placed as close together as possible during embedding in the preform.

4.2 Fiber Optic Cable Embedding Studies. The fiber optic sensors were embedded manually for this phase of the program as shown in Figure 8. To protect the sensor lead at the ingress/egress point into the panel, a hollow plastic tube is threaded over the cable and partially embedded into the panel. The plastic tubing from SID Tool Company, size 28 TW, has production number 167186. The tubing protects the fiber optic cable from any resin external to the panel and gives the cable additional flexibility. The tubing is partially embedded into the panel and extends out past the vacuum bag, going through the sealant tape (Figure 9). Since the RIM process requires full vacuum to pull the resin into the panel, and since the tubing is outside the vacuum bag, it is imperative that the tube end is plugged to eliminate air being pulled into the panel. Air bubbles around the sensor itself can result in an inadequate bond between the sensor and the resin, reducing sensor data accuracy.

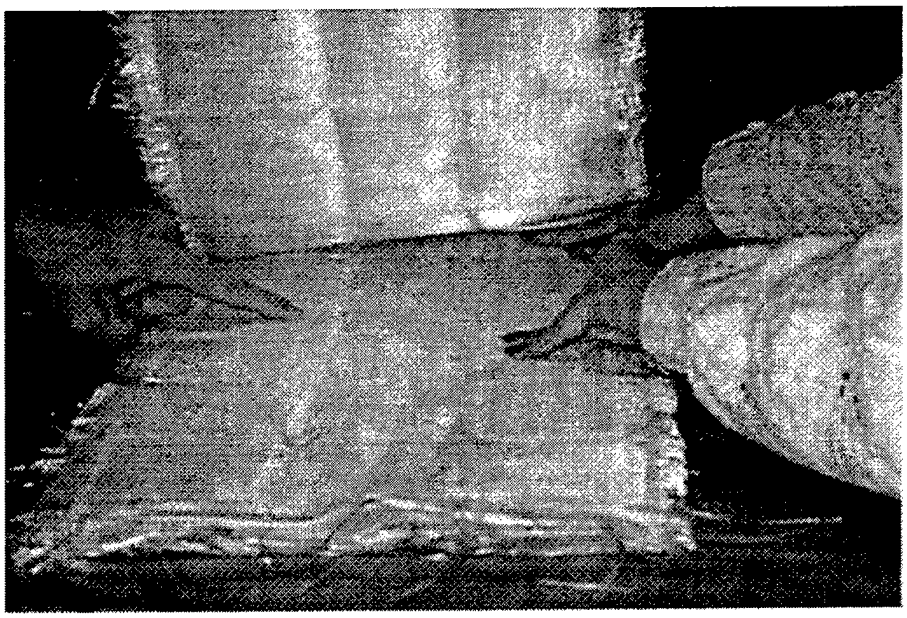

Figure 8. Embedding the Bragg Gratings and FOCS Into the 12- × 24-in Preform.

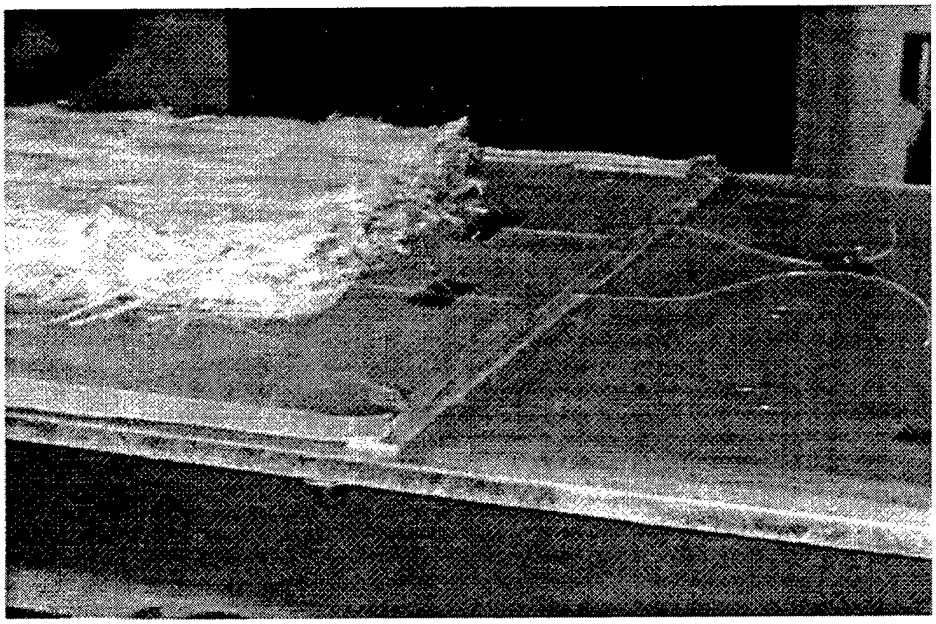

Figure 9. Egressing the Bragg Gratings and FOCS From the Preform and Vacuum Bag.

The FOCSs were also embedded manually. These sensors require that the cores of the two cables sit nearly parallel to each other to obtain the fluorescence data. To ensure that the two fibers were properly located and remained in place during preform assembly, they were stitched

together and stitched to the fiberglass preform. They were egressed the same as the Bragg gratings; however, the plastic protective tubing was not utilized since the FOCS is a substantially larger cable (200 vs. 125 μm) and is more durable. For the FOCS, it is desired that the polymer matrix adhere well to the fiber optic (same as for the Bragg grating) and that the matrix fill the volume immediately adjacent to the distil fiber end to wet it so that fluorescence is representative of the polymerized polymer employed. Any unoccupied volume at the distil end of the optical fiber will reduce the fluorescent radiation intensity. The issue of adhesion has been recently studied in detail (Green et al. 1996; Levin and Nilsson 1996; Denham et al. 1996). However, by using a low surface energy polymer that is compatible with the composite matrix better adhesion to the optical fiber can be obtained. For instance, using polyimide-coated optical fibers with a low surface energy, the adhesion to an epoxy polymer matrix can be enhanced substantially.

4.3 Stitching Studies. To reduce the bulk factor and to minimize damage propagation after impact, the CAV fiberglass preform is stitched. Therefore, in this program we attempted to demonstrate stitching of the flat fiberglass preform in two of the panels. As mentioned in the previous section, the fiberglass preform is made up of 108 plies of 7.5-oz, plain weave, 0.011-in-thick E-glass fabric from Fiberglast. The stitch material is size E Kevlar thread. Several unsuccessful attempts to stitch the full thickness of material were made before resorting to ply pack stitching for the demonstration articles. Using our process, the optimum number of plies that could be stitched was 20–25. Therefore, the demonstration articles contained 5-ply packs of 20 plies each and 2-ply packs of 4 plies each. The next paragraphs describe the process that we were using in the program as well as the recommended stitching process used by ARL at UD (Karl Bernetich).

For demonstration article preform stitching, a Consew stitching machine with a foot to index the material was used (Figure 10). With this machine, a Type 301 Lock Stitch was used, and we were attempting to achieve 5–7 stitches/inch. The mechanism for punching through the material is the needle. In the thicker preform stackings (50–100 plies), the friction buildup through the material caused the needle to heat up significantly and structurally fail (breakoff). We used both steel and high-strength titanium needles with the same result. Furthermore, the tight weave of

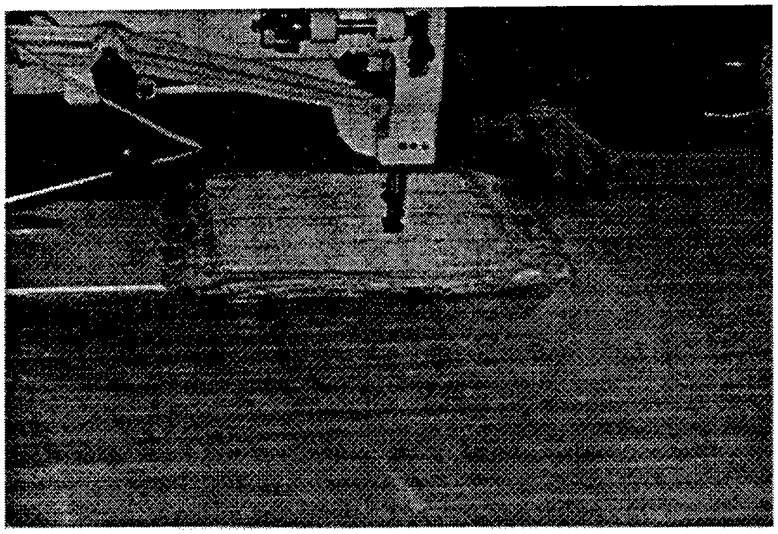

Figure 10. Stitching a 25-Ply Fiberglass Preform.

the material was adding to the friction problem. In the thinner preform stackings (<25), the needle was able to penetrate the material and stitch the required pattern.

To investigate a potential solution to stitching thicker preforms, Karl Bernetich of UD was consulted. At UD, a Hi-Post Puritan Chain Stitching Machine is used, allowing for preform stitching of up to 0.70-in-thick material. With this machine, an "awl" is used to punch through the material, leaving a hole for the needle to follow behind with a chain stitch. This takes the load off of the more fragile needle. Furthermore, ARL typically uses an 18-oz, 2 × 2 twill glass cloth, a looser weave than used in the demonstration article. ARL typically does two stitches/inch.

5. Fabrication of Demonstration Articles

Each of the four demonstration panels was fabricated using the VARTM process, whereby the fiberglass preform under vacuum pressure is infused with resin (Figure 11). After infusion, the panels were cured in an oven at the required processing temperature, as described in section 4.1. Throughout the infusion and cure cycles of the panels, the embedded optical fiber

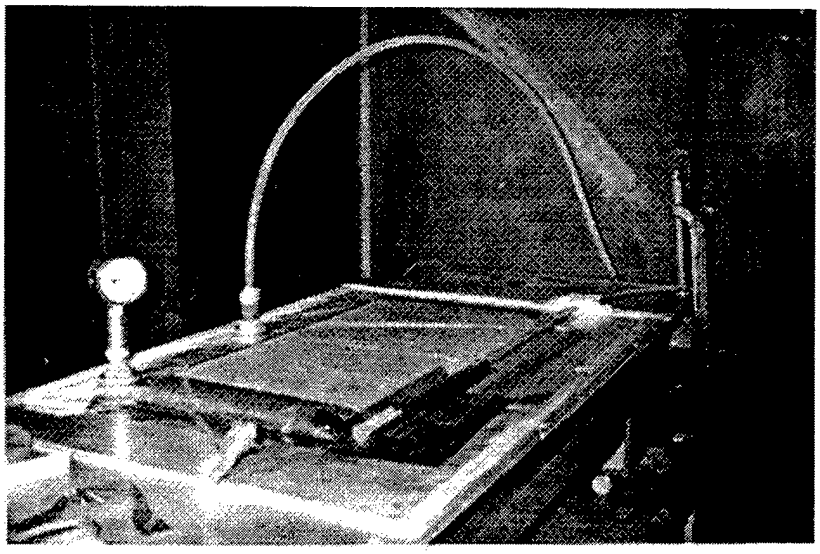

Figure 11. Infusion of a Demonstration Article Panel.

data were monitored and the oven temperature recorded. The following sections address the processing and strain data collected during cure of the demonstration panels.

5.1 Fabrication of Test Panel No. 1. As described in section 4.1, panel no. 1 is composed of an anhydride epoxy resin system and fiberglass cloth (no stitching). The anhydride system, along with the dramatic cure/cool cycle, was used to enable the introduction of maximum residual stress in the panel. The resin was heated to 110 °F to lower the viscosity for infusion. Infusion of the panel took longer than usual, 35 min, as a result of the cold day and the lack of heat on the tool. When the warm resin reached the cold tool, the viscosity increased slowing the infusion process. After resin fill was completed, the oven doors were closed and the cure cycle started (ramp to 275 °F, hold for 4 hr, cool quickly using ice packs). Oven temperature was measured using the existing oven control system. Measurement of internal part temperature is more meaningful and can be accomplished using fiber optic sensors as described in section 5.5.

Fiber Grating Results

As described earlier, this panel contained two Bragg grating fiber optic sensors, and each sensor was monitored using a different demodulation technique. The sensor embedded at the

midplane of the panel was interpreted by the optical spectrum analyzer, and the one embedded four plies deep from the tool surface was monitored by the BRR fast response demodulator. The BRR demodulator was set to take data for 400 min of the cure cycle. Therefore, the spectrum analyzer was hooked up to measure the sensor before infusion and after cure (cooled) to measure the residual strain in the panel near the surface of the tool. The following paragraphs describe the results of the data.

Figure 12 is a plot of the spectral data from the sensor embedded at the midplane of the panel at five discrete times during cure. It can be seen from this figure that the wavelength shifts throughout the cure, indicating a change in the resin and cure of the panel. The last spectrum, which was recorded after cool down, shows a wider bandwidth with some small local peaks indicating that strain varies as much as 200 με along the 4-mm Bragg grating length. Figure 13 is a plot of the strain on the sensor vs. time into cure. This figure was generated from the spectral data in Figure 12.

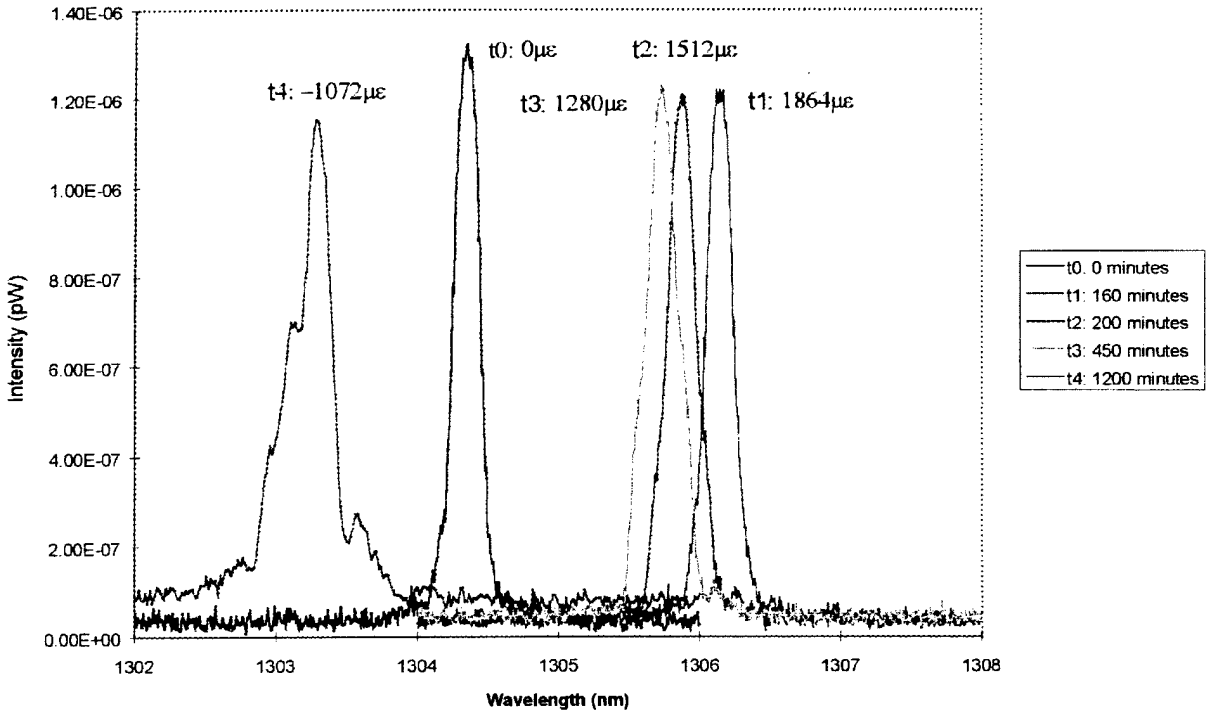

Figure 12. Spectra for Midplane Optical Fiber on Panel No. 1.

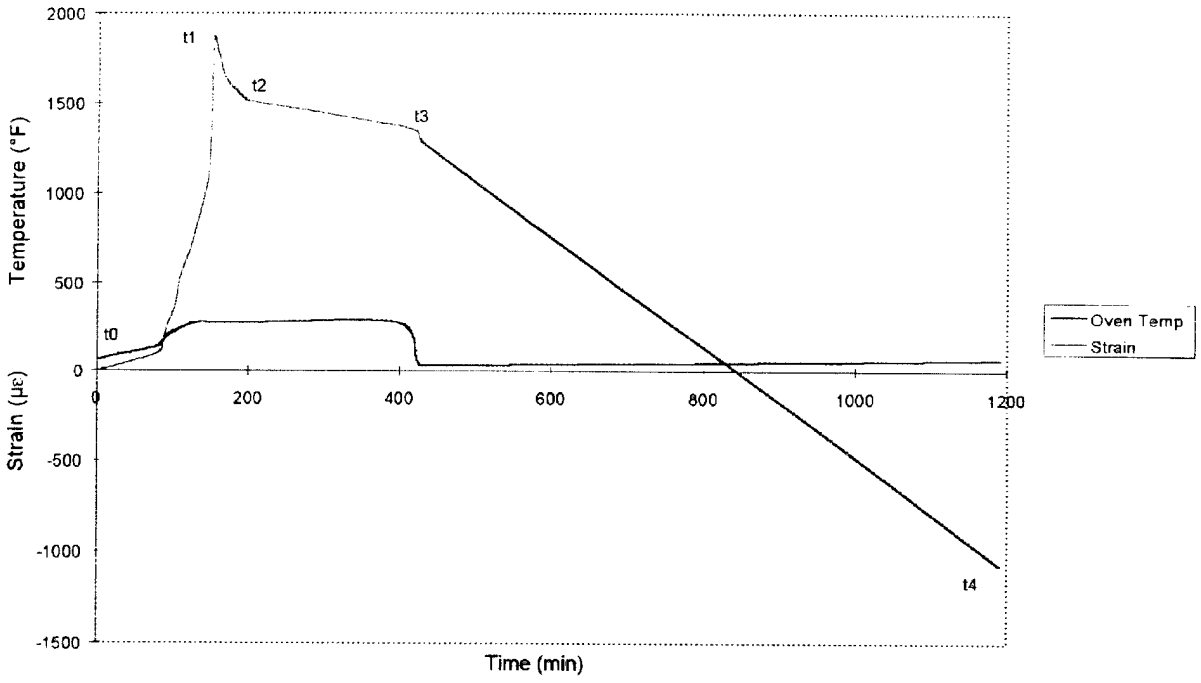

Figure 13. Optical Fiber Strain Midplane Sensor Panel No. 1.

An interpretation of the figures follows:

t_0 - 0 min depicts the wavelength of the fiber optic prior to infusion of the resin.

t_1 - 160 min is the time at which the maximum peak was achieved relating to the onset of cure. Up to this point, the strain values in the sensor were increasing as a result of thermal expansion of the fiber. At the maximum peak point, the resin starts to shrink due to cross-linking.

t_2 - 200 min, the cross-linking is complete and post cure begins.

t_3 - 450 min is the end of the post cure and the point at which ice packs were put onto the panel to rapidly cool.

t_4 - 1,200 min is the wavelength of the sensor and corresponding strain when the panel was completely cooled and the panel was measured the next morning.

The residual strain in the panel can be determined by the spectral shift from 1,304 nm (0 min) to 1303.28 nm (1,200 min) for a net spectral shift of 1.04 nm or 1,040 με.

Figure 14 is a plot of the strain-vs.-time data taken of the Bragg grating embedded four plies deep from the tool surface. The sensor data were measured using the BRR-developed demodulator. The surface sensor showed a temperature increase for curing at approximately 80 min, which is a little sooner than the center sensor, which was about 100 min. Onset of cure was the same at 160 min, and at 200 min, strain from cross-linking levels out and post cure begins. Once again, post cure ends at 400 min and the panel begins to cool. These data lead us to believe that the two sensors were seeing the same cure trends in the panel. As mentioned earlier, the spectrum analyzer was used to record the surface sensor spectrum before infusion and after cure. The resulting data showed a spectral net shift of 1.10 nm translating to a residual strain in the panel of 1,100 με. The starting wavelength was 1304.38 nm before infusion, and the final was 1303.28 nm.

FOCS Results

The bifurcated optical fibers were placed perpendicular to the ply pack at the top of the vacuum bag. These fibers were inserted through a hole in a wooden block, which was laid on top of the vacuum bag. The central fiber of the bifurcated fibers was attached to the xenon source, and the outer fibers were attached to the spectrometer using optical fiber extensions. One spectrum of the panel as it was being cured is shown in Figure 15. The other spectra, taken at different times during the cure, did not show any marked changes in the count rate as a function of wavelength. Thus, it was concluded that the optical fibers must be in direct contact with the resin to measure the cure rate.

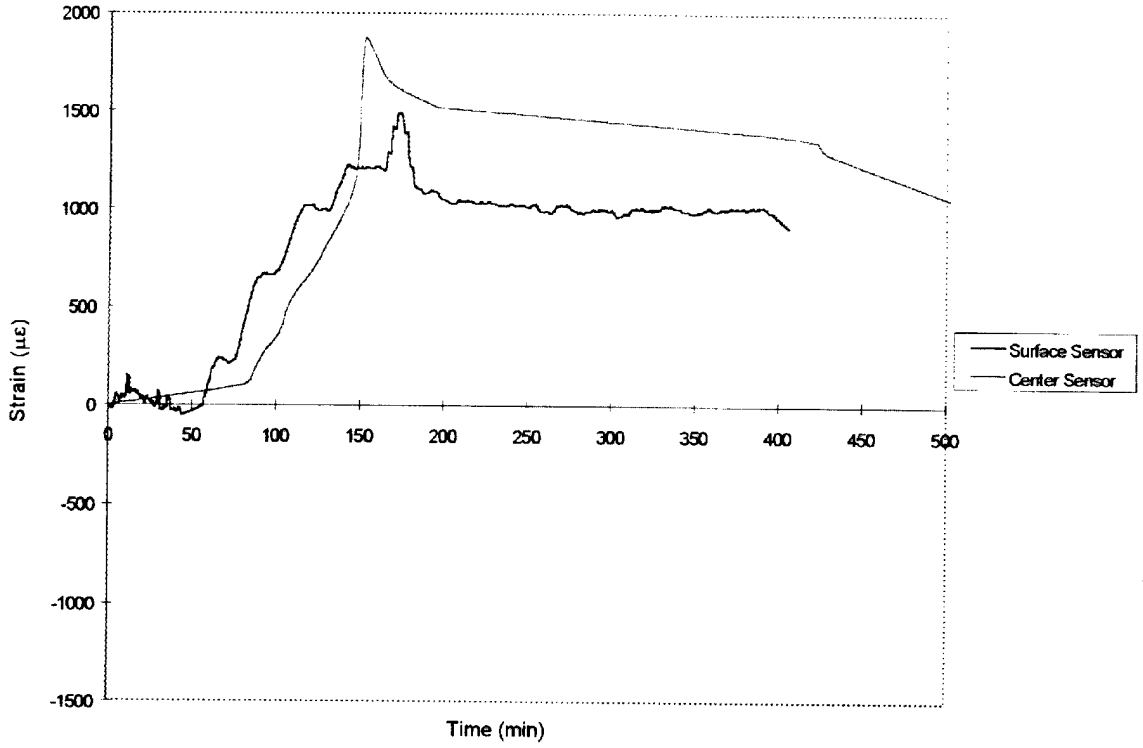

Figure 14. Fiber Strain vs. Time for Surface and Midplane Optical Fiber Panel No. 1.

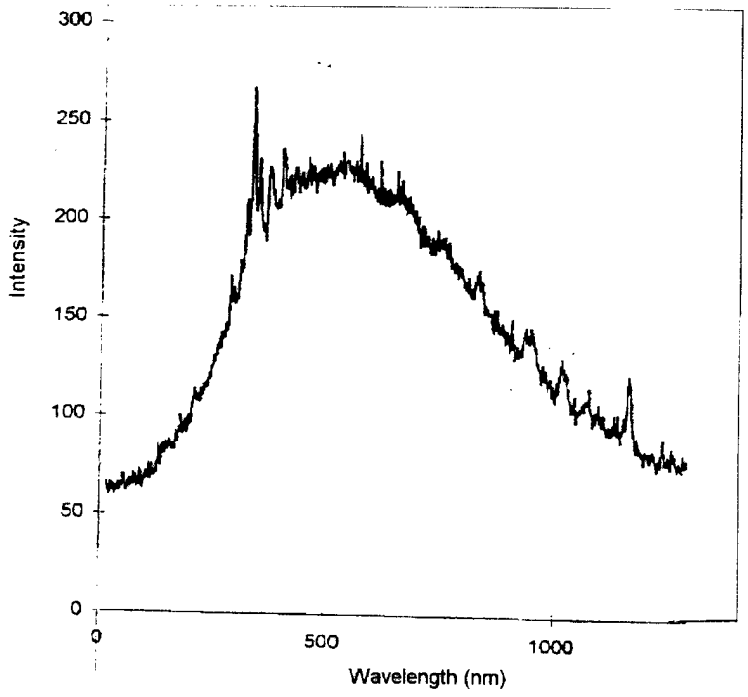

Figure 15. Spectrum of Panel No. 1 From Bifurcated Fiber During Cure.

5.2 Fabrication of Test Panel No. 2. As described in section 4.1, panel no. 2 is composed of an amine epoxy resin system and fiberglass cloth (with stitching). The amine system, along with the more gentle cure/cool cycle, was used to minimize residual stress in the panel. The resin was heated to 110 °F to lower the viscosity for infusion. The tool and preform were also preheated to ensure lower viscosity in the resin. This panel took approximately 10 min to infuse. After resin fill was completed, the oven doors were closed and the cure cycle started (ramp to 175 °F, hold for 2 hr, ramp to 250 °F, hold for 2 hr, cool at 8°/min).

Fiber Grating Results

Once again, this panel contained two Bragg grating fiber optic sensors, and each sensor was monitored using a different demodulation technique. However, this time the sensor at the midplane of the panel was a dual overlaid fiber grating at 1,300 and 1,550 nm written onto Fibercore polarization preserving fiber, and the sensor, four plies from the tool surface, was a single element 1,300-nm fiber grating. The sensor embedded at the midplane of the panel was interpreted by the optical spectrum analyzer, and the one embedded four plies deep from the tool surface was monitored by the BRR-developed demodulator. The BRR demodulator was set to take data for 400 min of the cure cycle. Therefore, the spectrum analyzer was hooked up to measure the sensor before infusion and after cure (cooled) to measure the residual strain in the panel near the surface of the tool. The following paragraphs describe the results of the data.

Figure 16 is a plot of the spectral data from the sensor embedded at the midplane of the panel. The plot shows the dual peaks for the two wavelengths. It can be seen from this figure that the wavelength shifts throughout the cure, indicating a change in the resin and cure of the panel. Figure 17 is a plot of the strain on the sensor vs. time into cure; the two wavelengths overlaid on the sensor are shown. This figure was generated from the spectral data in Figure 16.

From these figures, it appears that the onset of cure begins after the ramp to 175 °F at about 102 min into the cycle. After the peak wavelength and strain is seen, the curve slopes downward, indicating that cross-linking is continuing at the 175 °F hold. When the temperature

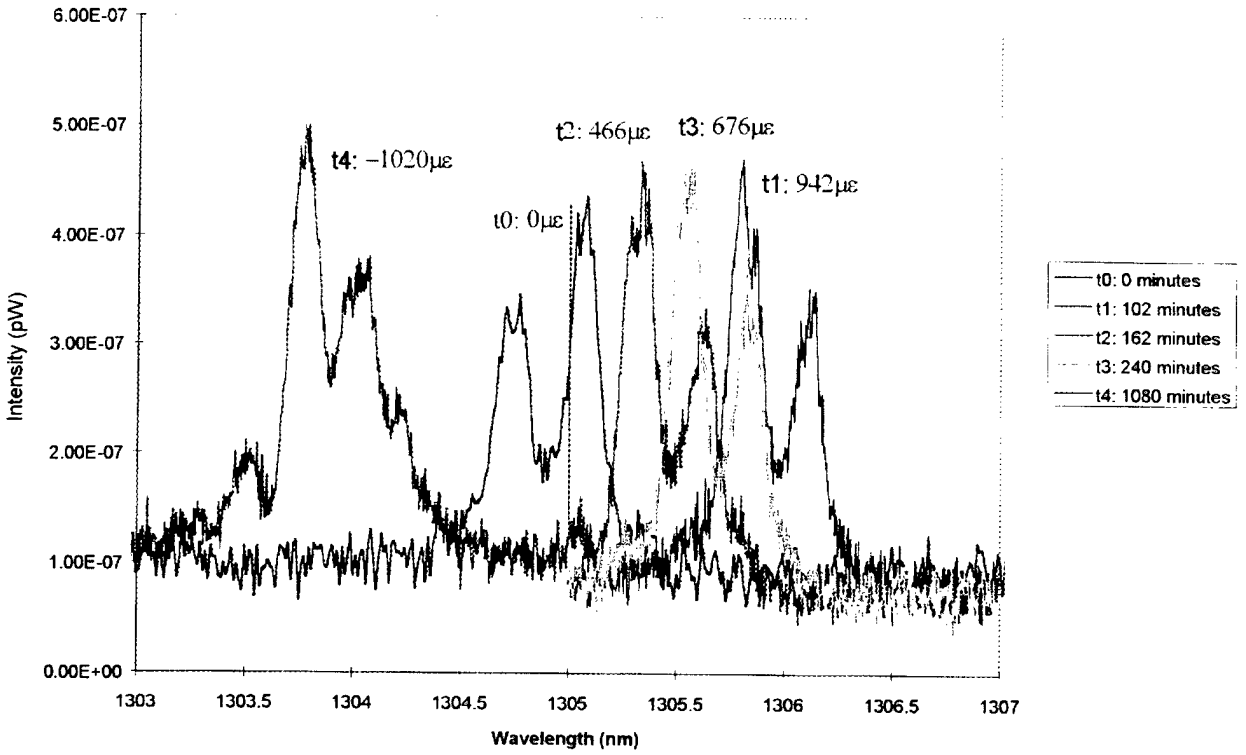

Figure 16. Spectra for Midplane Optical Fiber on Panel No. 2.

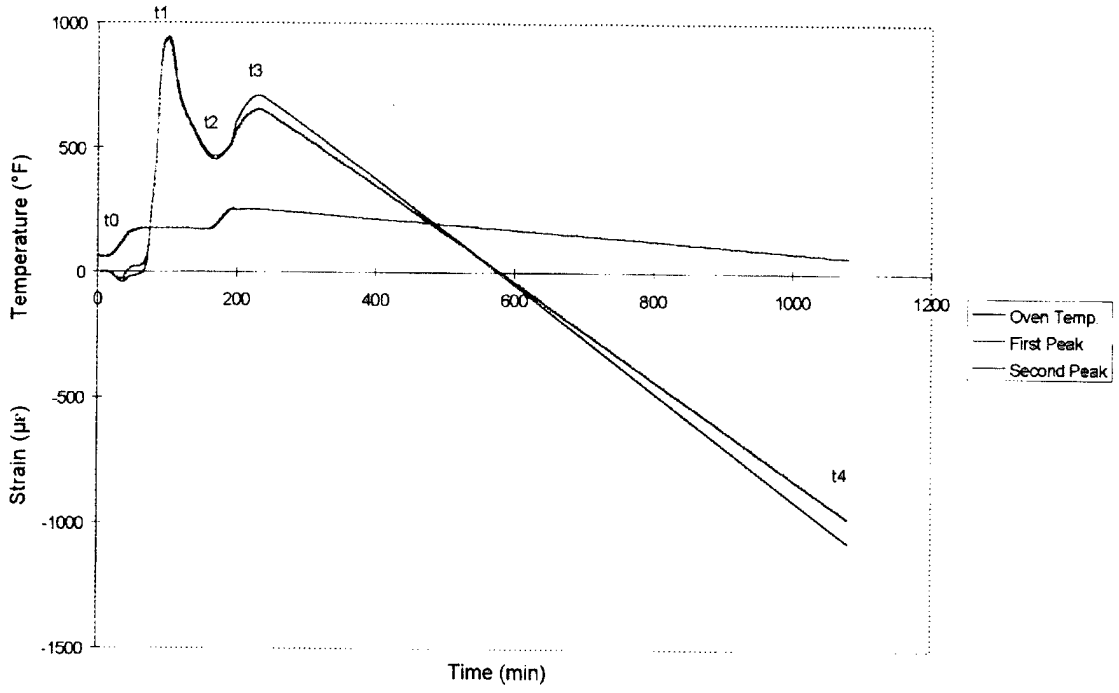

Figure 17. Optical Fiber Strain Midplane Sensor Panel No. 2.

ramps to 250 °F at about 162 min, cure is complete and post cure begins. At this point, another peak is seen due to the thermal expansion in the panel and sensor as the temperature goes up, giving a higher positive reading. The sensor data were taken for approximately 250 min into the cycle. The next morning, at about 1,080 min, the sensor data was taken again to measure the wavelength change at room temperature. This reading allowed calculation of a residual stress of 1,020 με in the sensor embedded in the center of the panel. As in the first panel, this final spectrum shows a wider bandwidth with two additional peaks indicating the presence of strains along the grating.

Figure 18 is a plot of the strain-vs.-time data taken from the Bragg grating embedded four plies deep from the tool surface. This sensor data was measured using the BRR-developed demodulator. The in-process cure data from this sensor were not as easy to interpret for this run. Interpretation of sensor output will be tied to modeling and simulation of the process in future work. The sensor indicates cross-linking at 90 min into processing, where the peak spikes and then goes down as compressive strains increase on the fiber. The 250 °F ramp temperature is also seen at approximately 162 min. This peak is achieved by expansion of the panel and sensor while the temperature goes up. The part then continues to cross-link and cure. The BRR demodulator results also appear to be shifted −400 με. As mentioned earlier, the spectrum analyzer was used to monitor the surface sensor before infusion and after cure on the surface sensor. Using this data, a residual stress of 1,000 με was measured in the panel.

FOCS Results

The FOCS data from cure of panel no. 2 tracked very well with the results from the Bragg grating sensor embedded at the midplane of the panel. Two bare 200-μm optical fibers (FOCS) were placed in the center of the ply pack so that their distil ends were side by side. One of the fibers was attached to the source, and the other was attached to the spectrometer. Transmission spectra of the resin system were taken at different times during the cure. These spectra data are recorded on disk and will be made available upon request.

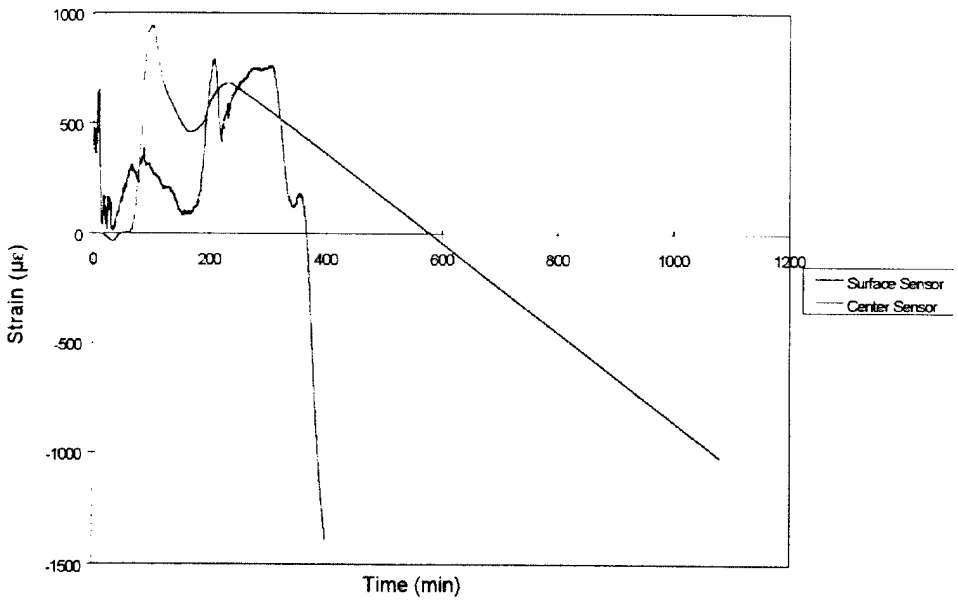

Figure 18. Fiber Strain vs. Time for Surface and Midplane Optical Fiber Panel No. 2.

Figure 19 is a plot of the summed counts for the 400–640-nm region (Table 2), which is the expected wavelengths for fluorescent radiation. The integrated counts over this wavelength region are directly proportional to the fluorescent radiation intensity. In Figure 19, the initial intensity decline is caused by the reduced viscosity of the resin mix produced by the increase in temperature. Then the fluorescent intensity increases as a result of some polymerization or gelation. A gel time between 78 and 88 min provides the most intense fluorescence, indicating the most rapid resin cure. The decline in fluorescent intensity after 88 min represents additional cure produced by additional heating and includes the "inner filter effect," which is caused by the absorption of the fluorescent radiation by the cured resin. The fluorescent radiation absorption increases with the amount of additional cured resin. The conclusions from Figure 19 concerning the time for gel are corroborated by examining the maximum intensity curve given in Figure 20.

5.3 Fabrication of Test Panel No. 3. As described in section 4.1, panel no. 3 is composed of a vinylester resin system and fiberglass cloth (with stitching). The mixture of components was designed to minimize residual stresses in the panel. The resin was mixed and infused at room temperature, since vinylesters generate their own exotherm to react. This panel took approximately 10 min to infuse. However, it did not react and exotherm as we expected. Since

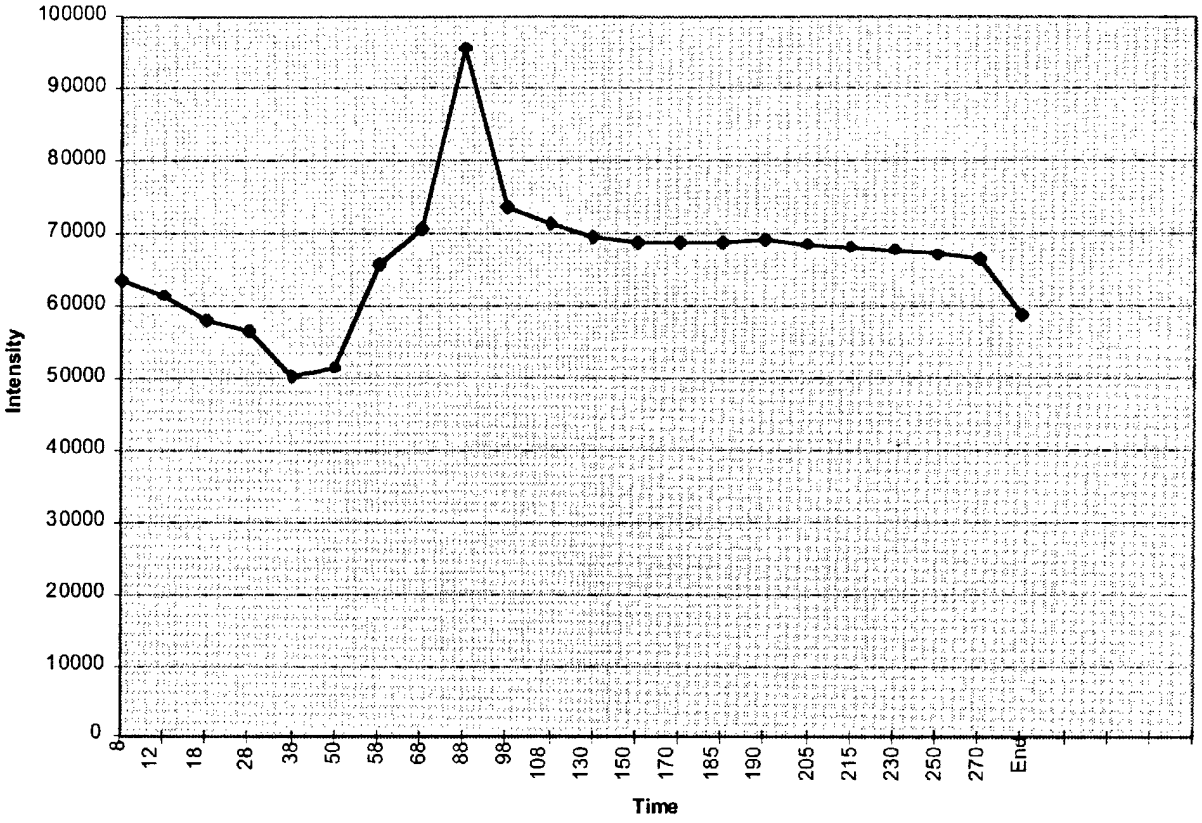

Figure 19. Panel No. 2 Fluorescence Optrode Data.

Table 2. Integrated Counts as a Function of Time for the 400–640-nm Region

Panel No. 2			
Time (min)	Counts	Time (min)	Counts
1	554,338	108	71,382
8	63,451	130	69,406
12	61,481	150	68,763
18	57,916	170	68,701
28	56,490	185	68,798
38	50,109	190	68,995
50	51,397	205	68,516
58	65,834	215	68,096
68	70,555	230	67,747
78	56,020	250	67,082
88	95,590	270	66,497
98	73,638	—	—

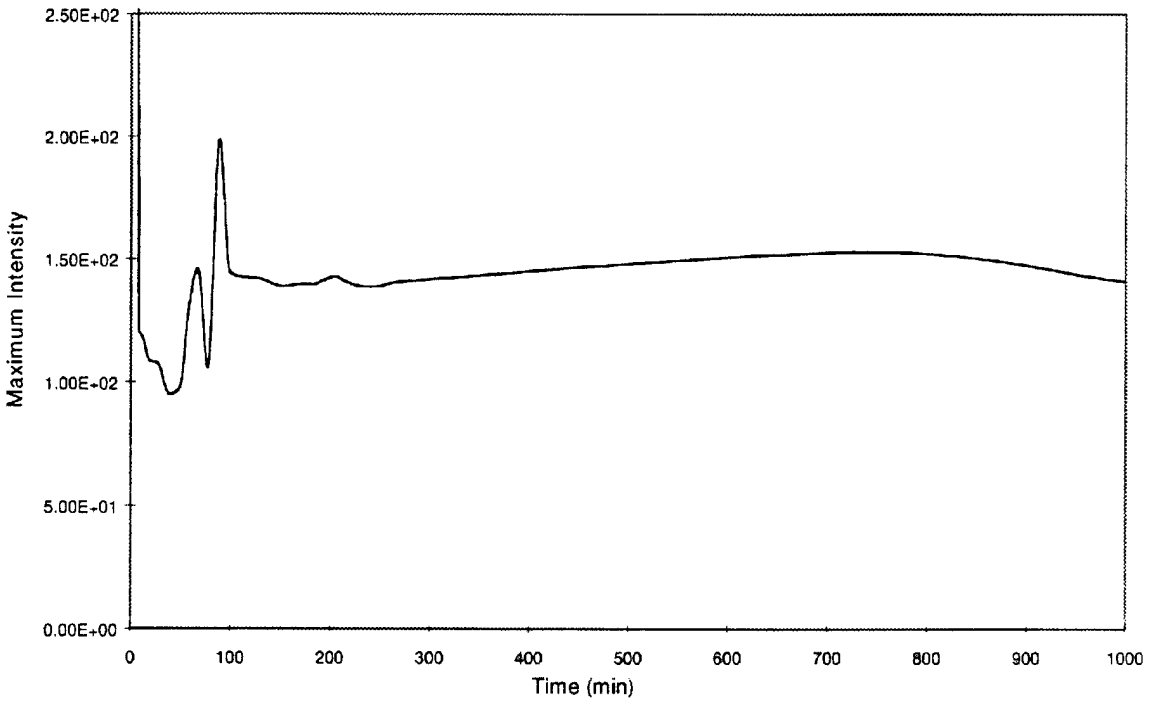

Figure 20. Fluorescence Optrode Maximum Intensity Panel No. 2.

it was approximately 45 °F in the plant, it was decided that the introduction of heat would help start the reaction; therefore, the oven was turned on at 125 °F. The panel finally exothermed in approximately 45 min (determined by examining the panel in the oven), at which time, the oven post cure cycle was started (ramp to 250 °F, hold for 2 hr, cool). The resultant panel was of less-than-expected quality, partially due to the excess air in the panel. The air is most likely caused by the lack of vacuum prior to exotherm. Also, air appears to be located around the Bragg grating sensor cables, indicating that the flexible tubing used to protect the sensor was not properly taped off during the infusion process.

Fiber Grating Results

Panel no. 3 contained two Bragg grating fiber optic sensors, and each sensor was monitored using a different demodulation technique. Once again, a three-axis fiber grating sensor consisting of a dual overlaid fiber grating at 1,300 and 1,550 nm written onto Fibercore polarization preserving fiber was embedded at the midplane of the panel, and the sensor four

plies from the tool surface was a single-element 1,300-nm fiber grating. The grating embedded at the midplane of the panel was interpreted by the optical spectrum analyzer, and the one embedded four plies deep from the tool surface was monitored by the BRR-developed demodulator. The BRR demodulator was set to take data for 300 min of the cure cycle. Therefore, the spectrum analyzer was hooked up to measure the sensor before infusion and after cure (cooled) to measure the residual strain in the panel near the surface of the tool. The following paragraphs describe the results of the data.

Panel no. 3 was an unusual panel for the Bragg grating sensor readings as well. As described previously, the mix ratio was selected to minimize residual stresses; however, an atypical reaction of the vinylester was seen—meaning that the typical hard cure of a vinylester, prior to increasing the oven temperature, was not achieved. The material did cure; it just did not undergo a violent exotherm, and there was very little net wavelength shift in the sensors during the cure.

Figure 21 is a plot of the spectral data from the sensor embedded at the midplane of the panel. The plot shows the dual peaks for the two wavelengths. Figure 22 is a plot of the strain on the sensor vs. time into cure; the two wavelengths overlaid on the sensor are shown. This figure was generated from the spectral data in Figure 21. According to these figures, the maximum strain peak is seen at about 86 min into the cycle, corresponding with the increase in oven temperature to 250 °F. The peak then slopes downward, indicating cross-linking in the panel applying a compression strain on the sensor. As the curve levels out, cross-linking is completed and the post cure is finished. At this time, the panel is cooled. The resulting residual stress in the panel, taken the next morning at room temperature, is 706 με.

Figure 23 is a plot of the strain-vs.-time data taken of the Bragg grating embedded four plies deep from the tool surface. The sensor data were measured using the BRR-developed demodulator. Comparing Figures 22 and 23, it appears that the surface and center sensors follow the same trend. The resulting residual stress is 1,000 με.

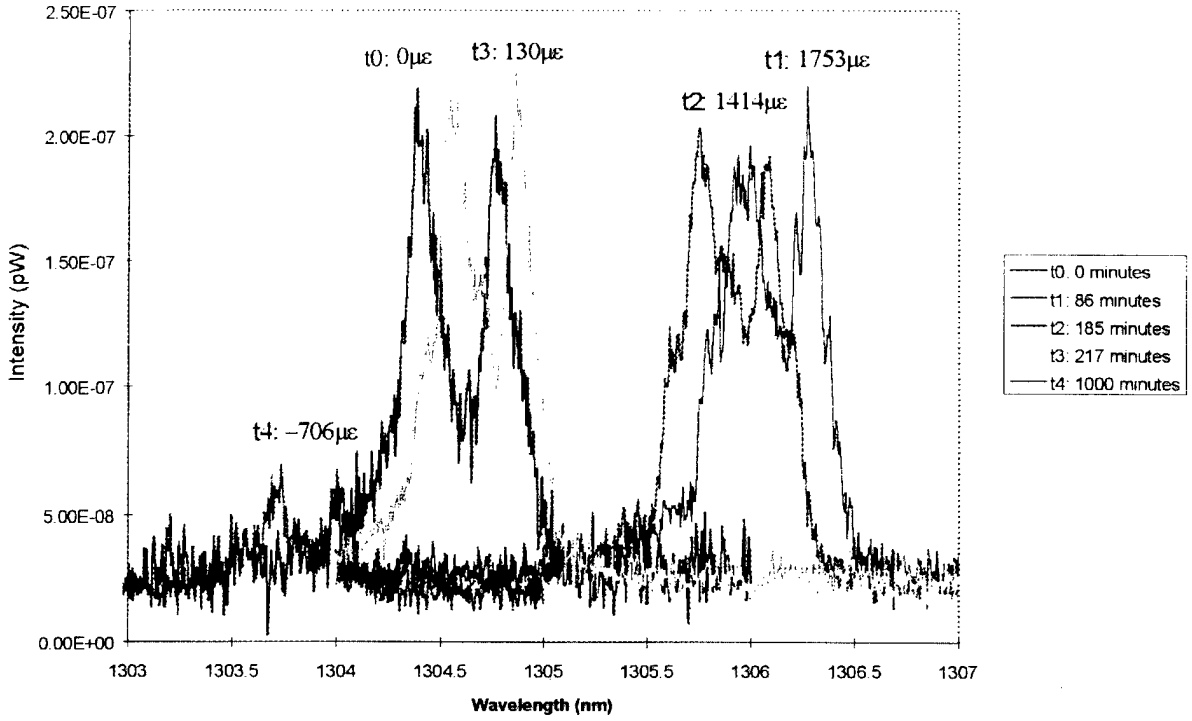

Figure 21. Spectra for Midplane Optical Fiber on Panel No. 3.

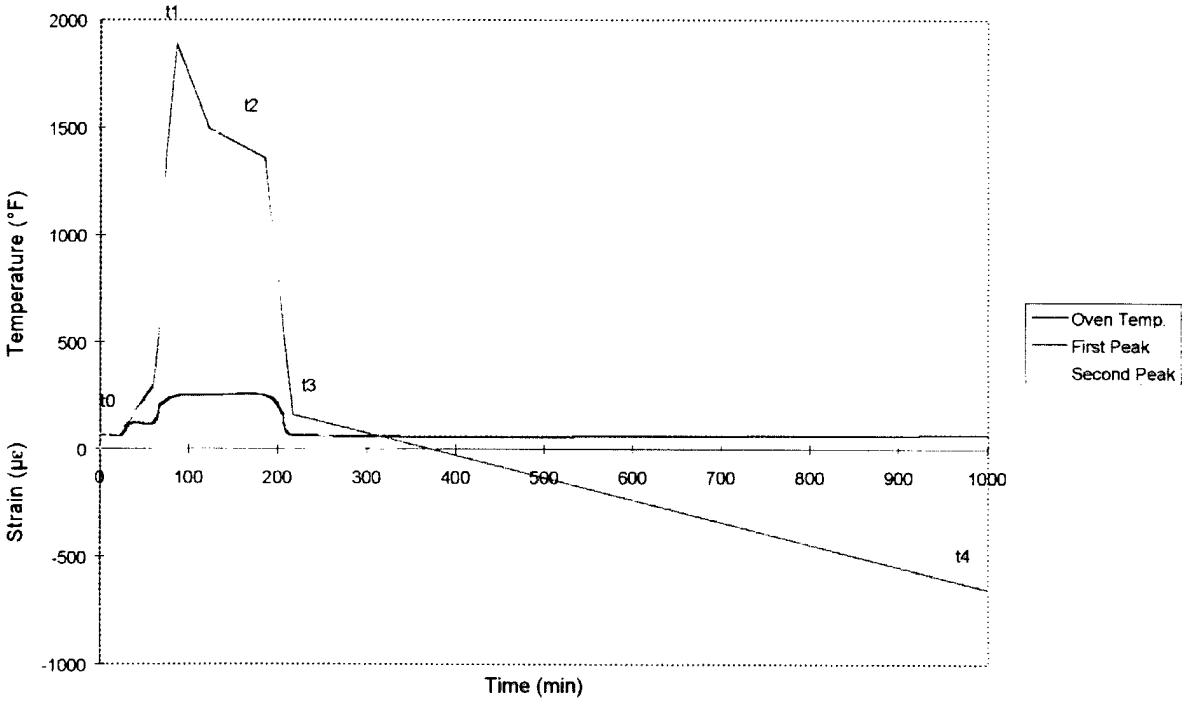

Figure 22. Optical Fiber Strain Midplane Sensor Panel No. 3.

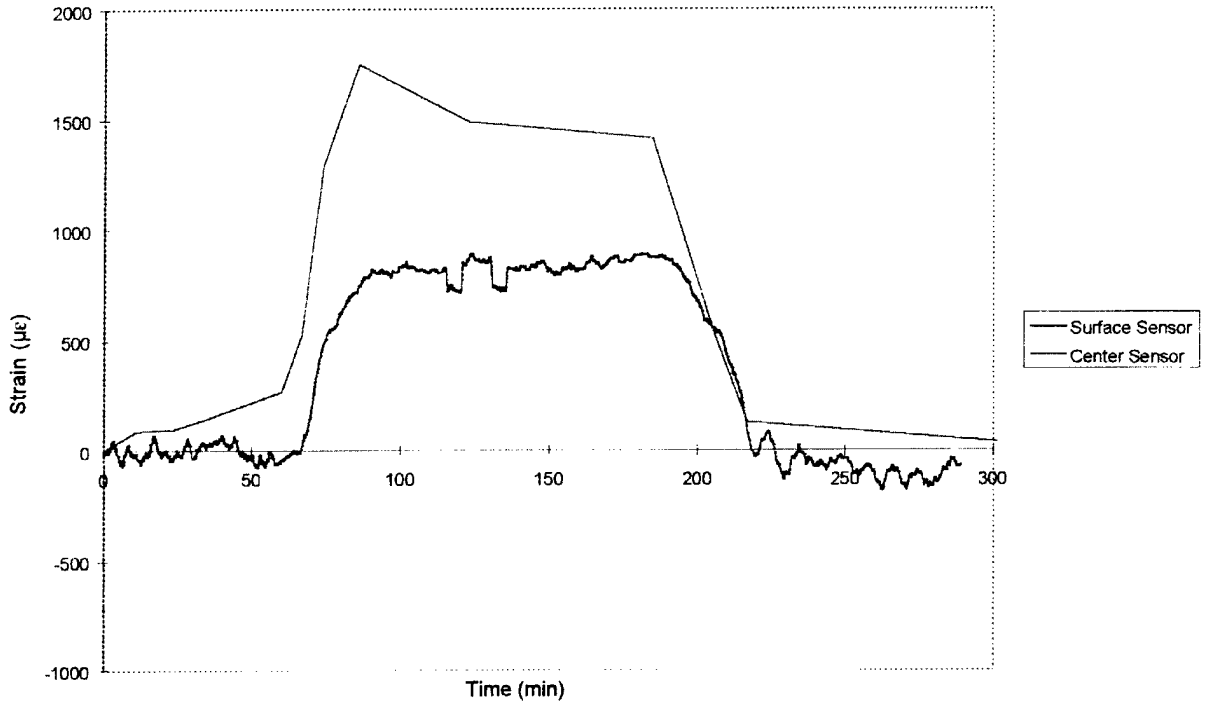

Figure 23. Fiber Strain vs. Time for Surface and Midplane Optical Fiber Panel No. 3.

5.4 Fabrication of Test Panel No. 4. As described in section 4.1, panel no. 4 is composed of a vinylester resin system and fiberglass cloth (without stitching). The mixture of components was designed to maximize residual stresses in the panel. The resin was mixed and infused at room temperature, since vinylesters generate their own exotherm to react. The tool was preheated to about 80 °F prior to infusion to avoid the cool down of the resin, and slow down of the reaction, that was experienced on panel no. 3. This panel took approximately 10 min to infuse, and it exothermed in 10 additional minutes (a more typical response for vinylesters). After exotherm, the oven cure cycle was started (ramp to 175 °F, hold for 1 hr, ramp to 250 °F, hold for 2 hr, cool rapidly).

Fiber Grating Results

Panel no. 4 contained two single-element 1,300-nm Bragg grating fiber optic sensors, and each sensor was monitored using a different demodulation technique. The sensor embedded at

the midplane of the panel was interpreted by the optical spectrum analyzer, and the one embedded four plies deep from the tool surface was monitored by the BRR-developed demodulator. The BRR demodulator was set to take data for 300 min of the cure cycle. Therefore, the spectrum analyzer was hooked up to measure the sensor before infusion and after cure (cooled) to measure the residual strain in the panel near the surface of the tool. The following paragraphs describe the results of the data.

This panel cured more typically for a vinylester resin, a distinct exotherm was achieved and the sensor was able to detect onset of cure. Figure 24 is a plot of the strain on the midplane sensor vs. time into cure. This figure was generated from the spectral data. On this panel, a thermocouple was mounted to the top of the panel throughout the cycle and these data are recorded on the charts. According to the sensor and thermocouple information, cure of the panel occurred at 30–35 min into the process. This is evident from the high wavelength shift and large peak shown in the figure and the exotherm temperature of 148 °F (measured by the thermocouple on top of the panel) realized prior to oven heat up. After exotherm, the oven was heated to 175 °F, at which point the strain curve (and wavelength) shifts down because the resin is shrinking and completing the cross-linking. After the 1 hr hold at 175 °F, a post cure of 250 °F was implemented for 2 hr, indicated by the second peak where the panel was expanding, until 200 min when cool down was started. The final spectral measurement taken when the part was completely cooled gave a wavelength of 1303.4 nm. Comparing this with the before infusion measurement of 1304.4 nm indicates a shift of 1.0 nm and a residual stress of 1,000 $\mu\varepsilon$.

Figure 25 is a plot of the strain-vs.-time data taken of the Bragg grating embedded four plies deep from the tool surface. The sensor data were measured using the BRR-developed demodulator. Data were not recorded during the infusion and initial part of the cure cycle. Comparing Figures 24 and 25, it appears that the surface and center sensors follow the same trend along the cure cycle of the process; however, the surface sensor sees slightly lower strain levels.

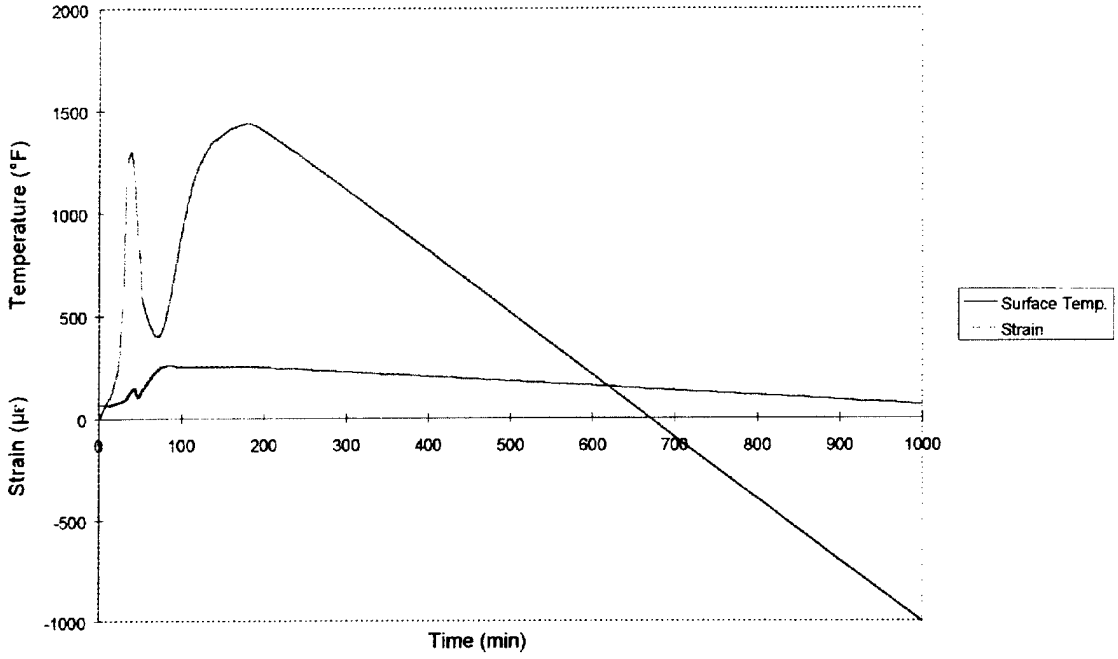

Figure 24. Optical Fiber Strain Midplane Sensor Panel No. 4.

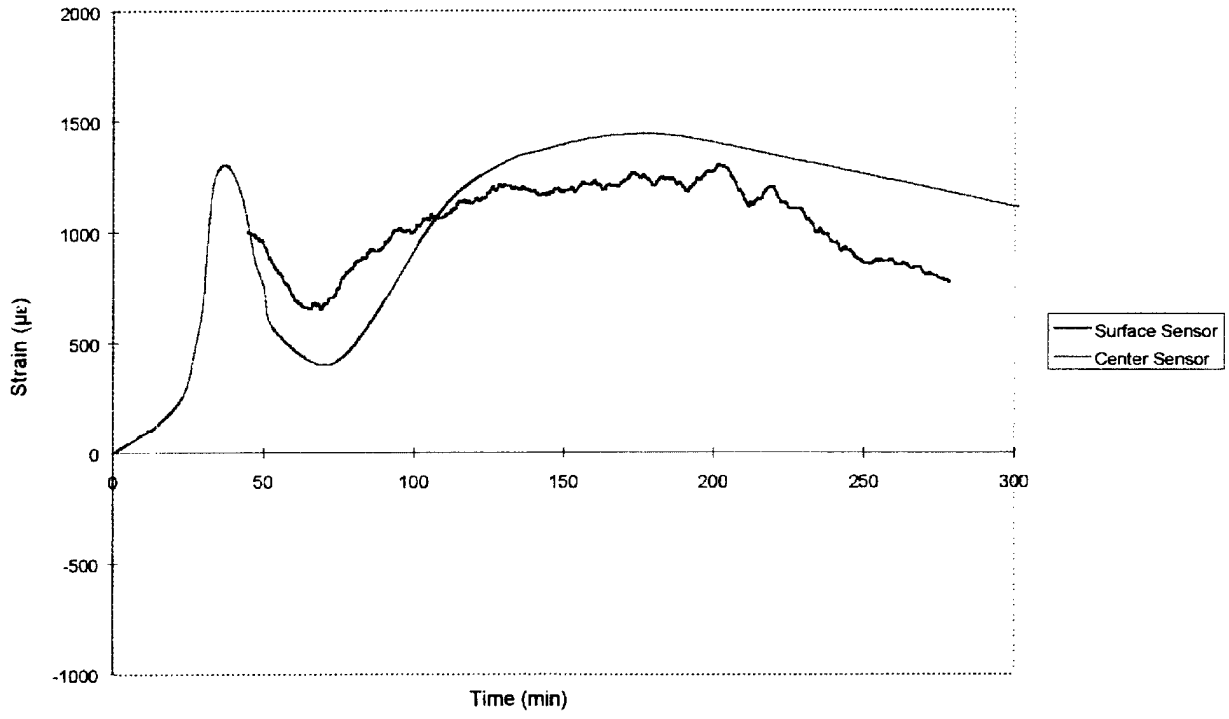

Figure 25. Optical Fiber Strain Surface Sensor Panel No. 4.

FOCS Results

The FOCS data from the cure of panel no. 4 tracked fairly well with the results of the Bragg grating sensor data embedded at the midplane of the panel. The intensity of the data is much less than that taken for the epoxy, indicating that vinylesters do not fluoresce as well as epoxies. Two bare 200-μm optical fibers (FOCS) were placed in the center of the ply pack so that their distil ends were side by side. The transmission spectra taken as a function of time and the intensity (in counts) as a function of wavelength and cure time are on disk and available upon request.

The summed counts representing the integration of the fluorescence intensity over the wavelengths 400–640 nm are plotted in Figure 26 (Table 3). Note that the fluorescent intensity of this resin is small compared to that of the epoxy used in panel no. 2.

Examination of Figure 26 indicates that the fluorescence increases immediately, suggesting that the resin begins to cure as it enters the vacuum bag. Gelation at the optical fiber ends began between 25 and 30 min. The decrease in fluorescence intensity after this gelation indicates emission absorption due to the 'inner filter effect' of the gel. With additional heating, further curing of the resin occurs as indicated by the increased fluorescence intensity. After 54 min, the polymer emission absorption (inner filter effect) predominates due to the accumulation of polymer at the optical fiber distil end. In Figure 27, the maximum fluorescence intensity corroborates the cited designation of the gel point for this resin.

A summary of the strain in the optical sensors after cool down of each panel is shown in Figure 28.

5.5 Recommendations for Sensing During Cure. During these tests, it has been shown that the embedded fiber gratings can be used to indicate temperature and strain internal to the part. It has also been shown that the fiber gratings can be used to determine the degree and onset of cure and that they can be used to measure strain gradients across the sensor. The three-axis

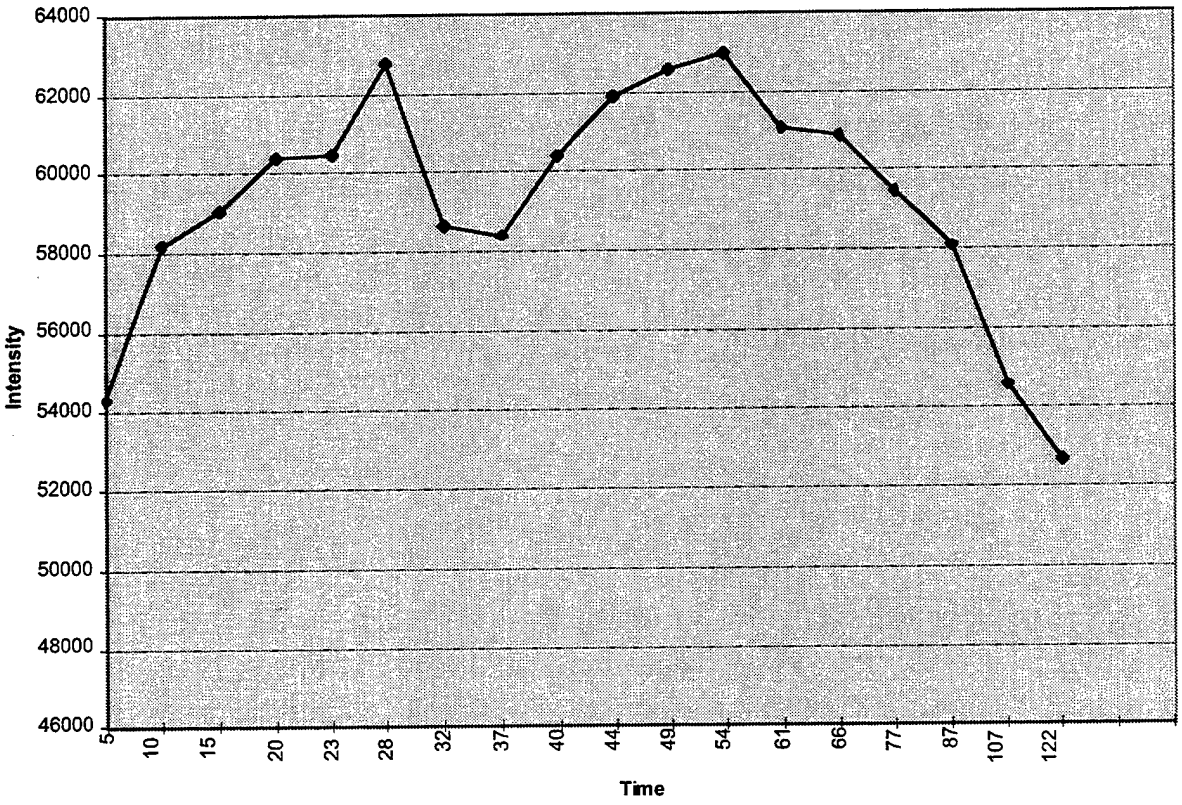

Figure 26. Panel No. 4 Fluorescence Optrode Data.

Table 3. Integrated Counts as a Function of Time for the 400–640-nm Region

Panel No. 4			
Time (min)	Counts	Time (min)	Counts
5	54,285	44	61,887
10	58,162	49	62,592
15	59,051	54	62,995
20	60,430	61	61,083
23	60,472	66	60,898
28	62,798	77	59,460
32	58,636	87	58,082
37	58,397	107	54,555
40	60,433	122	52,687

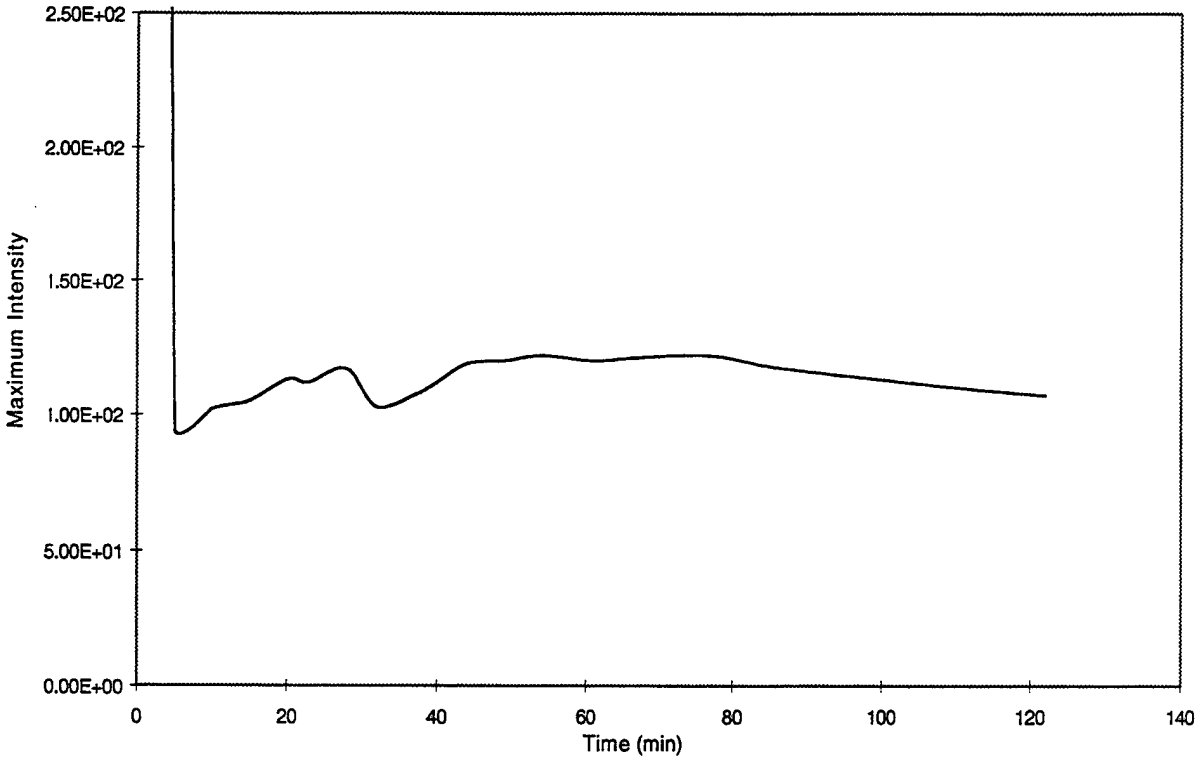

Figure 27. Fluorescence Optrode Maximum Intensity Panel No. 4.

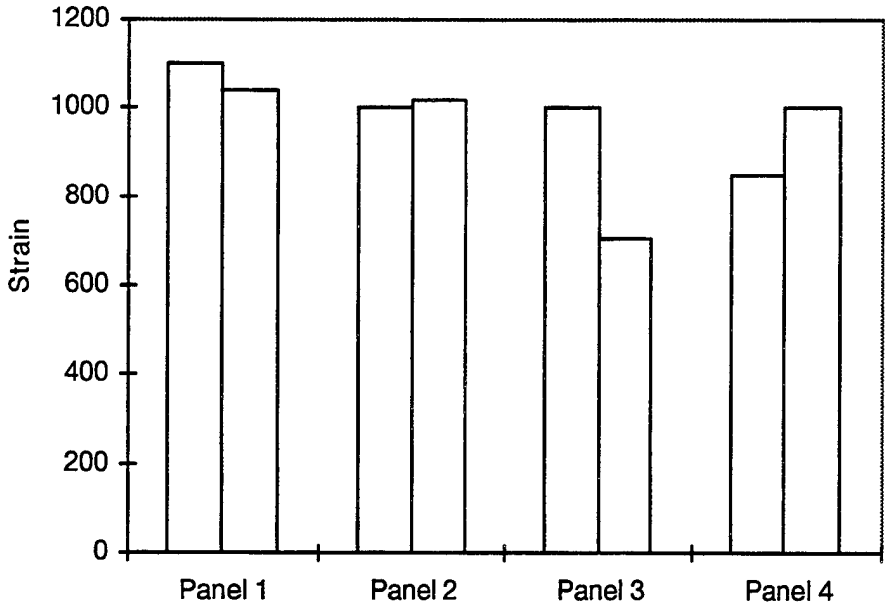

Figure 28. Optical Fiber Strain After Cool Down of Each Panel (Comparison of Surface on LHS and Center on RHS).

strain sensor in particular has been shown to have the potential to measure transverse strain gradients internal to the part. Furthermore, the fiber optic Bragg grating data have been verified by the FOCS, indicating that the cure of the part can be determined using both methods.

Coupling these new fiber optic sensing techniques with ARL modeling and simulation will provide scientific knowledge of the cure process, allowing optimization of the cure process, part quality improvements, and maximization of mechanical properties.

Bragg Grating Recommendations

One of the issues that must be addressed in the use of Bragg gratings for cure monitoring is the separation of temperature and strain measurements, and there are several ways to address temperature measurements using fiber optic grating sensors.

In the first case, which was used because of resource limitations in Phase I, fiber gratings were embedded into the 1-in-thick panels and the internal temperature of the panels could be measured before gel occurred by noting the thermal expansion of the fiber gratings and the consequential shift toward longer wavelengths that can, in turn, be used to measure temperature. At the point that gel starts to occur, resin strain induces compression and causes temperature-induced wavelength shifts to be counterbalanced. This has the effect of slowing and reversing the trend from longer wavelength output toward shorter wavelengths and provides an accurate measurement of where gel occurs. After the gelling process occurs, the single-element fiber gratings are measuring resin strain superimposed on optical fiber temperature strain via changes in their overall wavelength. From changes in their overall profiles, strain gradients can be monitored as discussed in the earlier test results. These strain gradient changes are particularly interesting in the post cure phase.

Several approaches are recommended to monitor strain and temperature simultaneously internal to the part. The first approach devised by BRR and PPMS involves writing two fiber gratings, one of which is encapsulated into a buffer tube, such as that used for strain relief for

ingress/egress so that it is free from strain. This is done by putting a connector on one end of the tube and sealing the other end of the tube with epoxy. A second fiber grating used to measure both strain and temperature is then placed in the part in a manner similar to that used during this effort. This approach offers the prospect of high accuracy strain and temperature measurements internal to the part and allows the use of fiber grating demodulator systems already developed, available, and tested by BRR.

The second approach uses dual overlaid fiber gratings of sufficiently different wavelength so that strain and temperature can be measured simultaneously. For good resolution, this involves using widely spaced wavelengths and would mean the development of improved demodulation designs. The approach is straightforward using existing BRR hardware. Additional testing would have to be performed to determine the accuracy of the temperature and strain measurements using this system. It is anticipated that the resolution of these devices would be somewhat less than the separated fiber grating approach but it would offer single point strain and temperature sensing.

The third approach would seek to leverage strongly off the BRR, NASA Phase II contract, Single Point Three-Axis Strain and Temperature Fiber Grating Sensor. This approach offers the prospect of transverse as well as longitudinal strain sensing as well as temperature measurements. Because the fiber grating sensors being developed under this program are experimental, the accuracy of the three-axis strain and temperature measurement with each fiber type will need to be determined. The information that this approach has the prospect of delivering offers potential breakthroughs as it has not been previously available.

It is recommended that all three approaches to internal temperature and strain measurement be applied in future work. Combinations of these three techniques should also be explored. Especially interesting would be combining the three-axis strain sensing approach with a loose-tube single-element fiber grating sensor for higher accuracy temperature measurements.

FOCS Recommendations

For the FOCS, the following recommendations should be examined:

(1) Use natural fluorescence wherever possible (such as occurs with epoxies); add a small amount of fluorophore to the resin or use a disk of resin containing the fluorophore when the resin has little or no fluorescence (vinylesters).

(2) Embed the fiber or fibers in the ply pack wherever information is desired. Place a optical fiber thermometer at the distil end of the sensing fibers.

(3) Use a multimode optical fiber that has a diameter approximately equal to that of the glass fibers; if those fibers are less than 100 μm in diameter, then obtain a fiber where the core is 100-μm silica with the total diameter of 125 μm. The cladding should be a polymer having a low surface energy such as polyimide so that maximum bonding between it and the resin will occur.

(4) Use a single-line excitation source such as He-Cd laser or a source high in UV radiation plus a filter to remove all lines above 400 nm to obtain the maximum fluorescence intensity and combine it with band pass filters.

(5) Measure the total fluorescence intensity continuously with a charge coupled device when curing a laminate. Use AC or synchronous detection to increase the sensitivity.

(6) Examine the possible use of the evanescent wave for cure detection. With the use of this detector, it may be possible to have a single embedded fiber stretching across the laminate to monitor the cure at different locations. Such a detector can also monitor water/absorbate and aging characteristics of the laminate.

5.6 Differential Scanning Calorimetry (DSC) Data. Washington University ran DSC on a section of each of the four panels fabricated. Dr. John Kardos of Washington University reviewed the data and determined that the panels were fully cured since there is no evidence of a large exotherm during the test. The DSC plots are in Figures 29–32.

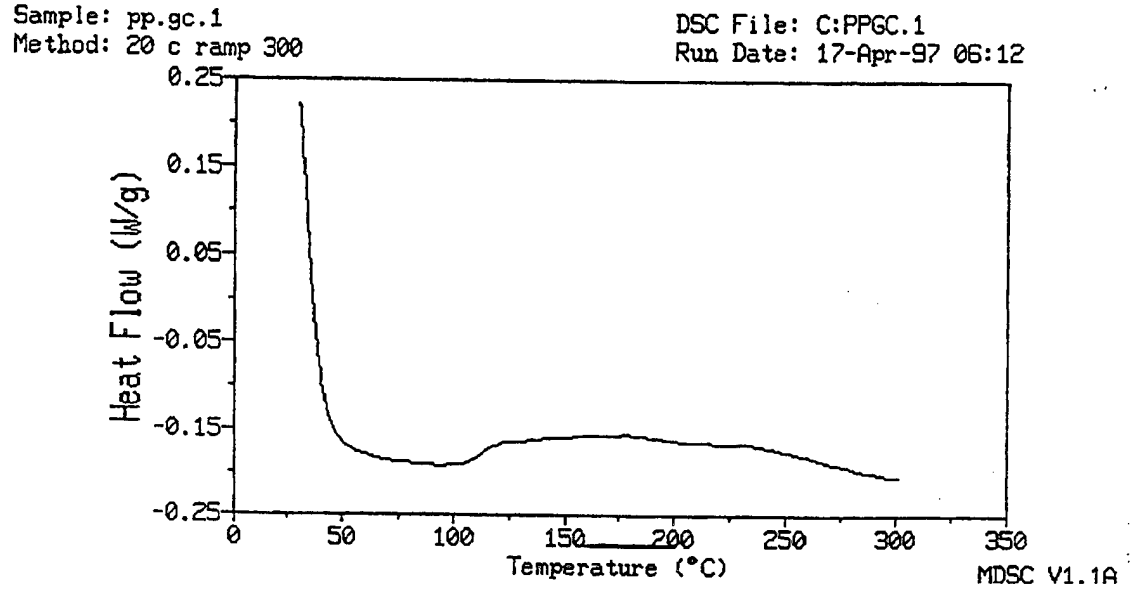

Figure 29. DSC Data for Panel No. 1.

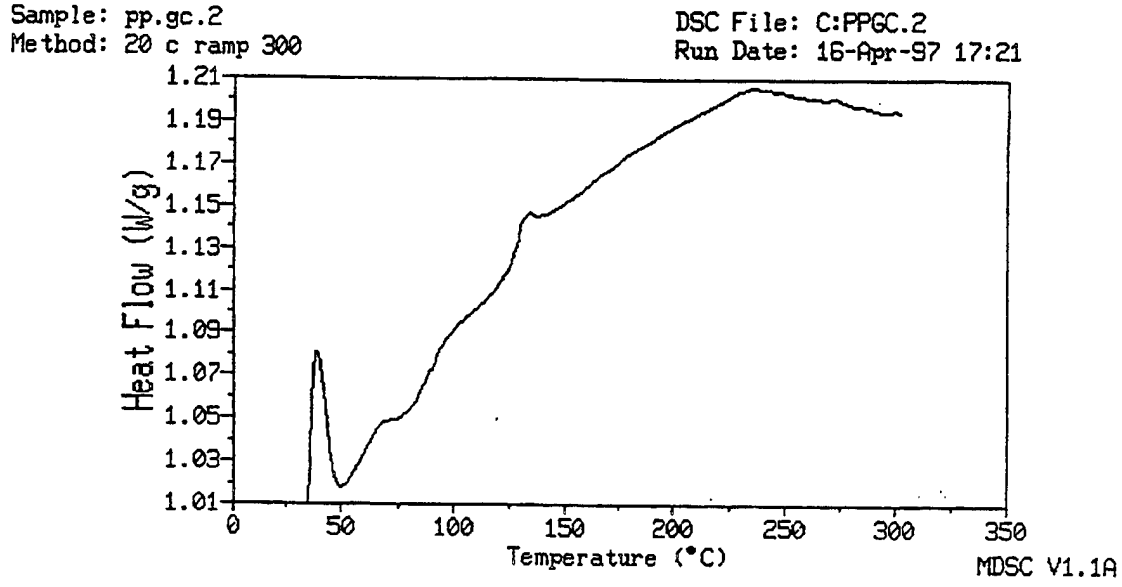

Figure 30. DSC Data for Panel No. 2.

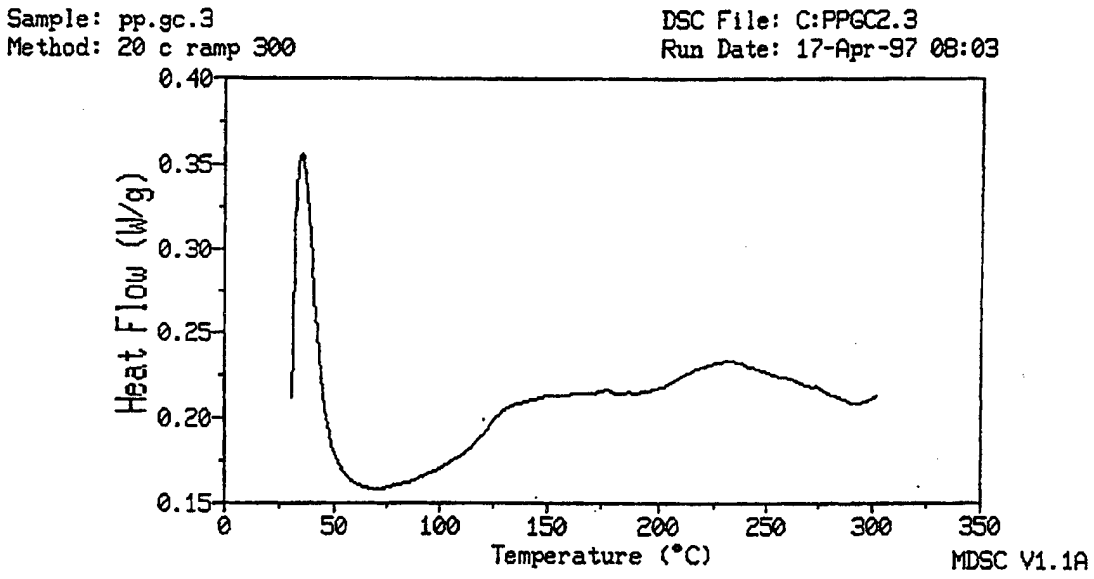

Figure 31. DSC Data for Panel No. 3.

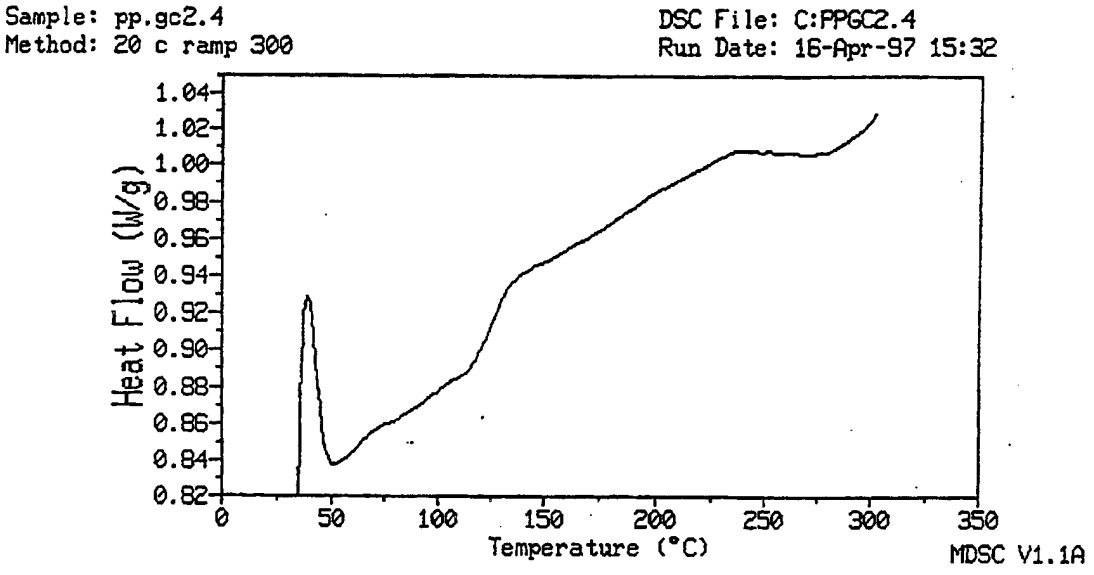

Figure 32. DSC Data for Panel No. 4.

6. Testing of Demonstration Articles

Representative results from selected flexural and impact tests performed on the composite panels are presented in the following section.

6.1 Four-Point Bend Testing.

Test Plan

Structural tests were performed on the four 24- × 12- × 1-in-thick panels. Panel nos. 1, 3, and 4 were initially proof-tested in four-point bending, as shown in Figure 33. Figure 34 shows a photograph of the overall bending test setup, with Figure 35 showing a closeup of a composite panel in the setup. A resistive strain gauge was bonded to the top of the panel near the surface optical fiber sensor. Two load cycles were applied. The spectrum analyzer read the center fiber, and the BRR demodulator read the surface sensor on the first cycle. The fibers were switched on the second cycle. The embedded optical fiber sensors, external resistive strain gauges, load cell, and panel displacement at the center were monitored throughout the test, and results were recorded. The specimen was loaded in increments of about 5,000 lb. The spectrum analyzer recorded the reflected spectrum during the hold at each increment.

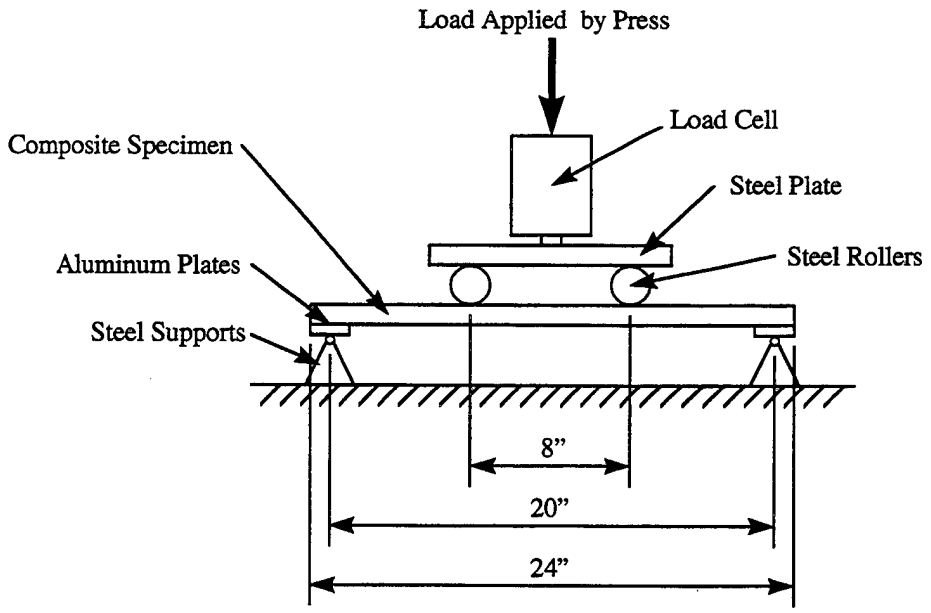

Figure 33. Four-Point Bending Test.

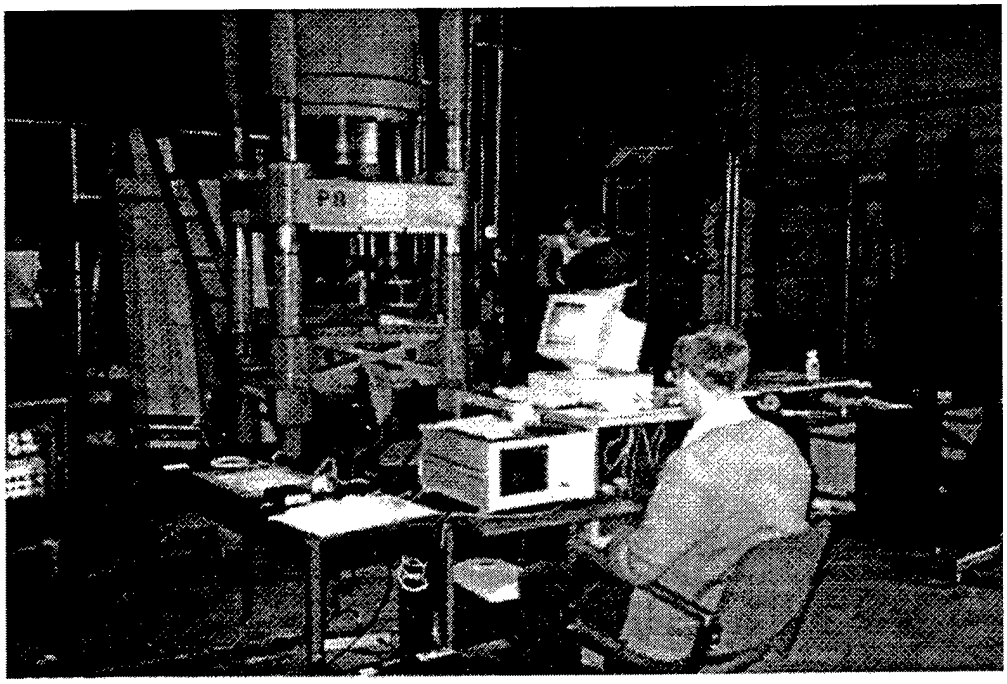

Figure 34. Four-Point Bending Setup.

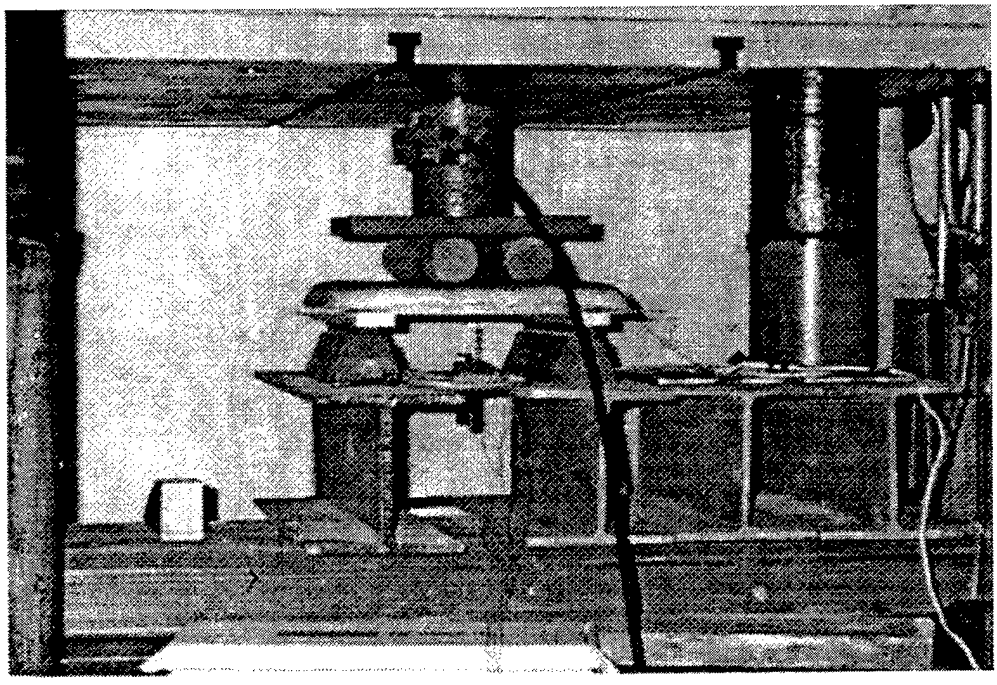

Figure 35. Closeup of Panel Loaded in Four-Point Bending Setup.

Test Results

Figure 36 is a plot of the load/deflection response during the proof test on panel no. 3. The response was linear with a maximum deflection of 0.65 in. The predicted displacement based on simple beam theory was 0.58 in. Small discontinuities in the curve were caused by holds during the loading cycle. The longest hold occurred at 5,000 lb while data was being recorded on the spectrum analyzer. Figure 37 shows the stress/strain plot for the resistive and surface optical fiber strain gauges during the first load cycle. The optical fiber sensor was read using the BRR demodulator. Stresses were estimated using beam theory accounting for the depth of the sensor. Figure 38 plots the spectra from the surface optical fiber gauge during the second load cycle at 0, 5,000, 10,000, and again at 0 lb. The peak shifts to the left under load, indicating compressive strain, as expected. The posttest spectrum is essentially identical to the pretest. The additional, smaller peaks on the spectra under load indicate strain gradients along the optical fiber.

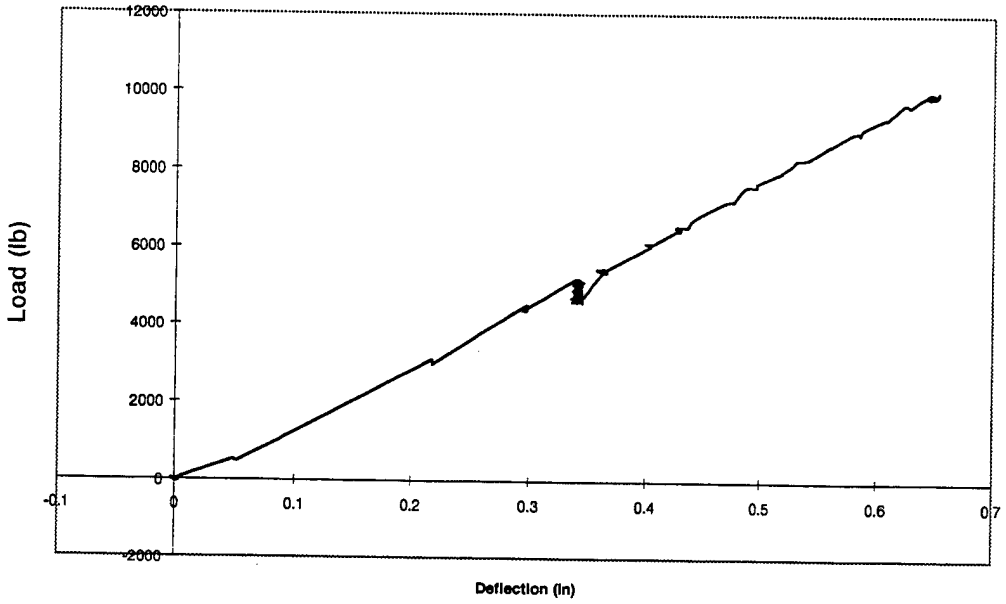

Figure 36. Load vs. Deflection During Four-Point Bend Test (Panel No. 3).

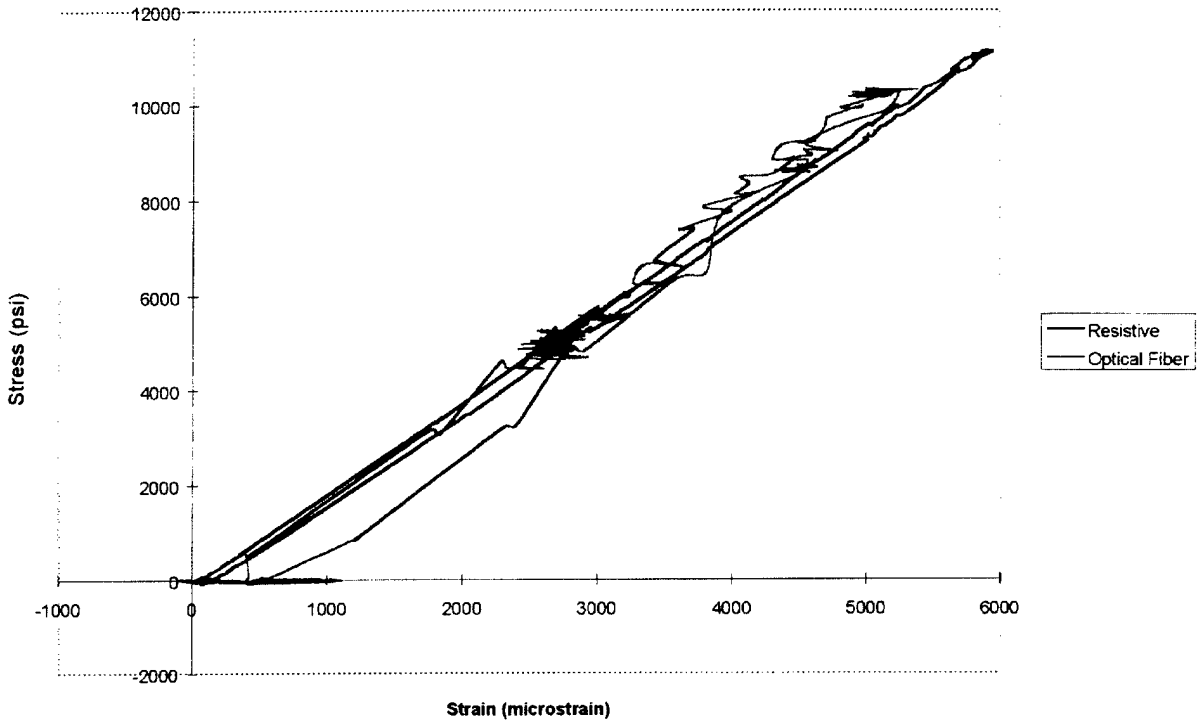

Figure 37. Stress vs. Strain Plot During Four-Point Bend Test (Panel No. 3).

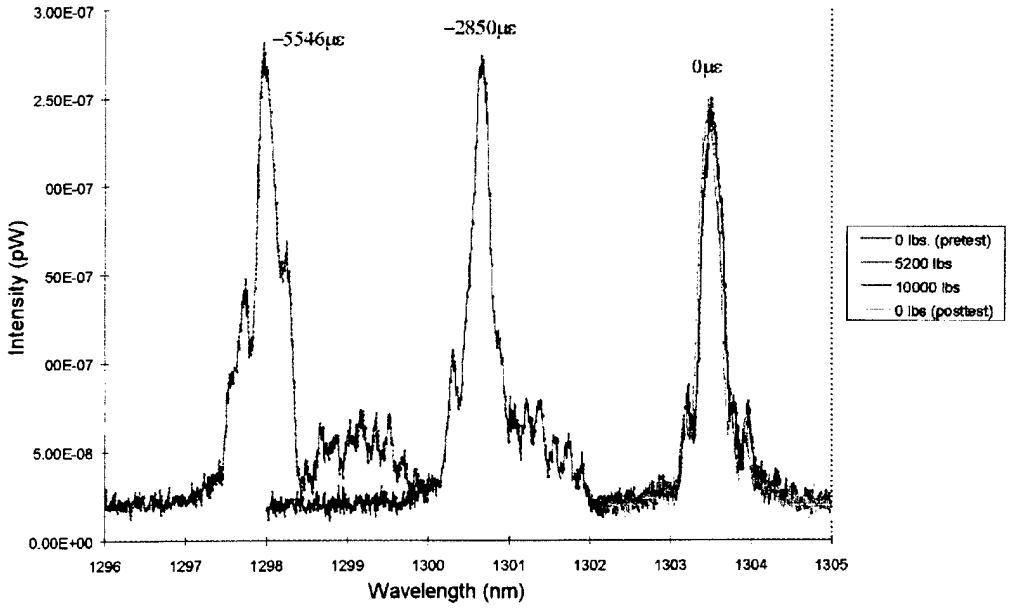

Figure 38. Surface Optical Fiber Spectrum During Various Four-Point Bend Loadings (Panel No. 3).

6.2 Impact Testing.

Test Plan

Impact tests were performed on the panels after the initial flexural test. Increasing levels of impact energy were applied as shown in Table 4. The impact test setup is shown in Figure 39. The surface-embedded optical fiber gauge, external strain gauge, and impactor acceleration were monitored and recorded at 2 kHz using the BRR demodulator during the dynamic events.

Table 4. Levels of Impact Energy

Test No.	Drop Height (in)	Energy (in-lb)
1	6	240
2	12	480
3	18	720
4	24	960
5	36	1,440
6	48	1,920
7	60	240
8	72	2,880
9	84	3,360
Impacter Weight = 40 lb		

Test Results

Plots of results from the impact tests on panel no. 2 are shown in Figures 40 and 41 for the 12-in drop. The results for the 84-in drop are shown in Figure 42. The negative of the resistive strain readings was plotted to improve readability. The 12-in test includes readings from the accelerometer attached to the impactor. These values were shifted and magnified to improve readability. The peak acceleration was about 25 g's. The accelerometer had a maximum range of 100 g's, so it was removed at higher impact energies. Minor damage in the form of surface delamination was observed at the high-impact energies. Figure 43 shows the chisel point impactor after impacting the composite panel, and Figure 44 shows a closeup of the surface

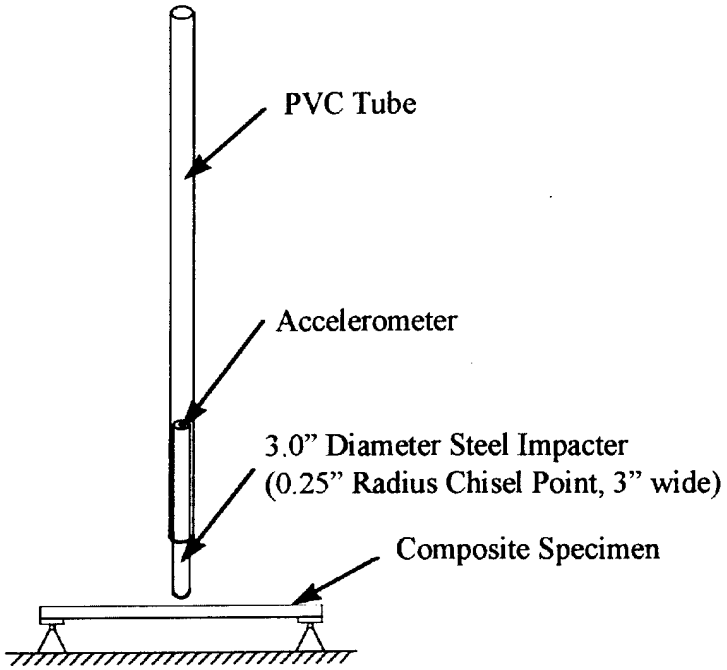

Figure 39. Impact Test Setup.

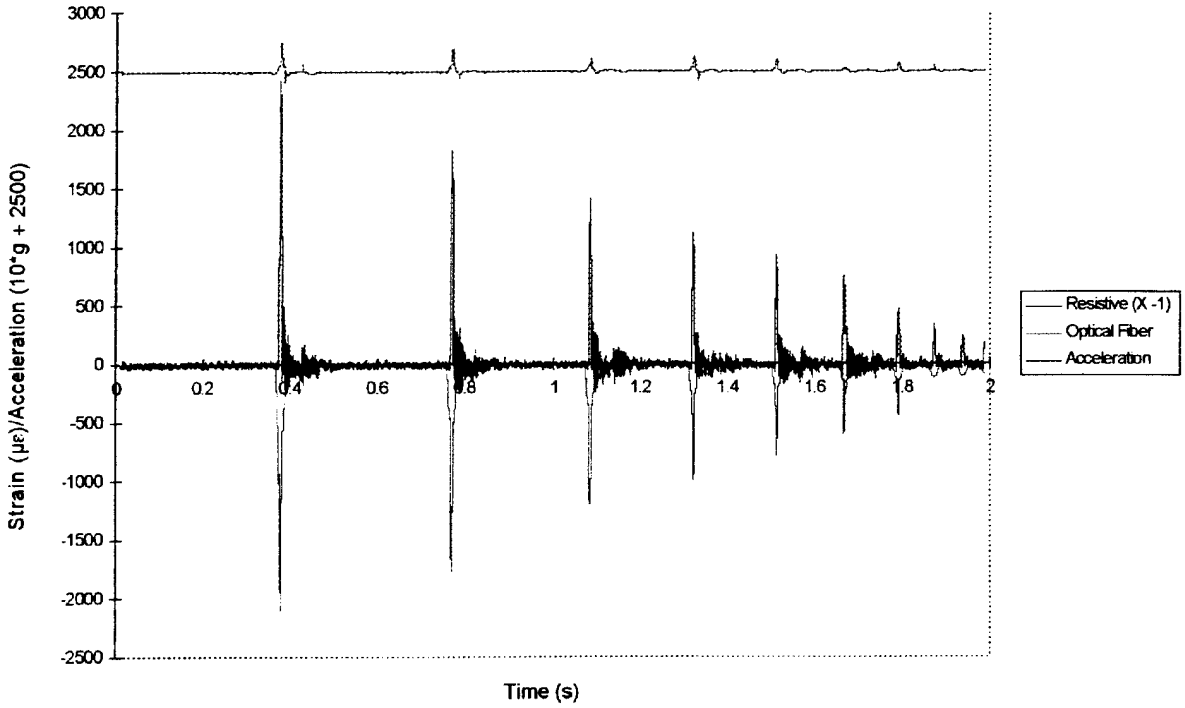

Figure 40. Impact Test Results (12-in Drop on Panel No. 2).

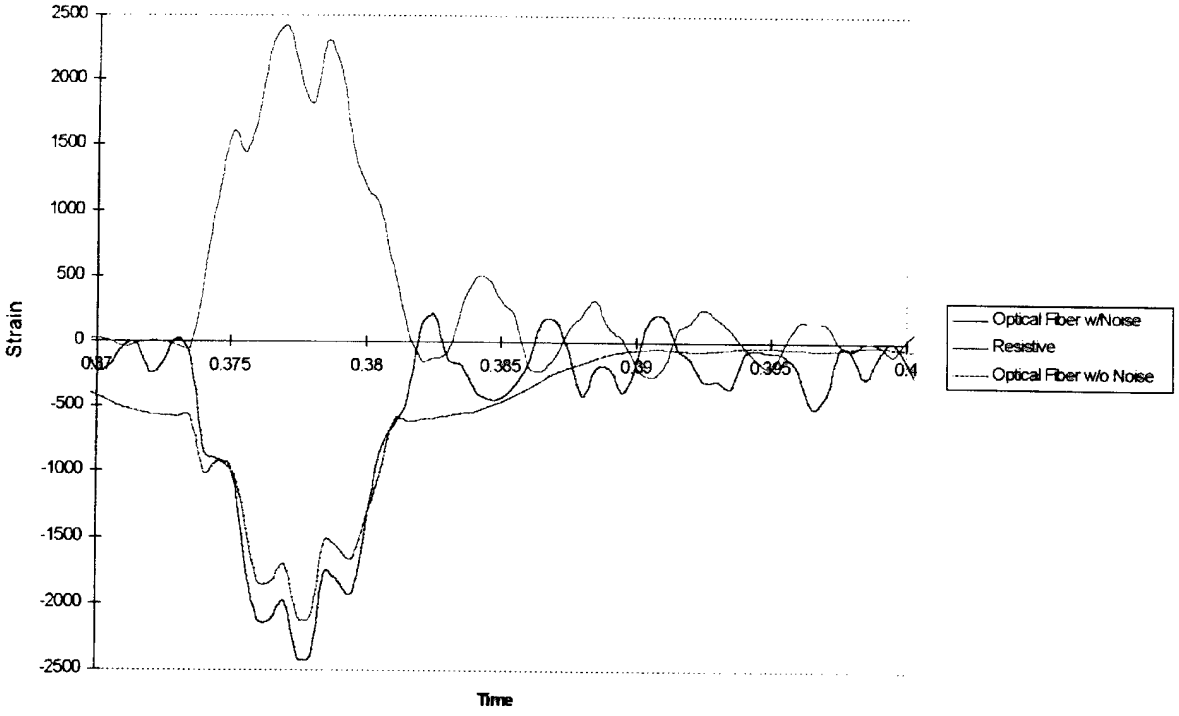

Figure 41. First Peak Magnification of 12-in Drop on Panel No. 2.

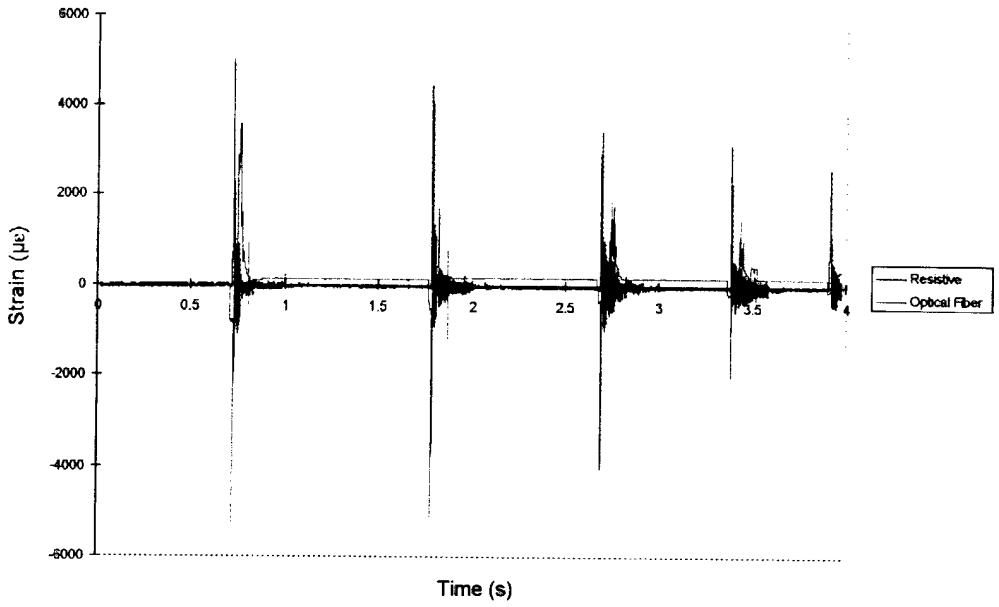

Figure 42. Impact Test Results (84-in Drop on Panel No. 2).

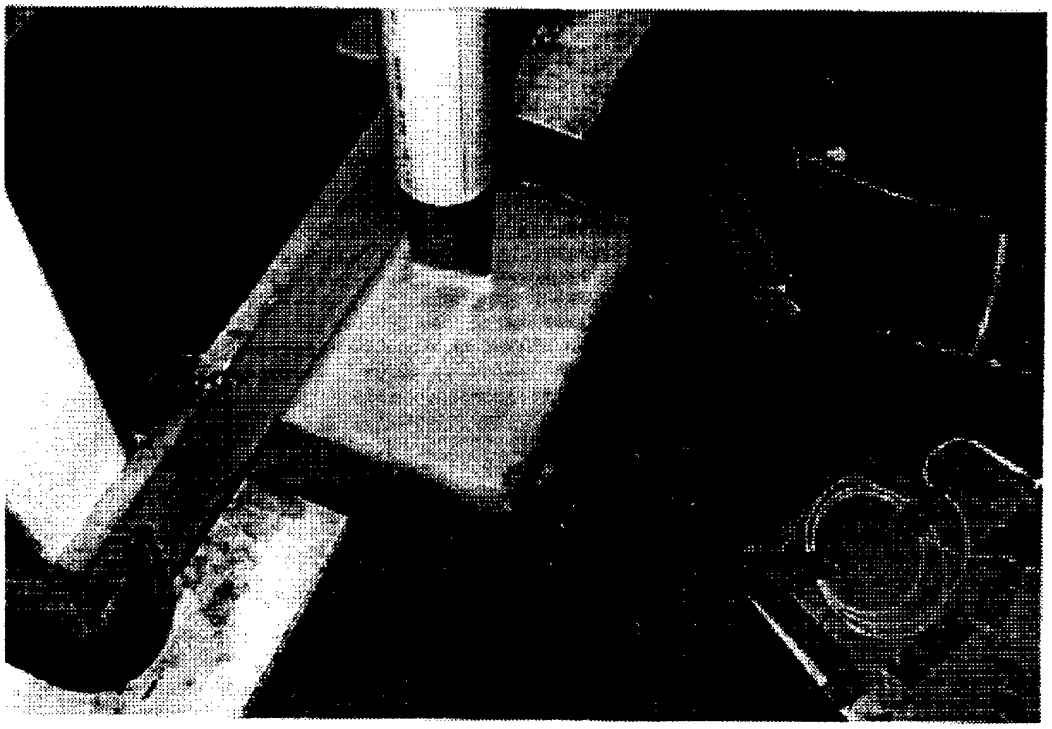

Figure 43. Chisel Point Impacting the Composite Panel.

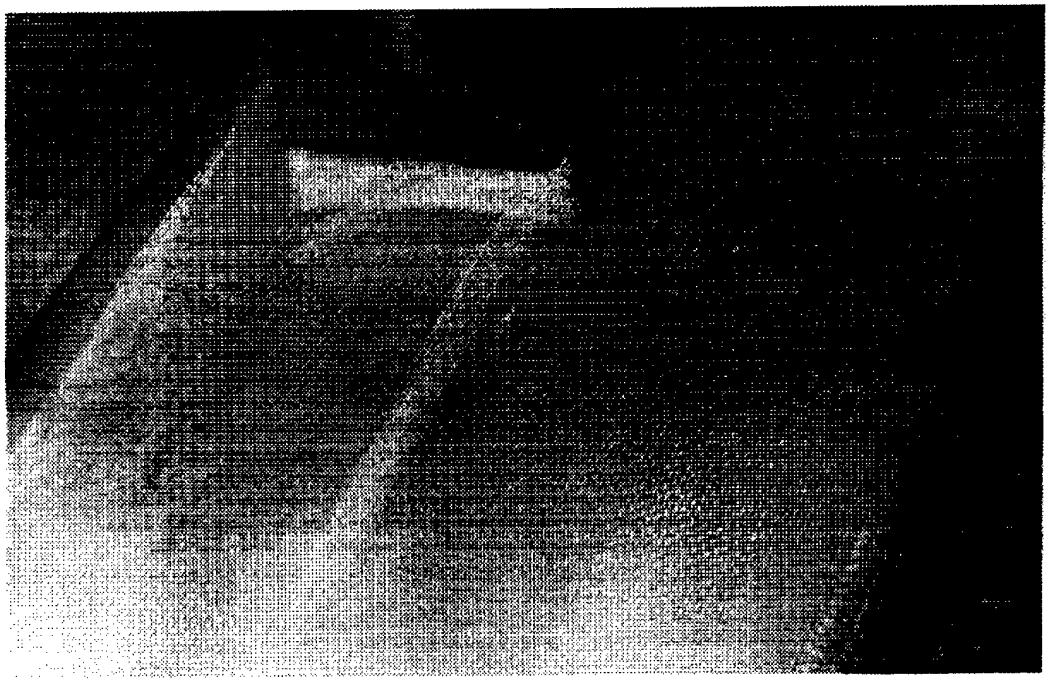

Figure 44. Closeup of Damage From Chisel Point.

damage. Optical fiber and resistive strain readings agree well at these high loading rates. The optical fiber strains tend to be about 10% lower than the resistive readings since they are embedded four plies below the surface.

Figure 41 shows a magnification of the response during the initial impact. Two plots of optical fiber output are shown. The first does not include averaging of low-level noise and used a less accurate fit to the spectral curve. The second plot attempts to clean up low-level noise by averaging but does not change the readings for the high strains. Residual vibration data indicate a natural period of about 0.004 s. This compares well with the natural frequency of a free-free beam with the properties of this panel.

6.3 Four-Point Bend Test After Impact.

Test Plan

The four panels were reloaded up to 20,000 lb or failure occurred (whichever comes first) in four-point bending after impact using the same procedure as in the initial flexure test previously described.

Test Results

Figure 45 shows panel no. 1 at 20,000 lb in the test machine. Results from the final test on panel no. 1 are shown in Figures 46 and 47. The load/deflection curve is linear up to the maximum load. The stress/strain curve for the resistive strain gauge is also linear. The strain gauge conditioner reached its maximum voltage output at about 7,200 $\mu\varepsilon$, so higher strains were not recorded electronically. The optical fiber strain began to decrease at stresses above 10 ksi, indicating possible nonlinear behavior near the embedded gauge.

The stitched, epoxy panel no. 2 failed during the proof test at 17,600 lb and a maximum compressive strain of 1.04%. Figure 48 is a picture of the failed panel no. 2. The failure in the

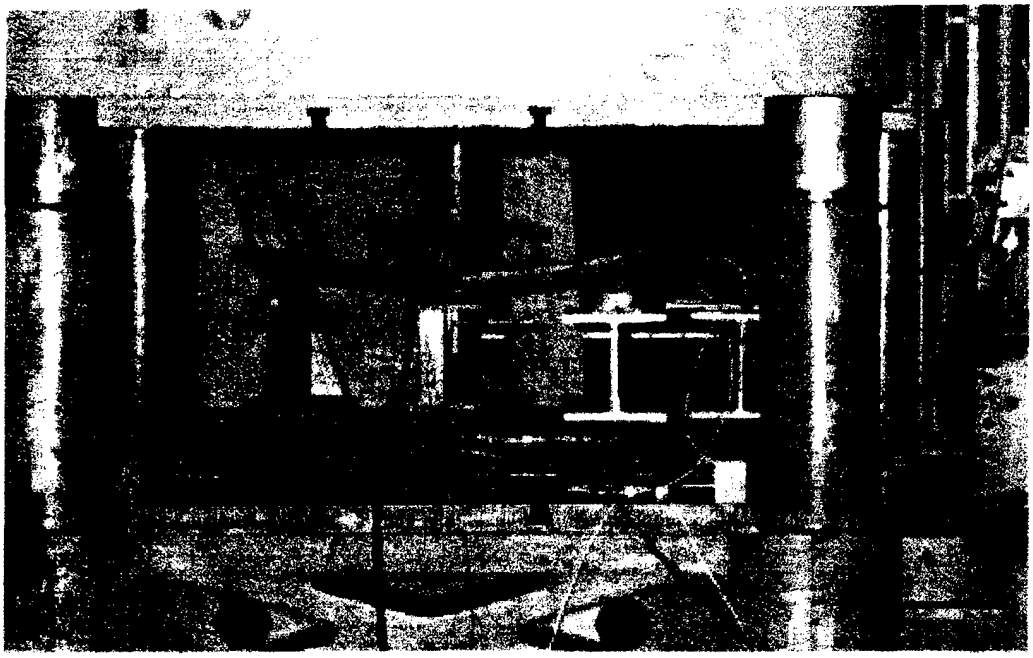

Figure 45. Panel No. 1 Loaded to 20,000 lb.

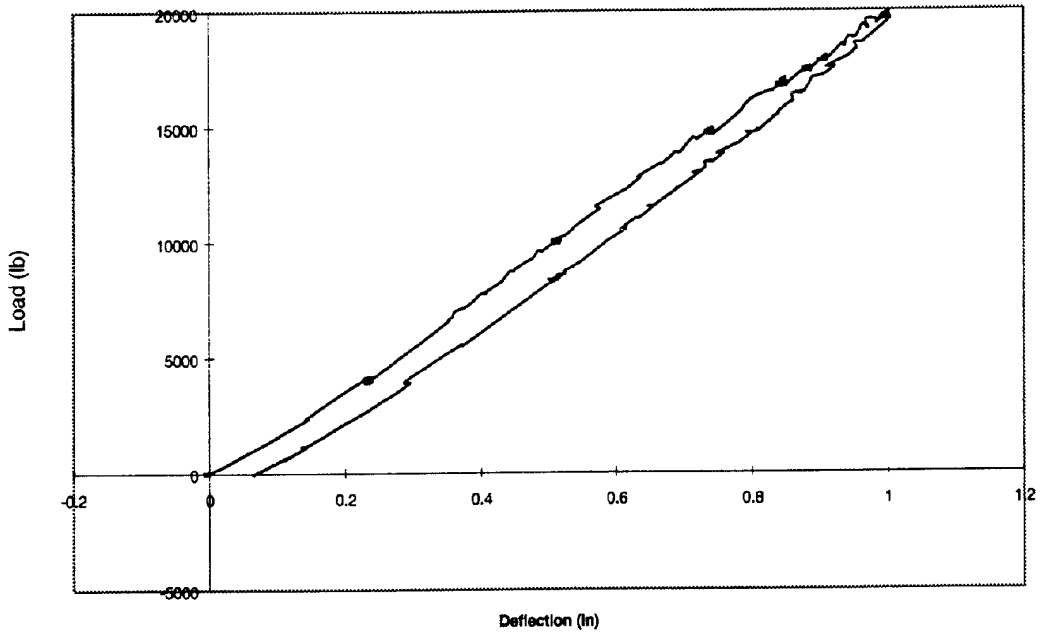

Figure 46. Panel No. 1 Load vs. Deflection During Four-Point Bend Test After Impact.

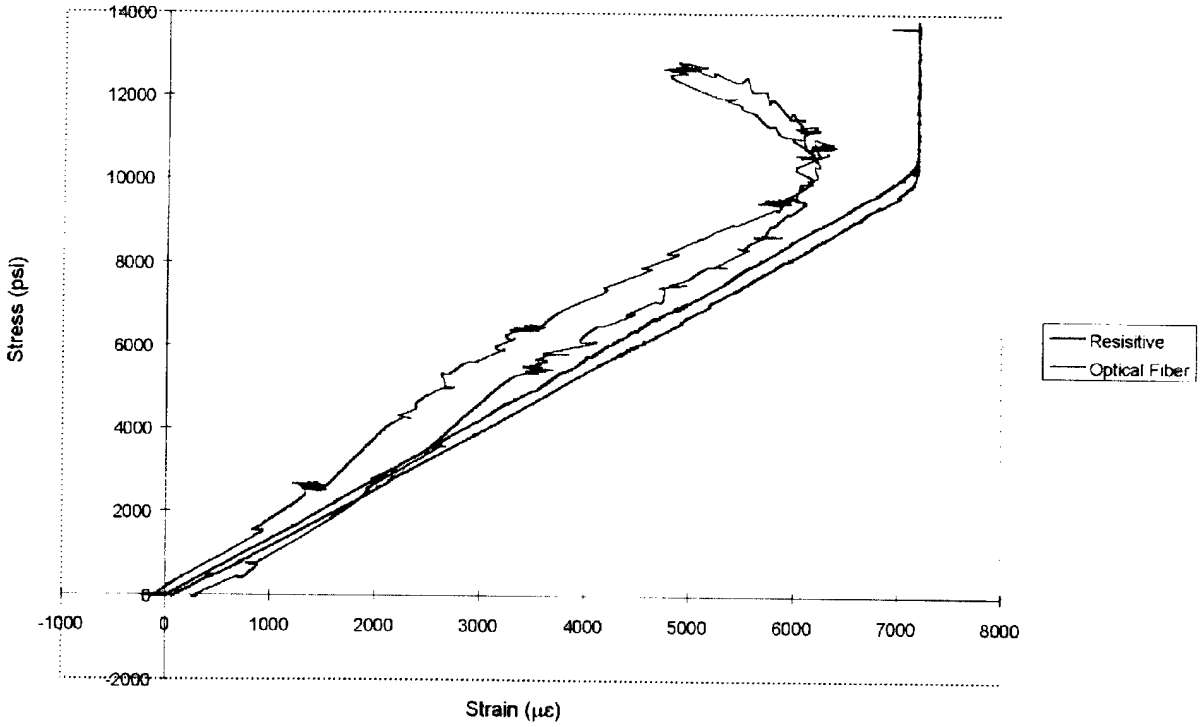

Figure 47. Panel No. 1 Stress vs. Strain During Four-Point Bend Test After Impact.

Figure 48. Failed Panel No. 2.

panel was along the stitch line. The stitching reduced the in-plane tension/compression strength of the E-glass, and impact damage also contributed to lower the strength of the panel compared to the nonstitched panels.

The stitched, vinylester panel no. 3 failed at 19,580 lb at a maximum compressive strain of 1.1% (Figure 49). Figure 50 shows the stress/strain response of panel no. 3 indicated by the resistive strain gauge before and after impact. These results indicate that the impact energy levels applied in the test program had little effect on overall structural stiffness and matched analytical predictions. Once again, the failure of the panel was along the stitch line. The unstitched panel nos. 1 and 4 did not fail at 20,000 lb.

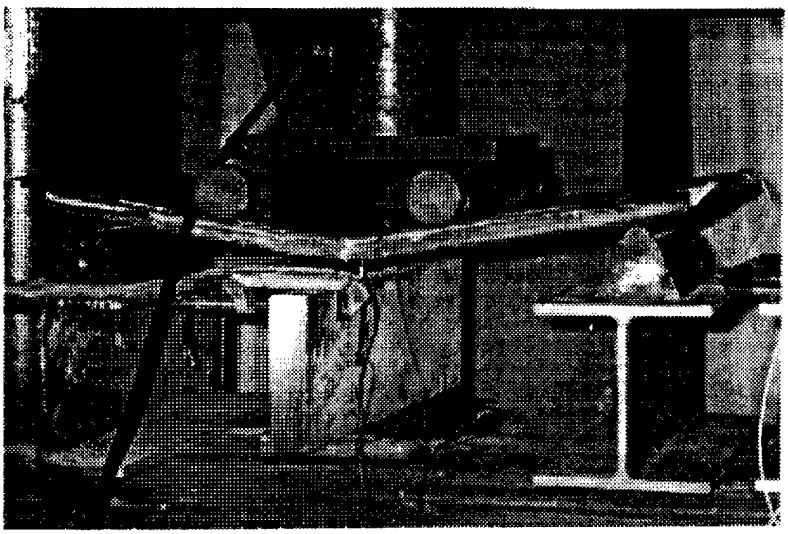

Figure 49. Failed Panel No. 3.

6.4 Ballistic Impact Testing. Panel no. 4 was rested against a backstop and struck by a .22-caliber rifle bullet fired from 20 ft. A .22 was used to create minimal damage (strain) and to see if we could measure the event. Figure 51 is a plot of strain vs. time for the test.

Figure 52 is a picture of the impacted panel, with initial impact on the right (4 in from sensor) and the two later impacts on the left, closer to the sensor (the resistive gauge is 1 in to the left of the left-hand upper impact and the fiber optic gauge is 2 in to the left of the lower

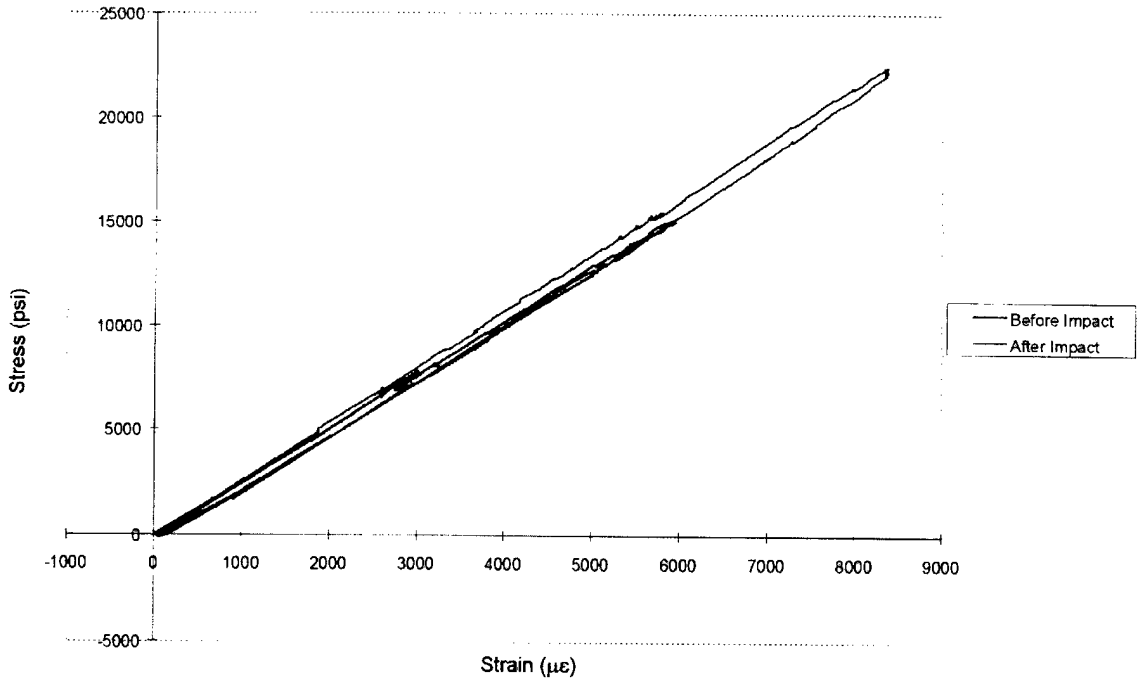

Figure 50. Stress/Strain Response of Panel No. 3 Before and After Impact.

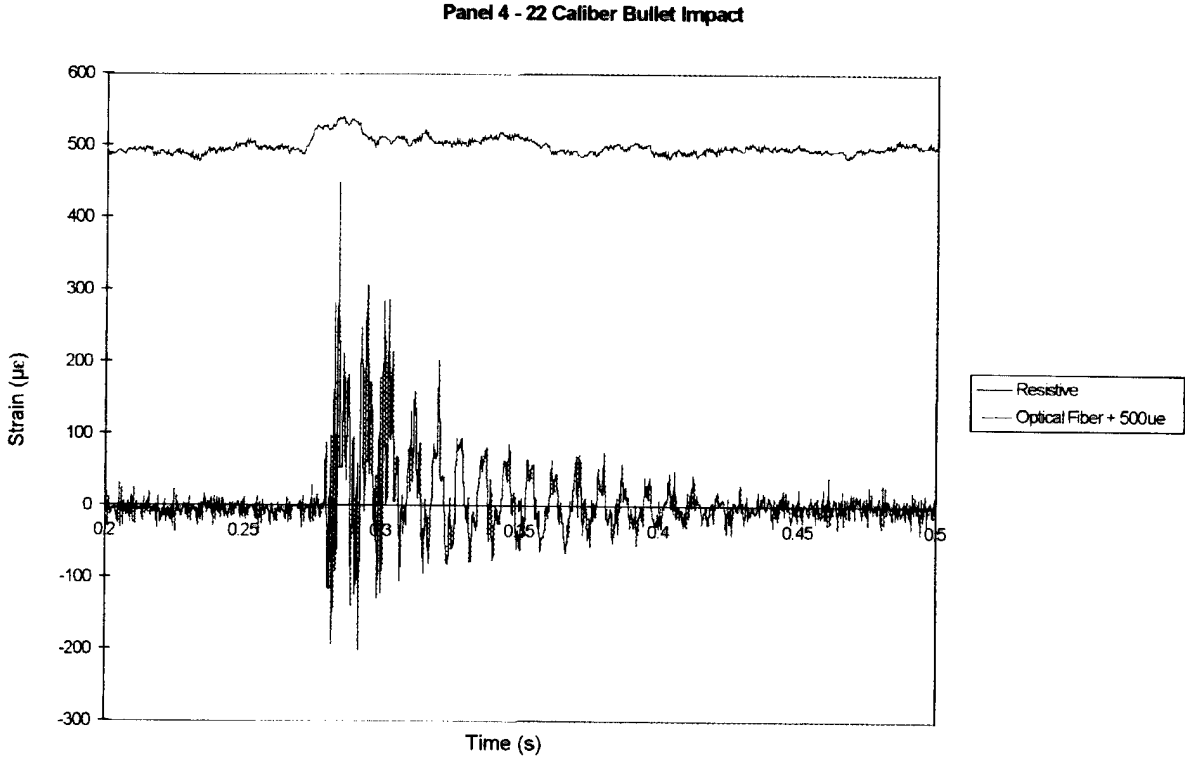

Figure 51. Panel No. 4 Strain-vs.-Time Plot During .22-Caliber Bullet Impact.

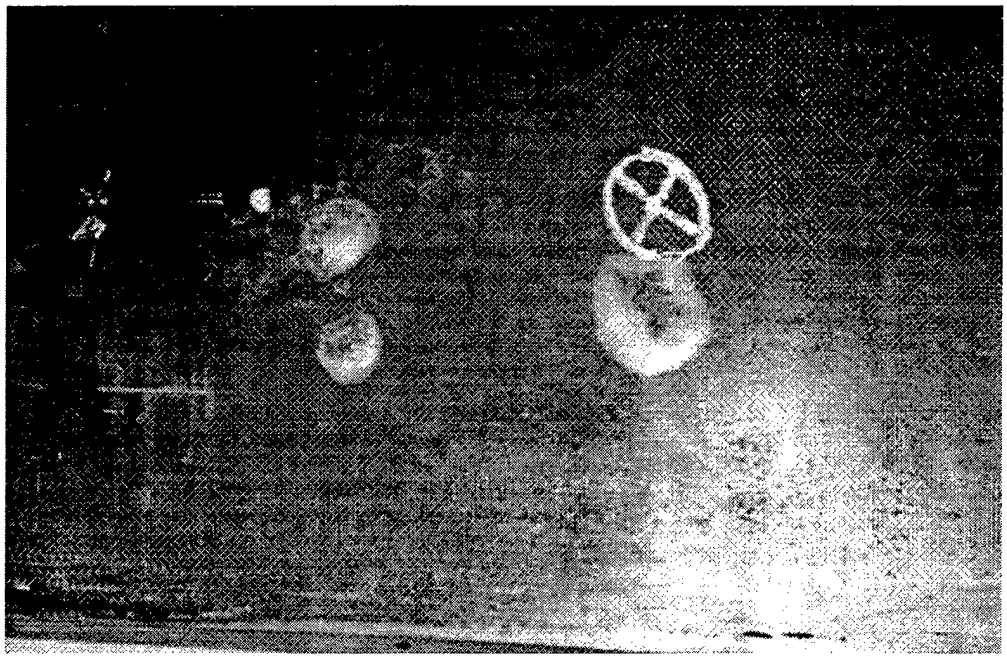

Figure 52. Ballistically Impacted Panel.

left-hand impact). The bullet became embedded in the panel and caused a 1-in-diameter delamination. This test was run to determine if we could sense the high dynamic rate ballistic event. Even though the signal from the optical fiber gauge was somewhat noisy at these low strain levels, we were able to get the reading even though the strains were low with the small-caliber bullet.

7. Conclusions

The research described in this report has demonstrated the potential benefits of embedded fiber optic sensors including Bragg grating sensors (three-axis sensors and single axis) and fluorescence optrode sensors:

- Precise cure monitoring at multiple points and planes in composite structures.

- Liquid molding (RIM/RTM) resin flow information.

- Residual stress at multiple points and planes in composite structures throughout the cure cycle.

- Temperature at multiple points in the composite structure during cure.

- Strain at multiple points in the composite structure during quasi-static loading.

- Strain-vs.-time and natural frequency data at multiple points in composite structure during dynamic events including high levels (280 ft· lb) of low-velocity impact and ballistic impact at high velocity.

- Transverse strain and strain gradients (three-axis sensor) at multiple points in composite structure.

- Damage to composite structures caused by low-velocity impact.

The BRR low-cost demodulator has been shown to be able to monitor the photonic information coming from the fiber optic sensors at very high data rates, and the prototype PPMS software has demonstrated our ability to convert the demodulator electronic signals to useful engineering information. PPMS has also developed and demonstrated the technology to successfully embed and protect the fiber optic sensors (0 sensors out of the 10 embedded were damaged throughout the program). The fiber optic sensors can be multiplexed using the BRR demodulator and significant amounts of data recorded in real time at high speed.

The ability to tailor the composite material constituents, panel design, and cure cycle to reduce residual stresses and produce composite structures with superior tailored mechanical properties should be demonstrated in future work. Combining detailed modeling and simulation of the composite structure and the cure process with the information gathered from a distributed embedded fiber optic network with sensors at precise preselected locations will provide a breakthrough in the knowledge of composite structures and the ability to scientifically formulate

resins, design composite structures, tailor cure processes and liquid molding processes, and produce high-quality, low-cost composite structures with tailored mechanical properties.

Future efforts should utilize the modeling and simulation capability of ARL and UD and scientifically controlled experiments with distributed embedded fiber optic sensors at strategic points throughout the liquid molded (resin infusion/transfer molded) composite structure. This should include development of a prototype production demodulation and software package to provide the desired automated, integrated engineering data on cure, three-dimensional strain, vibration, shock, temperature, and natural frequency of liquid-molded composite structures. This work will directly benefit the Army After Next's integral armor requirements, LHX Program, Composite Armor Bridge Program, and other Department of Defense and commercial composite structures programs.

INTENTIONALLY LEFT BLANK.

8. References

Bogetti, T., and J. Gillespie, Jr. "Two-Dimenesional Cure Simulation of Thick Thermosetting Composites." *Journal of Composite Materials*, vol. 25, no. 3, 1991.

Bogetti, T., and J. Gillespie, Jr. "Process-Induced Stress and Deformation in Thick-Section Thermoset Composite Laminates." *Journal of Composite Materials,* vol. 26, no. 5, 1992a.

Bogetti, T., and J. Gillespie, Jr. "Influence of Cure Shrinkage on Stress Development in Thick Thermosetting Composites." BRL-TR-3380, U.S. Army Ballistic Research Laboratory, Aberdeen Proving Ground, MD, July 1992b.

Denham, H., G. George, L. Rintol, and P. Calvert. *SPIE Proceedings on the Third International Conference on Intelligent Materials.* Vol. 2779, p. 742, 1996.

Dousa, P., C. Konak, V. Fidler, and D. Dusek. "Cure Monitoring of Epoxy Resins by Fluorescence Quenching." *Polymers Bulletin*, vol. 22, p. 585, 1989.

Draxler, S., and M. Lippitsch. *SPIE Proceedings.* Vol. 2085, p. 61, 1993.

Eloundou, J., M. Feve, J. Gerard, D. Harran, and J. Pascault. "Temperature Dependence of the Behavior of an Epoxy-Amine System Near the Gel Point Through Viscoelastic Study." *Macromolecules*, vol. 29, p. 6907, 1996.

England, K., J. Gillespie, Jr., and B. Fink. "In-Situ Sensing of Viscosity by Direct Current Measurements." *American Society of Mechanical Engineering Meeting*, Los Angeles, CA, 1996.

Fink, B., S. Walsh, D. DeSchepper, J. Gillespie, Jr., R. McCullough, R. Don, and B. Waibel. "Advances in Resin Transfer Molding Flow Monitoring Using SMART Weave Sensors." *Proceedings of the American Society of Mechanical Engineering Materials Division, International Mechanical Engineering Conference and Exposition*, vol. 69.2, pp. 999–1015, MD, 1995.

Forster, T., and G. Hoffmann. "Viscosity Dependence of Fluorescent Quantum Yields of Some Dye Systems." *Journal of Physical Chemistry–Frankfurt*, vol. 75, p. 4119, 1971.

Fuhs, M., J. Gillespie, Jr., B. Fink, and T. Bogetti. "Thermo-Chemical Characterization of S2-Glass/Binyl Ester Composites." *The 11th Technical Conference of the American Society for Composites*, pp. 529–538, Atlanta, GA, 7–9 October 1996.

Gillham, J., and J. Enns. "On the Cure and Properties of Thermosetting Polymers Using Torsional Braid Analysis." *Trends in Polymer Science*, vol. 2, no. 12, pp. 406–419, December 1994.

Green, A., S. Darvish, and E. Shafir. *SPIE Proceedings on the Third International Conference on Intelligent Materials.* Vol. 2779, p. 209, 1996.

Hill, K., Y. Fujii, D. Johnson, and B Kawasaki. "Photosensitivity in Optical Fiber Waveguides: Application to Reflection Filter Fabrication." *Applied Physics Letters*, vol. 32, p. 647, 1978.

Huang, X., T. Bogetti, and J. Gillespie, Jr. "Assessing Thermal Residual Stress in Integral Hybrid Composite Armor." *The 11th Technical Conference of the American Society for Composites*, pp. 787–796, Atlanta, GA, 7–9 October 1996.

Jacobs, J., E. W. Nelson, and A. B. Scranton. "Use of Fluorescence to Monitor Temperature and Observe Water Effects in Cationic Photopolymerization of Divinyl Ethers Photosynthesized by Anthracene." *Polymer Material Science and Engineering*, vol. 70, p. 74, 1994.

Lackowicz, J. *Topics in Fluorescence Spectroscopy.* Vol. 1–3, 1991.

Levin, K., and S. Nilsson. *SPIE Proceedings on the Third International Conference on Intelligent Materials.* Vol. 2779, p. 222, 1996.

Levy, R., and D. Ames. *Adhesive Chemistry Developments and Trends.* Seattle, WA: Plenum Press, p. 245, January 1984.

Levy, R., and D. Ames. "Effect of Absorbed Water on Epoxy Fluorescence." *Abstracted Papers of the American Chemical Society*, vol. 190, p. 37, 1985.

Levy, R. "Fluorescence Optrode Sensor for Monitoring the Composite Curing Process." *Abstracted Papers of the American Chemical Society*, vol. 191, p. 81, 1986.

Levy, R., and S. Schwab. "Cross-Linked Polymers." *ACS Symposium Series*, vol. 367, p. 113, 1988.

Loos, A., and G. Springer. "Curing of Epoxy Matrix Composites." *Journal of Composite Materials*, vol. 17, p. 135, 1983.

Loutfy, R. O. "High-Conversion Polymerization Fluorescence Probes: 1. Polymerization of Methyl-Methacrylate." *Macromolecules*, vol. 14, no. 2, p. 270, 1981.

Loutfy, R. O. "Fluorescence Probes for Polymer Free-Volume." *Pure and Applied Chemicals*, vol. 58, no. 9, p. 1239, 1986.

Meltz, G., W. Morey, and W. Glenn. "Formation of Bragg Gratings in Optical Fibers by Transverse Holographic Methods." *Optics Letters*, vol. 14, p. 823, 1989.

Miller, K., R. Krueger, and J. Torkelson. "Mobility-Sensitive Fluorescence Probes for Quantitative Monitoring of Water Sorption and Diffusion in Polymer Coatings." *J. Polymer Science and Polymer Physics*, vol. 33, no. 17, p. 2343, 1995.

Noel, C., F. Laupretre, C. Friedrich, C. Leonard, J. Halary, and L. Monnerie. "Electron-Spin-Resonance and Fluorescence Polarization Investigation of Molecular Motions in Poly(Vinylidene Fluoride) and Some Related Copolymers." *Macromolecules*, vol. 19, p. 201, 1986.

Park, H., and H. Song. "Optical Loss in Cured Epoxy Systems." *Polymer Material Science and Engineering*, vol. 76, p. 340, 1997.

Royal, J., and J. Torkelson. "Photochromic and Fluorescent-Probe Studies in Glassy Polymer Matrices." *Macromolecules*, vol. 25, no. 18, p. 1705, 1992.

Royal, J., and J. Torkelson. "Physical Aging Effects on Molecular-Scale Polymer Relaxations Monitored With Mobility-Sensitive Fluorescent Molecules." *Macromolecules*, vol. 26, no. 20, p. 5331, 1993.

Scarlata, S., and J. Ors. "Fluorescence Polarization—A Method to Monitor Polymer Cure." *Polymer Communication*, vol. 27, p. 41, 1986.

Schwab, S., and R. Levy. *Advanced Chemical Series*. Vol. 227, p. 397, 1990.

Song, J., and C. Sung. "Fluorescence Studies of Diaminodiphenyl Sulfone Curing Agent for Epoxy Cure Characterization." *Macromolecules*, vol. 26, no. 18, p. 4818, 1993.

Stroeks, A., M. Shmorhum, A. Jamieson, and R. Simha. "Cure Monitoring of Epoxy-Resins by Excimer Fluorescence." *Polymers*, vol. 29, p. 467, 1988.

Strehmel, B., V. Strehmel, H. Timpe, and K. Urban. "Time-Resolved Fluorescence Measurements for the Characterization of Epoxy Systems." *European Polymers Journal*, vol. 28, no. 5, p. 525, 1992.

Sun, X., and C. Sung. "Intrinsic Fluorescence of Curing Agent for Water-Uptake Monitoring in Epoxy Network." *Polymer Preprints*, vol. 34, p. 548, 1993.

Sun, X., and C. Sung. "Cure Characterization in Polyurethane and Model Urethane Reactions by an Intrinsic Fluorescence Technique." *Macromolecules*, vol. 29, no. 9, p. 3198, 1996.

Udd, E., and T. Clark. "Fiber Grating Sensor Systems for Sensing Environmental Effects." U.S. Patent 5,380,995, 10 January 1995.

Udd, E. "Multiparameter Sensor System Using a Multiple Grating Fiber Optic Birefringent Fiber." U.S. Patent 5,591,965, 7 January 1997.

Wang, F., R. Lowry, and B. Fanconi. "Novel Fluorescence Method for Cure Monitoring of Epoxy-Resins." *Polymers*, vol. 27, p. 1529, 1986.

Winans, J., and E. Seldin. *Handbook of Physics*. pp. 6–131, 1967.

Wolfbeis, O. *Fiber Optic Chemical Sensors and Biosensors*. Vols. 1 and 2, 1991.

Xu, M., H. Geiger, and J. Dakin. "Multiplexed Point and Stepwise Continuous Fiber Grating Based Sensors: Practical Sensor for Structural Monitoring." *Proceedings of SPIE*, vol. 2294, p. 69, 1994.

NO. OF COPIES	ORGANIZATION
2	DEFENSE TECHNICAL INFORMATION CENTER DTIC DDA 8725 JOHN J KINGMAN RD STE 0944 FT BELVOIR VA 22060-6218
1	HQDA DAMO FDT 400 ARMY PENTAGON WASHINGTON DC 20310-0460
1	OSD OUSD(A&T)/ODDDR&E(R) R J TREW THE PENTAGON WASHINGTON DC 20301-7100
1	DPTY CG FOR RDA US ARMY MATERIEL CMD AMCRDA 5001 EISENHOWER AVE ALEXANDRIA VA 22333-0001
1	INST FOR ADVNCD TCHNLGY THE UNIV OF TEXAS AT AUSTIN PO BOX 202797 AUSTIN TX 78720-2797
1	DARPA B KASPAR 3701 N FAIRFAX DR ARLINGTON VA 22203-1714
1	NAVAL SURFACE WARFARE CTR CODE B07 J PENNELLA 17320 DAHLGREN RD BLDG 1470 RM 1101 DAHLGREN VA 22448-5100
1	US MILITARY ACADEMY MATH SCI CTR OF EXCELLENCE DEPT OF MATHEMATICAL SCI MADN MATH THAYER HALL WEST POINT NY 10996-1786

NO. OF COPIES	ORGANIZATION
1	DIRECTOR US ARMY RESEARCH LAB AMSRL D D R SMITH 2800 POWDER MILL RD ADELPHI MD 20783-1197
1	DIRECTOR US ARMY RESEARCH LAB AMSRL DD 2800 POWDER MILL RD ADELPHI MD 20783-1197
1	DIRECTOR US ARMY RESEARCH LAB AMSRL CS AS (RECORDS MGMT) 2800 POWDER MILL RD ADELPHI MD 20783-1145
3	DIRECTOR US ARMY RESEARCH LAB AMSRL CI LL 2800 POWDER MILL RD ADELPHI MD 20783-1145
	ABERDEEN PROVING GROUND
4	DIR USARL AMSRL CI LP (BLDG 305)

NO. OF COPIES	ORGANIZATION
1	DIRECTOR US ARMY RESEARCH LAB AMSRL CP CA D SNIDER 2800 POWDER MILL RD ADELPHI MD 20783-1145
1	DIRECTOR US ARMY RESEARCH LAB AMSRL OP SD TA 2800 POWDER MILL ROAD ADELPHI MD 20783-1145
3	DIRECTOR US ARMY RESEARCH LAB AMSRL OP SD TL 2800 POWDER MILL ROAD ADELPHI MD 20783-1145
1	DIRECTOR US ARMY RESEARCH LAB AMSRL OP SD TP 2800 POWDER MILL ROAD ADELPHI MD 20783-1145
2	DIRECTOR US ARMY RESEARCH LAB AMSRL OP CI AD TECH PUB BR RECORDS MGMT ADMIN 2800 POWDER MILL ROAD ADELPHI MD 20783-1197
1	HQDA DAMI FIT NOLAN BLDG WASHINGTON DC 20310-1025
1	DIRECTOR DA OASARDA SARD SO 103 ARMY PENTAGON WASHINGTON DC 20310-0103
1	DEPUTY ASST SCY FOR R&T SARD TT RM 3EA79 THE PENTAGON WASHINGTON DC 20301-7100

NO. OF COPIES	ORGANIZATION
1	COMMANDER US ARMY MATERIEL CMD AMXMI INT 5001 EISENHOWER AVE ALEXANDRIA VA 22333-0001
2	COMMANDER US ARMY ARDEC AMSTA AR AE WW E BAKER J PEARSON PICATINNY ARSENAL NJ 07806-5000
1	COMMANDER US ARMY ARDEC AMSTA AR TD C SPINELLI PICATINNY ARSENAL NJ 07806-5000
1	COMMANDER US ARMY ARDEC AMSTA AR FSE T GORA PICATINNY ARSENAL NJ
6	COMMANDER US ARMY ARDEC AMSTA AR CCH A W ANDREWS S MUSALLI R CARR M LUCIANO E LOGSDEN T LOUZEIRO PICATINNY ARSENAL NJ 07806-5000
4	COMMANDER US ARMY ARDEC AMSTA AR CC G PAYNE J GEHBAUER C BAULIEU H OPAT PICATINNY ARSENAL NJ 07806-5000

NO. OF COPIES	ORGANIZATION
1	COMMANDER US ARMY ARDEC AMSTA AR CCH P J LUTZ PICATINNY ARSENAL NJ 07806-5000
1	COMMANDER US ARMY ARDEC AMSTA AR FSF T C LIVECCHIA PICATINNY ARSENAL NJ 07806-5000
1	COMMANDER US ARMY ARDEC AMSTA AR QAC T C C PATEL PICATINNY ARSENAL NJ 07806-5000
2	COMMANDER US ARMY ARDEC AMSTA AR M D DEMELLA F DIORIO PICATINNY ARSENAL NJ 07806-5000
3	COMMANDER US ARMY ARDEC AMSTA AR FSA A WARNASH B MACHAK M CHIEFA PICATINNY ARSENAL NJ 07806-5000
2	COMMANDER US ARMY ARDEC AMSTA AR FSP G M SCHIKSNIS D CARLUCCI PICATINNY ARSENAL NJ 07806-5000
1	COMMANDER US ARMY ARDEC AMSTA AR FSP A P KISATSKY PICATINNY ARSENAL NJ 07806-5000
2	COMMANDER US ARMY ARDEC AMSTA AR CCH C H CHANIN S CHICO PICATINNY ARSENAL NJ 07806-5000
9	COMMANDER US ARMY ARDEC AMSTA AR CCH B P DONADIA F DONLON P VALENTI C KNUTSON G EUSTICE S PATEL G WAGNECZ R SAYER F CHANG PICATINNY ARSENAL NJ 07806-5000
6	COMMANDER US ARMY ARDEC AMSTA AR CCL F PUZYCKI R MCHUGH D CONWAY E JAROSZEWSKI R SCHLENNER M CLUNE PICATINNY ARSENAL NJ 07806-5000
1	COMMANDER US ARMY ARDEC AMSTA AR QAC T D RIGOGLIOSO PICATINNY ARSENAL NJ 07806-5000

NO. OF COPIES	ORGANIZATION
1	COMMANDER US ARMY ARDEC AMSTA AR SRE D YEE PICATINNY ARSENAL NJ 07806-5000
1	COMMANDER US ARMY ARDEC AMSTA AR WET T SACHAR BLDG 172 PICATINNY ARSENAL NJ 07806-5000
1	COMMANDER US ARMY ARDEC SMCAR ASF PICATINNY ARSENAL NJ 07806-5000
1	COMMANDER US ARMY ARDEC AMSTA AR WEL F INTELLIGENCE SPECIALIST M GUERRIERE PICATINNY ARSENAL NJ 07806-5000
11	PROJECT MANAGER US ARMY TMAS SFAE GSSC TMA R MORRIS C KIMKER D GUZOWICZ E KOPACZ R ROESER R DARCY R MCDANOLDS L D ULISSE C ROLLER J MCGREEN B PATTER PICATINNY ARSENAL NJ 07806-5000
2	PEO FIELD ARTILLERY SYSTEMS SFAE FAS PM H GOLDMAN T MCWILLIAMS PICATINNY ARSENAL NJ 07806-5000
6	PM SADARM SFAE GCSS SD COL B ELLIS M DEVINE R KOWALSKI W DEMASSI J PRITCHARD S HROWNAK PICATINNY ARSENAL NJ 07806-5000
1	COMMANDER US ARMY ARDEC PRODUCTION BASE MODERN ACTY AMSMC PBM K PICATINNY ARSENAL NJ 07806-5000
3	COMMANDER US ARMY TACOM PM TACTICAL VEHICLES SFAE TVL SFAE TVM SFAE TVH 6501 ELEVEN MILE RD WARREN MI 48397-5000
1	COMMANDER US ARMY TACOM PM ABRAMS SFAE ASM AB 6501 ELEVEN MILE RD WARREN MI 48397-5000
1	COMMANDER US ARMY TACOM PM BFVS SFAE ASM BV 6501 ELEVEN MILE RD WARREN MI 48397-5000

NO. OF COPIES	ORGANIZATION
1	COMMANDER US ARMY TACOM PM AFAS SFAE ASM AF 6501 ELEVEN MILE RD WARREN MI 48397-5000
2	COMMANDER US ARMY TACOM PM SURV SYS SFAE ASM SS T DEAN SFAE GCSS W GSI M D COCHRAN 6501 ELEVEN MILE RD WARREN MI 48397-5000
1	COMMANDER US ARMY TACOM PM RDT&E SFAE GCSS W AB J GODELL 6501 ELEVEN MILE RD WARREN MI 48397-5000
1	COMMANDER US ARMY TACOM PM SURVIVABLE SYSTEMS SFAE GCSS W GSI H M RYZYI 6501 ELEVEN MILE RD WARREN MI 48397-5000
1	COMMANDER US ARMY TACOM PM BFV SFAE GCSS W BV S DAVIS 6501 ELEVEN MILE RD WARREN MI 48397-5000
1	COMMANDER US ARMY TACOM PM LIGHT TACTICAL VEHICLES AMSTA TR S AJ J MILLS MS 209 6501 ELEVEN MILE RD WARREN MI 48397-5000
1	COMMANDER US ARMY TACOM PM GROUND SYSTEMS INTEGRATION SFAE GCSS W GSI R LABATILLE 6501 ELEVEN MILE RD WARREN MI 48397-5000
1	COMMANDER US ARMY TACOM CHIEF ABRAMS TESTING SFAE GCSS W AB QT T KRASKIEWICZ 6501 ELEVEN MILE RD WARREN MI 48397-5000
1	COMMANDER US ARMY TACOM AMSTA SF WARREN MI 48397-5000
1	COMMANDER SMCWV QAE Q B VANINA BLDG 44 WATERVLIET ARSENAL WATERVLIET NY 12189-4050
14	COMMANDER US ARMY TACOM ASMTA TR R J CHAPIN R MCCLELLAND D THOMAS J BENNETT D HANSEN AMSTA JSK S GOODMAN J FLORENCE K IYER J THOMSON AMSTA TR D D OSTBERG L HINOJOSA B RAJU AMSTA CS SF H HUTCHINSON F SCHWARZ WARREN MI 48397-5000

NO. OF COPIES	ORGANIZATION
1	COMMANDER SMCWV SPM T MCCLOSKEY BLDG 253 WATERVLIET ARSENAL WATERVLIET NY 12189-4050
10	BENET LABS AMSTA AR CCB R FISCELLA G D ANDREA M SCAVULO G SPENCER P WHEELER K MINER J VASILAKIS G FRIAR R HASENBEIN SMCAR CCB R S SOPOK WATERVLIET NY 12189
2	TSM ABRAMS ATZK TS S JABURG W MEINSHAUSEN FT KNOX KY 40121
3	ARMOR SCHOOL ATZK TD R BAUEN J BERG A POMEY FT KNOX KY 40121
2	HQ IOC TANK AMMO TEAM AMSIO SMT R CRAWFORD W HARRIS ROCK ISLAND IL 61299-6000
1	DIRECTOR US ARMY AMCOM SFAE AV RAM TV D CALDWELL BUILDING 5300 REDSTONE ARSENAL AL 35898

NO. OF COPIES	ORGANIZATION
4	DIRECTOR US ARMY CECOM NIGHT VISION & ELECTRONIC SENSORS DIRECTORATE AMSEL RD NV CM CCD R ADAMS R MCLEAN A YINGST AMSEL RD NV VISP E JACOBS 10221 BURBECK RD FT BELVOIR VA 22060-5806
2	CDR US ARMY AMCOM AVIATION APPLIED TECH DIR J SCHUCK FT EUSTIS VA 23604-5577
1	US ARMY CRREL P DUTTA 72 LYME RD HANOVER NH 03755
1	US ARMY CERL R LAMPO 2902 NEWMARK DR CHAMPAIGN IL 61822
2	US ARMY CORP OF ENGINEERS CERD C T LIU CEW ET T TAN 20 MASS AVE NW WASHINGTON DC 20314
10	DIRECTOR US ARMY NATL GRND INTEL CTR D LEITER S EITELMAN M HOLTUS M WOLFE S MINGLEDORF H C ARDLEIGH J GASTON W GSTATTENBAUER R WARNER J CRIDER 220 SEVENTH STREET NE CHARLOTTESVILLE VA 22091

NO. OF COPIES	ORGANIZATION
6	US ARMY SBCCOM SOLDIER SYSTEMS CTR BALLISTICS TEAM J WARD MARINE CORPS TEAM J MACKIEWICZ BUS AREA ADVOCACY TEAM W HASKELL SSCNC WST W NYKVIST T MERRILL S BEAUDOIN KANSAS ST NATICK MA 01760-5019
1	US ARMY COLD REGIONS RSCH & ENGRNG LAB P DUTTA 72 LYME RD HANOVER NH 03755
1	SYSTEM MANAGER ABRAMS ATZK TS LTC J H NUNN BLDG 1002 RM 110 FT KNOX KY 40121
9	US ARMY RESEARCH OFFICE A CROWSON J CHANDRA H EVERETT J PRATER R SINGLETON G ANDERSON D STEPP D KISEROW J CHANG PO BOX 12211 RESEARCH TRIANGLE PARK NC 27709-2211
1	DIRECTORATE OF CMBT DEVELOPMENT C KJORO 320 ENGINEER LOOP STE 141 FT LEONARD WOOD MO 65473-8929

NO. OF COPIES	ORGANIZATION
1	COMMANDANT US ARMY FIELD ARTILLERY CTR ATFS CD LTC BUMGARNER FT SILL OK 73503 5600
1	CHIEF USAIC LTC T J CUMMINGS ATZB COM FT BENNING GA 31905-5800
1	NAVAL AIR SYSTEMS CMD J THOMPSON 48142 SHAW RD UNIT 5 PATUXENT RIVER MD 20670
1	NAVAL SURFACE WARFARE CTR DAHLGREN DIV CODE G06 DAHLGREN VA 22448
1	NAVAL SURFACE WARFARE CTR TECH LIBRARY CODE 323 17320 DAHLGREN RD DAHLGREN VA 22448
3	NAVAL RESEARCH LAB I WOLOCK CODE 6383 R BADALIANCE CODE 6304 L GAUSE WASHINGTON DC 20375
1	NAVAL SURFACE WARFARE CTR CRANE DIVISION M JOHNSON CODE 20H4 LOUISVILLE KY 40214-5245
2	COMMANDER NAVAL SURFACE WARFARE CTR CADEROCK DIVISION R PETERSON CODE 2020 M CRITCHFIELD CODE 1730 BETHESDA MD 20084
2	NAVAL SURFACE WARFARE CTR U SORATHIA C WILLIAMS CD 6551 9500 MACARTHUR BLVD WEST BETHESDA MD 20817

NO. OF COPIES	ORGANIZATION
1	DAVID TAYLOR RESEARCH CTR SHIP STRUCTURES & PROTECTION DEPARTMENT CODE 1702 J CORRADO BETHESDA MD 20084
2	DAVID TAYLOR RESEARCH CTR R ROCKWELL W PHYILLAIER BETHESDA MD 20054-5000
1	OFFICE OF NAVAL RESEARCH D SIEGEL CODE 351 800 N QUINCY ST ARLINGTON VA 22217-5660
8	NAVAL SURFACE WARFARE CTR J FRANCIS CODE G30 D WILSON CODE G32 R D COOPER CODE G32 J FRAYSSE CODE G33 E ROWE CODE G33 T DURAN CODE G33 L DE SIMONE CODE G33 R HUBBARD CODE G33 DAHLGREN VA 22448
1	NAVAL SEA SYSTEMS CMD D LIESE 2531 JEFFERSON DAVIS HIGHWAY ARLINGTON VA 22242-5160
1	NAVAL SURFACE WARFARE CTR M LACY CODE B02 17320 DAHLGREN RD DAHLGREN VA 22448
1	OFFICE OF NAVAL RESEARCH J KELLY 800 NORTH QUINCEY ST ARLINGTON VA 22217-5000
2	NAVAL SURFACE WARFARE CTR CARDEROCK DIVISION R CRANE CODE 2802 C WILLIAMS CODE 6553 3A LEGGETT CIR BETHESDA MD 20054-5000

NO. OF COPIES	ORGANIZATION
1	NAVSEA OJRI PEO DD21 PMS500 G CAMPONESCHI 2351 JEFFERSON DAVIS HWY ARLINGTON VA 22242-5165
1	EXPEDITIONARY WARFARE DIV N85 F SHOUP 2000 NAVY PENTAGON WASHINGTON DC 20350-2000
1	AFRL MLBC 2941 P STREET RM 136 WRIGHT PATTERSON AFB OH 45433-7750
1	AFRL MLSS R THOMSON 2179 12TH STREET RM 122 WRIGHT PATTERSON AFB OH 45433-7718
2	AFRL F ABRAMS J BROWN BLDG 653 2977 P STREET STE 6 WRIGHT PATTERSON AFB OH 45433-7739
1	AFRL MLS OL L COULTER BLDG 100 BAY D 7278 4TH STREET HILL AFB UT 84056-5205
1	OSD JOINT CCD TEST FORCE OSD JCCD R WILLIAMS 3909 HALLS FERRY RD VICKSBURG MS 29180-6199
1	DEFENSE NUCLEAR AGENCY INNOVATIVE CONCEPTS DIV R ROHR 6801 TELEGRAPH RD ALEXANDRIA VA 22310-3398

NO. OF COPIES	ORGANIZATION
1	WATERWAYS EXPERIMENT D SCOTT 3909 HALLS FERRY RD SC C VICKSBURG MS 39180
3	DARPA M VANFOSSEN S WAX L CHRISTODOULOU 3701 N FAIRFAX DR ARLINGTON VA 22203-1714
2	SERDP PROGRAM OFC PM P2 C PELLERIN B SMITH 901 N STUART ST SUITE 303 ARLINGTON VA 22203
1	FAA MIL HDBK 17 CHAIR L ILCEWICZ 1601 LIND AVE SW ANM 115N RENTON VA 98055
2	FAA TECH CTR D OPLINGER AAR 431 P SHYPRYKEVICH AAR 431 ATLANTIC CITY NJ 08405
1	OFC OF ENVIRONMENTAL MGMT US DEPT OF ENERGY P RITZCOVAN 19901 GERMANTOWN RD GERMANTOWN MD 20874-1928
1	LOS ALAMOS NATL LAB F ADDESSIO MS B216 PO BOX 1633 LOS ALAMOS NM 87545
1	OAK RIDGE NATL LAB R M DAVIS PO BOX 2008 OAK RIDGE TN 37831-6195

NO. OF COPIES	ORGANIZATION
5	DIRECTOR LAWRENCE LIVERMORE NATL LAB R CHRISTENSEN S DETERESA F MAGNESS M FINGER MS 313 M MURPHY L 282 PO BOX 808 LIVERMORE CA 94550
7	NIST R PARNAS J DUNKERS M VANLANDINGHAM MS 8621 J CHIN MS 8621 D HUNSTON MS 8543 J MARTIN MS 8621 D DUTHINH MS 8611 100 BUREAU DR GAITHERSBURG MD 20899
1	OAK RIDGE NATL LAB C EBERLE MS 8048 PO BOX 2009 OAK RIDGE TN 37831
1	OAK RIDGE NATL LAB C D WARREN MS 8039 PO BOX 2009 OAK RIDGE TN 37922
4	DIRECTOR SANDIA NATL LABS APPLIED MECHANICS DEPT DIVISION 8241 W KAWAHARA K PERANO D DAWSON P NIELAN PO BOX 969 LIVERMORE CA 94550-0096
1	LAWRENCE LIVERMORE NATIONAL LAB M MURPHY PO BOX 808 L 282 LIVERMORE CA 94550

NO. OF COPIES	ORGANIZATION
3	NASA LANGLEY RESEARCH CTR MS 266 AMSRL VS W ELBER F BARTLETT JR G FARLEY HAMPTON VA 23681-0001
1	NASA LANGLEY RESEARCH CTR T GATES MS 188E HAMPTON VA 23661-3400
1	USDOT FEDERAL RAILROAD RDV 31 M FATEH WASHINGTON DC 20590
1	DOT FHWA J SCALZI 400 SEVENTH ST SW 3203 HNG 32 WASHINGTON DC 20590
1	FHWA E MUNLEY 6300 GEORGETOWN PIKE MCLEAN VA 22101
1	CENTRAL INTELLIGENCE AGENCY OTI WDAG GT W L WALTMAN PO BOX 1925 WASHINGTON DC 20505
1	MARINE CORPS INTEL ACTY D KOSITZKE 3300 RUSSELL RD SUITE 250 QUANTICO VA 22134-5011
1	NATL GRND INTELLIGENCE CTR DIRECTOR IANG TMT 220 SEVENTH ST NE CHARLOTTESVILLE VA 22902-5396
1	DIRECTOR DEFENSE INTELLIGENCE AGENCY TA 5 K CRELLING WASHINGTON DC 20310

NO. OF COPIES	ORGANIZATION
1	GRAPHITE MASTERS INC J WILLIS 3815 MEDFORD ST LOS ANGELES CA 90063-1900
1	ADVANCED GLASS FIBER YARNS T COLLINS 281 SPRING RUN LN STE A DOWNINGTON PA 19335
1	COMPOSITE MATERIALS INC D SHORTT 19105 63 AVE NE PO BOX 25 ARLINGTON WA 98223
1	COMPOSITE MATERIALS INC R HOLLAND 11 JEWEL COURT ORINDA CA 94563
1	COMPOSITE MATERIALS INC C RILEY 14530 S ANSON AVE SANTA FE SPRINGS CA 90670
2	COMPOSIX D BLAKE L DIXON 120 O NEILL DR HEBRUN OHIO 43025
4	CYTEC FIBERITE R DUNNE D KOHLI M GILLIO R MAYHEW 1300 REVOLUTION ST HAVRE DE GRACE MD 21078
2	SIMULA J COLTMAN R HUYETT 10016 S 51ST ST PHOENIX AZ 85044
1	SIOUX MFG B KRIEL PO BOX 400 FT TOTTEN ND 58335

NO. OF COPIES	ORGANIZATION
2	PROTECTION MATERIALS INC M MILLER F CRILLEY 14000 NW 58 CT MIAMI LAKES FL 33014
3	FOSTER MILLER J J GASSNER M ROYLANCE W ZUKAS 195 BEAR HILL RD WALTHAM MA 02354-1196
1	ROM DEVELOPMENT CORP R O MEARA 136 SWINEBURNE ROW BRICK MARKET PLACE NEWPORT RI 02840
2	TEXTRON SYSTEMS T FOLTZ M TREASURE 201 LOWELL ST WILMINGTON MA 08870-2941
1	JPS GLASS L CARTER PO BOX 260 SLATER RD SLATER SC 29683
1	O GARA HESS & EISENHARDT M GILLESPIE 9113 LESAINT DR FAIRFIELD OH 45014
2	MILLIKEN RESEARCH CORP H KUHN M MACLEOD PO BOX 1926 SPARTANBURG SC 29303
1	CONNEAUGHT INDUSTRIES INC J SANTOS PO BOX 1425 COVENTRY RI 02816

NO. OF COPIES	ORGANIZATION
1	BATTELLE C R HARGREAVES 505 KING AVE COLUMBUS OH 43201-2681
2	BATTELLE NATICK OPERATIONS J CONNORS B HALPIN 209 W CENTRAL ST STE 302 NATICK MA 01760
1	BATTELLE NW DOE PNNL T HALL MS K231 BATTELLE BLVD RICHLAND WA 99352
3	PACIFIC NORTHWEST LAB M SMITH G VAN ARSDALE R SHIPPELL PO BOX 999 RICHLAND WA 99352
1	ARMTEC DEFENSE PRODUCTS S DYER 85 901 AVE 53 PO BOX 848 COACHELLA CA 92236
2	ADVANCED COMPOSITE MATLS CORP P HOOD J RHODES 1525 S BUNCOMBE RD GREER SC 29651-9208
2	GLCC INC J RAY M BRADLEY 103 TRADE ZONE DR STE 26C WEST COLUMBIA SC 29170
2	AMOCO PERFORMANCE PRODUCTS M MICHNO JR J BANISAUKAS 4500 MCGINNIS FERRY RD ALPHARETTA GA 30202-3944

NO. OF COPIES	ORGANIZATION
1	SAIC M PALMER 2109 AIR PARK RD S E ALBUQUERQUE NM 87106
1	SAIC G CHRYSSOMALLIS 3800 W 80TH ST STE 1090 BLOOMINGTON MN 55431
1	AAI CORPORATION T G STASTNY PO BOX 126 HUNT VALLEY MD 21030-0126
1	JOHN HEBERT PO BOX 1072 HUNT VALLEY MD 21030-0126
12	ALLIANT TECHSYSTEMS INC C CANDLAND C AAKHUS R BECKER B SEE N VLAHAKUS R DOHRN S HAGLUND D FISHER W WORRELL R COPENHAFER M HISSONG D KAMDAR 600 2ND ST NE HOPKINS MN 55343-8367
3	ALLIANT TECHSYSTEMS INC J CONDON E LYNAM J GERHARD WV01 16 STATE RT 956 PO BOX 210 ROCKET CENTER WV 26726-0210
1	APPLIED COMPOSITES W GRISCH 333 NORTH SIXTH ST ST CHARLES IL 60174

NO. OF COPIES	ORGANIZATION
1	PROJECTILE TECHNOLOGY INC 515 GILES ST HAVRE DE GRACE MD 21078
1	CUSTOM ANALYTICAL ENG SYS INC A ALEXANDER 13000 TENSOR LN NE FLINTSTONE MD 21530
2	LORAL VOUGHT SYSTEMS G JACKSON K COOK 1701 W MARSHALL DR GRAND PRAIRIE TX 75051
5	AEROJET GEN CORP D PILLASCH T COULTER C FLYNN D RUBAREZUL M GREINER 1100 WEST HOLLYVALE ST AZUSA CA 91702-0296
3	HEXCEL INC R BOE F POLICELLI J POESCH PO BOX 98 MAGNA UT 84044
3	HERCULES INC G KUEBELER J VERMEYCHUK B MANDERVILLE JR HERCULES PLAZA WILMINGTON DE 19894
1	BRIGS COMPANY J BACKOFEN 2668 PETERBOROUGH ST HERNDON VA 22071-2443
1	ZERNOW TECHNICAL SERVICES L ZERNOW 425 W BONITA AVE STE 208 SAN DIMAS CA 91773

NO. OF COPIES	ORGANIZATION
2	OLIN CORPORATION FLINCHBAUGH DIV E STEINER B STEWART PO BOX 127 RED LION PA 17356
1	OLIN CORPORATION L WHITMORE 10101 9TH ST NORTH ST PETERSBURG FL 33702
1	DOW UT S TIDRICK 15 STERLING DR WALLINGFORD CT 06492
5	SIKORSKY AIRCRAFT G JACARUSO T CARSTENSAN B KAY S GARBO M S S330A J ADELMANN 6900 MAIN ST PO BOX 9729 STRATFORD CT 06497-9729
1	PRATT & WHITNEY D HAMBRICK 400 MAIN ST MS 114 37 EAST HARTFORD CT 06108
1	AEROSPACE CORP G HAWKINS M4 945 2350 E EL SEGUNDO BLVD EL SEGUNDO CA 90245
2	CYTEC FIBERITE M LIN W WEB 1440 N KRAEMER BLVD ANAHEIM CA 92806
1	HEXCEL T BITZER 11711 DUBLIN BLVD DUBLIN CA 94568

NO. OF COPIES	ORGANIZATION
1	BOEING R BOHLMANN PO BOX 516 MC 5021322 ST LOUIS MO 63166-0516
2	BOEING DEFENSE & SPACE GRP W HAMMOND J RUSSELL S 4X55 PO BOX 3707 SEATTLE WA 98124-2207
2	BOEING ROTORCRAFT P MINGURT P HANDEL 800 B PUTNAM BLVD WALLINGFORD PA 19086
1	BOEING DOUGLAS PRODUCTS DIV L J HART SMITH 3855 LAKEWOOD BLVD D800 0019 LONG BEACH CA 90846-0001
1	LOCKHEED MARTIN S REEVE 8650 COBB DR D 73 62 MZ 0648 MARIETTA GA 30063-0648
1	LOCKHEED MARTIN SKUNK WORKS D FORTNEY 1011 LOCKHEED WAY PALMDALE CA 93599-2502
1	LOCKHEED MARTIN R FIELDS 1195 IRWIN CT WINTER SPRINGS FL 32708
1	MATERIALS SCIENCES CORP B W ROSEN 500 OFFICE CENTER DR STE 250 FORT WASHINGTON PA 19034

NO. OF COPIES	ORGANIZATION
1	NORTHROP GRUMMAN CORP ELECTRONIC SENSORS & SYSTEMS DIV E SCHOCH MAILSTOP V 16 1745A WEST NURSERY RD LINTHICUM MD 21090
2	NORTHROP GRUMMAN ENVIRONMENTAL PROGRAMS R OSTERMAN A YEN 8900 E WASHINGTON BLVD PICO RIVERA CA 90660
1	UNITED DEFENSE LP D MARTIN PO BOX 359 SANTA CLARA CA 95052
1	UNITED DEFENSE LP G THOMAS PO BOX 58123 SANTA CLARA CA 95052
2	UNITED DEFENSE LP R BARRETT V HORVATICH MAIL DROP M53 328 W BROKAW RD SANTA CLARA CA 95052-0359
3	UNITED DEFENSE LP GROUND SYSTEMS DIVISION M PEDRAZZI MAIL DROP N09 A LEE MAIL DROP N11 M MACLEAN MAIL DROP N06 1205 COLEMAN AVE SANTA CLARA CA 95052
4	UNITED DEFENSE LP 4800 EAST RIVER RD R BRYNSVOLD P JANKE MS170 T GIOVANETTI MS236 B VAN WYK MS389 MINNEAPOLIS MN 55421-1498

NO. OF COPIES	ORGANIZATION
2	GENERAL DYNAMICS LAND SYSTEMS D REES M PASIK PO BOX 2074 WARREN MI 48090-2074
1	GENERAL DYNAMICS LAND SYSTEMS D BARTLE PO BOX 1901 WARREN MI 48090
1	GENERAL DYNAMICS LAND SYSTEMS MUSKEGON OPERATIONS W SOMMERS JR 76 GETTY ST MUSKEGON MI 49442
1	GENERAL DYNAMICS AMPHIBIOUS SYS SURVIVABILITY LEAD G WALKER 991 ANNAPOLIS WAY WOODBRIDGE VA 22191
5	INST FOR ADVANCED TECH T KIEHNE H FAIR P SULLIVAN W REINECKE I MCNAB 4030 2 W BRAKER LN AUSTIN TX 78759
2	CIVIL ENGR RSCH FOUNDATION H BERNSTEIN PRESIDENT R BELLE 1015 15TH ST NW STE 600 WASHINGTON DC 20005
1	ARROW TECH ASSO 1233 SHELBURNE RD STE D 8 SOUTH BURLINGTON VT 05403-7700

NO. OF COPIES	ORGANIZATION
1	CONSULTANT R EICHELBERGER 409 W CATHERINE ST BEL AIR MD 21014-3613
1	UCLA MANE DEPT ENGR IV H THOMAS HAHN LOS ANGELES CA 90024-1597
2	UNIV OF DAYTON RESEARCH INST RAN Y KIM AJIT K ROY 300 COLLEGE PARK AVE DAYTON OH 45469-0168
1	MIT P LAGACE 77 MASS AVE CAMBRIDGE MA 01887
1	IIT RESEARCH CTR D ROSE 201 MILL ST ROME NY 13440-6916
1	GEORGIA TECH RESEARCH INST GEORGIA INST OF TECHNOLOGY P FRIEDERICH ATLANTA GA 30392
1	MICHIGAN ST UNIV R AVERILL 3515 EB MSM DEPT EAST LANSING MI 48824-1226
1	UNIV OF KENTUCKY L PENN 763 ANDERSON HALL LEXINGTON KY 40506-0046
1	UNIV OF WYOMING D ADAMS PO BOX 3295 LARAMIE WY 82071

NO. OF COPIES	ORGANIZATION
1	UNIV OF UTAH DEPT OF MECH & INDUSTRIAL ENGR S SWANSON SALT LAKE CITY UT 84112
2	PENNSYLVANIA STATE UNIV R MCNITT C BAKIS 227 HAMMOND BLDG UNIVERSITY PARK PA 16802
1	PENNSYLVANIA STATE UNIV RENATA S ENGEL 245 HAMMOND BLDG UNIVERSITY PARK PA 16801
1	PURDUE UNIV SCHOOL OF AERO & ASTRO C T SUN W LAFAYETTE IN 47907-1282
1	STANFORD UNIV DEPARTMENT OF AERONAUTICS AND AEROBALLISTICS DURANT BUILDING S TSAI STANFORD CA 94305
1	UNIV OF DAYTON J M WHITNEY COLLEGE PARK AVE DAYTON OH 45469-0240
7	UNIV OF DELAWARE CTR FOR COMPOSITE MATRLS J GILLESPIE M SANTARE G PALMESE S YARLAGADDA S ADVANI D HEIDER D KUKICH 201 SPENCER LABORATORY NEWARK DE 19716

NO. OF COPIES ORGANIZATION

1 UNIV OF ILLINOIS
AT URBANA CHAMPAIGN
NATL CTR FOR COMPOSITE
MATERIALS RESEARCH
216 TALBOT LABORATORY
J ECONOMY
104 S WRIGHT ST
URBANA IL 61801

3 THE UNIV OF TEXAS
AT AUSTIN
CTR FOR ELECTROMECHANICS
J PRICE
A WALLS
J KITZMILLER
10100 BURNET RD
AUSTIN TX 78758-4497

3 VA POLYTECHNICAL INST
STATE UNIV
DEPT OF ESM
M W HYER
K REIFSNIDER
R JONES
BLACKSBURG VA 24061-0219

1 NORTH CAROLINA STATE
UNIV
CIVIL ENGINEERING DEPT
W RASDORF
PO BOX 7908
RALEIGH NC 27696-7908

1 UNIV OF MARYLAND
DEPT OF AEROSPACE ENGINEERING
ANTHONY J VIZZINI
COLLEGE PARK MD 20742

1 DREXEL UNIV
ALBERT S D WANG
32ND AND CHESTNUT STREETS
PHILADELPHIA PA 19104

1 SOUTHWEST RSCH INST
ENGR & MATL SCIENCES DIV
J RIEGEL
6220 CULEBRA RD
PO DRAWER 28510
SAN ANTONIO TX 78228-0510

NO. OF COPIES ORGANIZATION

ABERDEEN PROVING GROUND

1 COMMANDER
US ARMY MATERIEL SYS
ANALYSIS
P DIETZ
392 HOPKINS RD
AMXSY TD
APG MD 21005-5071

1 DIRECTOR
US ARMY RESEARCH LAB
AMSRL OP AP L
APG MD 21005 5066

115 DIR USARL
AMSRL CI
AMSRL CI H
W STUREK
AMSRL CI S
A MARK
AMSRL CS IO FI
M ADAMSON
AMSRL SL B
J SMITH
AMSRL SL BA
AMSRL SL BL
D BELY
R HENRY
AMSRL SL BG
A YOUNG
AMSRL SL I
AMSRL WM B
A HORST
E SCHMIDT
AMSRL WM BA
W D AMICO
F BRANDON
AMSRL WM BC
P PLOSTINS
D LYON
J NEWILL
S WILKERSON
A ZIELINSKI
AMSRL WM BD
B FORCH
R FIFER
R PESCE RODRIGUEZ
B RICE

NO. OF COPIES ORGANIZATION

ABERDEEN PROVING GROUND (CONT)

AMSRL WM BE
G WREN
C LEVERITT
D KOOKER
AMSRL WM BR
C SHOEMAKER
J BORNSTEIN
AMSRL WM M
D VIECHNICKI
G HAGNAUER
J MCCAULEY
B TANNER
AMSRL WM MA
R SHUFORD
P TOUCHET
N BECK TAN
D FLANAGAN
L GHIORSE
D HARRIS
S MCKNIGHT
P MOY
S NGYUEN
P PATTERSON
G RODRIGUEZ
A TEETS
R YIN
AMSRL WM MB
B FINK
J BENDER
T BLANAS
T BOGETTI
R BOSSOLI
L BURTON
K BOYD
S CORNELISON
P DEHMER
R DOOLEY
W DRYSDALE
G GAZONAS
S GHIORSE
D GRANVILLE
D HOPKINS
C HOPPEL
D HENRY
R KASTE
M KLUSEWITZ
M LEADORE
R LIEB

NO. OF COPIES ORGANIZATION

ABERDEEN PROVING GROUND (CONT)

AMSRL WM MB
E RIGAS
J SANDS
D SPAGNUOLO
W SPURGEON
J TZENG
E WETZEL
A ABRAHAMIAN
M BERMAN
A FRYDMAN
T LI
W MCINTOSH
E SZYMANSKI
AMRSL WM MC
J BEATTY
J SWAB
E CHIN
J MONTGOMERY
A WERESCZCAK
J LASALVIA
J WELLS
AMSRL WM MD
W ROY
S WALSH
AMSRL WM T
B BURNS
AMSRL WM TA
W GILLICH
T HAVEL
J RUNYEON
M BURKINS
E HORWATH
B GOOCH
W BRUCHEY
AMSRL WM TC
R COATES
AMSRL WM TD
A DAS GUPTA
T HADUCH
T MOYNIHAN
F GREGORY
A RAJENDRAN
M RAFTENBERG
M BOTELER
T WEERASOORIYA
D DANDEKAR
A DIETRICH

NO. OF
COPIES ORGANIZATION

ABERDEEN PROVING GROUND (CONT)

AMSRL WM TE
A NIILER
J POWELL
AMSRL SS SD
H WALLACE
AMSRL SS SE R
R CHASE
AMSRL SS SE DS
R REYZER
R ATKINSON
AMSRL SE L
R WEINRAUB
J DESMOND
D WOODBURY

NO. OF COPIES	ORGANIZATION
1	R MARTIN MERL LTD TAMWORTH RD HERTFORD SG13 7DG UNITED KINGDOM
1	PW LAY SMC SCOTLAND DERA ROSYTH ROSYTH ROYAL DOCKYARD DUNFERMLINE FIFE KY 11 2XR UNITED KINGDOM
1	T GOTTESMAN CIVIL AVIATION ADMINISTRATION PO BOX 8 BEN GURION INTERNL AIRPORT LOD 70150 ISRAEL
1	S ANDRE AEROSPATIALE A BTE CC RTE MD132 316 ROUTE DE BAYONNE TOULOUSE 31060 FRANCE
1	J BAUER DAIMLER BENZ AEROSPACE D 81663 MUNCHEN MUNICH GERMANY
3	DRA FORT HALSTEAD PETER N JONES DAVID SCOTT MIKE HINTON SEVEN OAKS KENT TN 147BP UNITED KINGDOM
1	FRANCOIS LESAGE DEFENSE RESEARCH ESTAB VALCARTIER PO BOX 8800 COURCELETTE QUEBEC COA IRO CANADA

NO. OF COPIES	ORGANIZATION
2	ROYAL MILITARY COLLEGE OF SCIENCE SHRIVENHAM D BULMAN B LAWTON SWINDON WILTS SN6 8LA UNITED KINGDOM
1	SWISS FEDERAL ARMAMENTS WKS WALTER LANZ ALLMENDSTRASSE 86 3602 THUN SWITZERLAND
1	PROFESSOR SOL BODNER ISRAEL INST OF TECHNOLOGY FACULTY OF MECHANICAL ENGR HAIFA 3200 ISRAEL
1	DSTO MATERIALS RSRCH LAB DR NORBERT BURMAN NAVAL PLATFORM VULNERABILITY SHIP STRUCTURES & MATERIALS DIV PO BOX 50 ASCOT VALE VICTORIA AUSTRALIA 3032
1	PROFESSOR EDWARD CELENS ECOLE ROYAL MILITAIRE AVE DE LA RENAISSANCE 30 1040 BRUXELLE BELGIQUE
1	DEF RES ESTABLISHMENT VALCARTIER ALAIN DUPUIS 2459 BOULEVARD PIE XI NORTH VALCARTIER QUEBEC CANADA PO BOX 8800 COURCELETTE GOA IRO QUEBEC CANADA

NO. OF COPIES	ORGANIZATION
1	INSTITUT FRANCO ALLEMAND DE RECHERCHES DE SANIT LOUIS DE MARC GIRAUD RUE DU GENERAL CASSAGNOU BOITE POSTALE 34 F 68301 SAINT LOUIS CEDEX FRANCE
1	J MANSON ECOLE POLYTECH DMX LTC CH 1015 LAUSANNE SWITZERLAND
1	TNO PRINS MAURITS LAB ROB IJSSELSTEIN LANGE KLEIWEG 137 PO BOX 45 2280 AA RIJSWIJK THE NETHERLANDS
2	FOA NAT L DEFENSE RESEARCH ESTAB BO JANZON R HOLMLIN DIR DEPT OF WEAPONS & PROTECTION S 172 90 STOCKHOLM SWEDEN
2	DEFENSE TECH & PROC AGENCY GRND I CREWTHER GENERAL HERZOG HAUS 3602 THUN SWITZERLAND
1	MINISTRY OF DEFENCE RAFAEL MEIR MAYSELESS ARMAMENT DEVELOPMENT AUTH PO BOX 2250 HAIFA 31021 ISRAEL
1	AKE PERSSON DYNAMEC RESEARCH AB PARADISGRND 7 S 151 36 SODERTALJE SWEDEN

NO. OF COPIES	ORGANIZATION
1	ERNST MACH INSTITUT EMI DIRECTOR HAUPTSTRASSE 18 79576 WEIL AM RHEIN GERMANY
1	ERNST MACH INSTITUT EMI ALOIS STILP ECKERSTRASSE 4 7800 FREIBURG GERMANY
1	IR HANS PASMAN TNO DEFENSE RESEARCH POSTBUS 6006 2600 JA DELFT THE NETHERLANDS
1	BITAN HIRSCH TACHKEMONY ST 6 NETAMUA 42611 ISRAEL
1	MANFRED HELD DEUTSCHE AEROSPACE AG DYNAMICS SYSTEMS PO BOX 1340 D 86523 SCHROBENHAUSEN GERMANY

REPORT DOCUMENTATION PAGE

Form Approved
OMB No. 0704-0188

1. AGENCY USE ONLY *(Leave blank)*	2. REPORT DATE	3. REPORT TYPE AND DATES COVERED
	September 2000	Final, Jan 96–Jul 96

4. TITLE AND SUBTITLE
Embedded Fiber Optic Sensors for Integral Armor

5. FUNDING NUMBERS
DAAL01-97-C-0034

6. AUTHOR(S)
Bruce K. Fink and Kelli Corona-Bittick*

7. PERFORMING ORGANIZATION NAME(S) AND ADDRESS(ES)
U.S. Army Research Laboratory
ATTN: AMSRL-WM-MB
Aberdeen Proving Ground, MD 21005-5069

8. PERFORMING ORGANIZATION REPORT NUMBER
ARL-TR-2267

9. SPONSORING/MONITORING AGENCY NAMES(S) AND ADDRESS(ES)

10.SPONSORING/MONITORING AGENCY REPORT NUMBER

11. SUPPLEMENTARY NOTES
Production Products Manufacturing & Sales, Inc.
St. Louis, MO 63138

12a. DISTRIBUTION/AVAILABILITY STATEMENT
Approved for public release; distribution is unlimited.

12b. DISTRIBUTION CODE

13. ABSTRACT *(Maximum 200 words)*

This report describes the work performed with Production Products Manufacturing & Sales (PPMS), Inc., under the "Liquid Molded Composite Armor Smart Structures Using Embedded Sensors" Small Business Innovative Research (SBIR) Program sponsored by the U.S. Army Research Laboratory (ARL). In the Phase I effort, fiber optic sensor systems were investigated for in-process cure monitoring and in-service health and dynamic response monitoring of monocoque and hybrid liquid molded composite armor structural parts. Sensor embedding techniques during resin infusion molding were developed, thick panels with varying residual stress characteristics were fabricated, two fiber optic sensor types were utilized and compared, several demodulation techniques were studied, and information processing programs were written for converting the sensor signal to engineering data. Bragg grating and fluorescence optrode fiber optic sensors were selected and embedded in armor panels to monitor the cure of the systems and health of the panels during impact and four-point bend tests. During panel curing, the Bragg gratings detected the change in strain in the material at the onset of cross-linking as well as the strain changes (residual stress) resulting from panel processing. The Bragg gratings, serving a dual purpose, measured the resulting strain from the external loads applied due to impact and bending. The fluorescence optrode was used during the cure process only to measure the changes in the material as it cured (degree of cure). Stitching of thick-section fiberglass preforms was also investigated.

14. SUBJECT TERMS	15. NUMBER OF PAGES
fiber optic sensors, composite materials, integral armor, resin transfer molding	103
	16. PRICE CODE

17. SECURITY CLASSIFICATION OF REPORT	18. SECURITY CLASSIFICATION OF THIS PAGE	19. SECURITY CLASSIFICATION OF ABSTRACT	20. LIMITATION OF ABSTRACT
UNCLASSIFIED	UNCLASSIFIED	UNCLASSIFIED	UL

INTENTIONALLY LEFT BLANK.

USER EVALUATION SHEET/CHANGE OF ADDRESS

This Laboratory undertakes a continuing effort to improve the quality of the reports it publishes. Your comments/answers to the items/questions below will aid us in our efforts.

1. ARL Report Number/Author ARL-TR-2267 (Fink) Date of Report September 2000

2. Date Report Received _____

3. Does this report satisfy a need? (Comment on purpose, related project, or other area of interest for which the report will be used.) _____

4. Specifically, how is the report being used? (Information source, design data, procedure, source of ideas, etc.) _____

5. Has the information in this report led to any quantitative savings as far as man-hours or dollars saved, operating costs avoided, or efficiencies achieved, etc? If so, please elaborate. _____

6. General Comments. What do you think should be changed to improve future reports? (Indicate changes to organization, technical content, format, etc.) _____

CURRENT ADDRESS

_____
Organization

_____
Name E-mail Name

_____
Street or P.O. Box No.

_____
City, State, Zip Code

7. If indicating a Change of Address or Address Correction, please provide the Current or Correct address above and the Old or Incorrect address below.

OLD ADDRESS

_____
Organization

_____
Name

_____
Street or P.O. Box No.

_____
City, State, Zip Code

(Remove this sheet, fold as indicated, tape closed, and mail.)
(DO NOT STAPLE)